

Shape Changing Transformations: Interactions with Plasticity and Electrochemical Processes

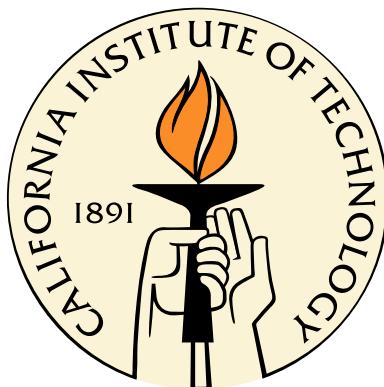
Thesis by

Farshid Roumi

In Partial Fulfillment of the Requirements

for the Degree of

Doctor of Philosophy



California Institute of Technology

Pasadena, California

2010

(Defended May 28, 2010)

© 2010

Farshid Rumi

All Rights Reserved

To my family

I can't wait to see them again.

Acknowledgments

I never forget anyone who taught me even a word, and my parents were the first to teach me anything, so I should thank them the first. I think at Caltech I have learned how to learn. It was not easy, but it is very rewarding. I feel I can do anything that I want, almost. I, especially, want to thank my advisor Professor Kaushik Bhattacharya, for teaching me some of the most important rules of any profession. I believe he is a professional scientist and I am hoping that I never forget the rules he taught me, especially the one that says: "Always distinguish between what you are sure is true, with what you expect to be true." I want to thank Jim Endrizzi and others at International Student Program , especially Jim for answering the complicated questions of an Iranian student. Also I want to thank Natalie Gilmore, and Icy Ma at the Graduate office for being very friendly and helpful. Thanks to Drs. Ken Pickar, Nadia Lapusta and Morteza Gharib for being available when I wanted to ask their opinions. I thank Christine Silva and Cheryl Geer at Thomas building for being very helpful. I also thank my sister Mahshid, and my friends here for helping me have a good social life so I could work better: Branislav Kecman, Shervin Taghavi, Ashley Woodmansee, Luca Giacchino, and many others. I also should not forget Jose, the friendly custodian of Thomas building.

I also want to thank Professors Nadia Lapusta, Guruswami Ravichandran, and William L. Johnson for accepting to be on my committee and reading my thesis. I hope they find it interesting.

I should also thank Marcial Gonzalez for reading part of this thesis, Bharat Prasad Penmecha for his comments on my presentation, Asghar Aryanfar, Mohsen Chitsaz, and my sister Mahshid for their help with some of the figures.

Abstract

Solids undergo phase transformations where the crystal structure changes with temperature, chemical potential, stress, applied electric fields, or other external parameters. These occur by either long-range diffusion of atoms (diffusional phase transformation) or by some form of cooperative, homogeneous movement of many atoms that results in changes in crystal structure (displacive phase transformation). In the latter case, these movements are usually less than the interatomic distances, and the atoms maintain their coordination. The most common example of displacive phase transformations is martensitic transformation. The martensitic transformation in steel is economically very important and can result in very different behavior in the product. Other examples of martensitic transformations are shape memory alloys which are lightweight, solid-state alternatives to conventional actuators such as hydraulic, pneumatic, and motor-based systems.

The martensitic transformation usually only depends on temperature and stress and, in contrast to diffusion-based transformations, is not time dependent. In shape memory alloys the transformation is reversible. On the other hand in steel, the martensite formation from austenite by rapidly cooling carbon-steel is not reversible; so steel does not have shape memory properties.

In Chapters 2 and 3, we study the interesting yet very complicated behavior of martensitic transformation interactions with plastic deformations. A good example here is steel, which has been known for thousands of years but still is believed to be a very complicated material. Steel

can show different behavior depending on its complex microstructure. Thus understanding the formation mechanisms is crucial for the interpretation and optimization of its properties. As an example, low alloyed steels with transformation induced plasticity (TRIP), metastable austenite steels, are known for strong hardening and excellent elongation and strength. It is suggested that the strain-induced transformation of small amounts of untransformed (retained) austenite into martensite during plastic deformation is a key to this excellent behavior.

In Chapters 4 and 5, we study the interactions of solid-solid phase transformations with electrochemical processes. It is suggested that electronic and ionic structures depends on lattice parameters, thus it is expected that structural transformations can lead to dramatic changes in material properties. These transformations can also change the energy barrier and hysteresis. It is known that compatible interfaces can reduce elastic energy and hysteresis, thus may extend the life of the system. Solid-solid transformations change the crystalline structure. These geometry changes can have long range effects and cause stresses in the whole material. The generated stress field itself changes the total free energy, due to the change in elastic energy, and thus, the electrochemical potential and processes are affected. An example is olivine phosphates which are candidates for cathode material in Li-ion batteries. These materials undergo an orthorhombic to orthorhombic phase transition. Experiments in the literature have suggested that elastic compatibility can affect rates of charge/discharge in the battery. Our theory provides some insight into this observation.

Contents

Acknowledgments	iv
Abstract	vi
Contents	viii
List of Figures	ix
List of Tables	x
1 Introduction	1
2 Martensitic Phase Transformation in the Presence of Plasticity	7
2.1 Introduction	7
2.2 Model	12
2.2.1 Phase-field parameter (order parameter)	13
2.2.1.1 Chemical energy	13
2.2.1.2 Interfacial energy	15
2.2.2 Austenite-martensite phase transformation	15
2.2.2.1 Transformation strain	16

2.2.2.2	Kinematics compatibility: prediction of A-M and M-M boundaries .	16
2.2.3	Plasticity	18
2.2.3.1	Plastic strain	18
2.2.3.2	Hardening	18
2.2.3.3	Yield criteria	20
2.2.4	Elastic energy	21
2.2.5	Total potential energy	21
2.2.6	Driving forces, equilibrium, and evolution	22
2.2.7	Time-discrete model	23
2.3	Parameters	28
2.3.1	Nucleation barrier	28
2.3.1.1	One- dimension two-well model	28
2.3.1.2	Two-dimension axi-symmetric three-well model	30
2.3.2	Physical range of parameters and scaling	35
2.4	Numerical Exploration	36
2.4.1	Effect of material parameters on the morphology during the quenching process	37
2.4.1.1	Role of transformation barrier	37
2.4.1.2	Role of surface energy	37
2.4.1.3	Role of elastic moduli	39
2.4.1.4	Role of volume change	40
2.4.1.5	Role of plastic deformation	40
2.4.1.6	Role of under-cooling	40

2.4.2	Lath microstructure and retained austenite: combined role of volume change and plasticity	42
2.4.3	Effect of loading on the morphology of the quenched microstructure	43
2.5	Discussions and experimental verifications	43
2.6	References	54
3	Yielding and Overall Plastic Behavior of Orthotropic Polycrystalline Metals	58
3.1	Introduction	58
3.2	Anisotropic plastic behavior of a single crystal	59
3.2.1	Yield criteria	61
3.2.2	Flow rule	63
3.2.3	Hardening	65
3.2.4	Orthotropic behavior: Two slip systems	66
3.2.5	Incremental work function	68
3.3	Overall plastic behavior of a polycrystal	71
3.3.1	Voronoi tessellation	74
3.3.2	Algorithm to estimate overall plastic behavior of a polycrystal	75
3.3.3	Numerical results and discussion	76
3.4	References	78
4	The Role of Size, Geometry, and Mechanical Compatibility in Diffusive Phase Transformations	80
4.1	Introduction	80
4.2	Model	84

4.3	Small and large body limit	88
4.3.1	Small particle limit	89
4.3.2	Large body limit	90
4.4	Thin film limit	96
4.4.1	Transition layers in the thin film limit	102
4.5	Conclusion	105
4.6	References	106
5	General Continuum Mechanics of Elasto-Electro-Chemical Systems with Moving	
	Boundaries	107
5.1	Introduction	107
5.2	Kinematics	108
5.3	Deformable solids with mass transport	109
5.3.1	Conservation of mass	109
5.4	Electrodynamics	111
5.4.1	Space charge density	111
5.4.2	Electric field	113
5.4.3	Discontinuities in the electric field	114
5.5	Rate of dissipation of the system	118
5.6	Elasto-chemical dissipation	119
5.7	Electrical dissipation	121
5.7.1	Rate of change of field energy: step 1	122
5.7.2	Rate of change of field energy: step 2	123
5.7.3	Rate of change of field energy: step 3	126

5.8 Rate of dissipation: the final expression	127
5.9 Governing equations	130
5.10 References	134

List of Figures

2.1	Chemical energy as a function of the order parameter. $\phi = 0$ means untransformed austenite, $\phi = \pm\phi_0$ indicates the two variants of the transformed martensite.	14
2.2	Phase transformation of a plastic region. Left shows the untransformed austenite. Right shows the transformed martensite. It is shown that plastic deformation is inherited from the old phase on left by the new phase on right.	19
2.3	Simple two-well model. Normalized energy as a function of the normalized order parameter	31
2.4	Transition zone is defined as the width of the region between $\phi = 0$ and $\phi = \pm\phi_0$. Transition length depends on the coefficient of the interfacial energy and defined the physical length scale of the problem.	31
2.5	A three-well model. Left: Normalized energy as a function of the normalized order parameter for different values of $\alpha = 0.55, 0.45, 0.35$. Right: A closer look at the chemical energy function for $\alpha = 0.35$	33

2.6 Martensitic transformation upon quenching. Volume change=0, average strain=0. Here we show some middle time steps, $t = 0, 16, 20, 30$ and not the final morphology. The color bar shows the order parameter. We observe that the stress field due to the neighboring nuclei plays a key role on how a nucleus grows into a plate of a specific thickness dictated by minimizing the sum of the elastic energy and surface energy. . . . 38

2.7 Martensitic transformation upon quenching. Volume change=0.08, average strain=0. When the transformation barrier or the coefficients of surface energy or elastic energy are very high (right figure) the energy barrier can get too high and the material would prefer to stay at the metastable austenite phase (green) instead of the twined martensite structure (red and blue). 39

2.8 Martensitic transformation upon quenching. Volume change=0.08, average strain=0. Here we show some middle time steps, $t = 0, 16, 20, 30$ and not the final morphology. The color bar shows the order parameter. Here we observe that the stress field due to one nucleus results in the nucleation of the other variant. We further observe the twined plates which grow together and nucleate more plates. 41

2.9 Effect of plasticity: Observed twinning and retained austenite in the final morphology, a simple cartoon 42

2.10 Martensitic transformation with no volume change, average strain=0, no plasticity, average surface energy. In the absence of volume change and plasticity, the material makes long twined plates of martensite to minimize the total elastic energy. The surface energy forces the morphology to be a coarse one. 44

2.11 Martensitic transformation with no volume change, average strain=0, $\sigma_y = 200$ MPa, average surface energy. In the absence of volume change, the plasticity reduces the deviatoric and total stresses and thus reduces the elastic energy barrier to transformation, and thus makes the transformation easier. The material still makes long twined plates of martensite to minimize the total elastic energy. The surface energy forces the morphology to be a coarse one. 45

2.12 Martensitic transformation with volume change=0.08, average strain=0, no plasticity, average surface energy. Volume change causes higher stresses and thus higher elastic energy barrier in the material, and thus makes the phase transformation slower. The boundary conditions, average strain=0, results in higher stresses in general, and thus the phase transformation stops as the driving force from the chemical energy difference between the austenite and martensite is not enough to overcome the elastic energy barrier. 46

2.13 Martensitic transformation with volume change=0.08, average strain=0, $\sigma_y = 200$ MPa, average surface energy. Volume change causes higher stresses and thus higher elastic energy barrier in the material, and thus makes the phase transformation slower. On the other hand plastic deformation reduces the deviatoric stresses and thus makes the transformation easier. The boundary conditions, average strain=0, results in higher stresses in general. In this case the competition between lower deviatoric stress due to plastic deformation and higher volumetric stresses due to volume change results in a complex morphology with regions of retained austenite. 47

- 2.14 Martensitic transformation with volume change=0.08, average stress=0, no plasticity, average surface energy. Volume change causes higher stresses and thus higher elastic energy barrier in the material, and thus makes the phase transformation slower. . . . 48
- 2.15 Martensitic transformation with volume change=0.08, average stress=0, $\sigma_y = 200$ MPa, average surface energy. Volume change causes higher stresses and thus higher elastic energy barrier in the material, and thus makes the phase transformation slower. On the other hand plastic deformation reduces the deviatoric stresses and thus makes the transformation easier. The boundary conditions, average stress=0, results in lower stresses in general. The phase transformation completes. 49
- 2.16 Martensitic transformation with volume change=0.08, average strain=0, $\sigma_y = 200$ MPa, average surface energy. It is observed that the combination of the volume change at plastic deformation results in a complex morphology including regions of twinning and retained austenite). Due to plastic deformation the preferred angle between austenite and martensite differs from that of the no plastic case $\sim 6^\circ$ 50
- 2.17 Martensitic transformation with volume change=0.08, average stress=0, $\sigma_y = 200$ MPa, low surface energy. It is observed that the combination of the volume change at plastic deformation results in the presence of some untransformed regions of austenite (retained austenite). Due to plastic deformation the preferred angle between austenite and martensite, $\sim 15^\circ$ here, differs from that of the no plastic case $\sim 6^\circ$ 51

2.18 Martensitic transformation with volume change=0.08, average strain=0, $\sigma_y=200$ MPa, low surface energy. With applied $\epsilon_{12}^0 = 0.1$. It's observed that upon applying far-field strain, the material tries to accommodate it by increasing the volume fraction of the preferred martensite variant at the expense of reduction of the other variant. We also see that some of the retained austenite transforms to the preferred martensite variant. 52

3.1 Stress-strain curve for different steels compared to aluminum according to United States Steel Corporation 60

3.2 Stress-strain curve for martensite, TRIP steel, and austenite 61

3.3 A schematic figure showing lath microstructure: martensitic layers (blue), with retained austenite (white) between them 68

3.4 Optical micrographs of lath martensite in (a) Fe-0.0026C, (b) Fe-0.18C, (c) Fe-0.38C and (d) Fe-0.61C alloys. Etching solution: 3% nital. Morito et al. (2005) 72

3.5 Voronoi tessellation 75

3.6 Estimated mechanical behavior of the polycrystal for different values of domain sizes, $n \times n$, and number of grains nG . $n = 200$ for series *A* and *B*, $n = 400$ for series *C* and *D*. $nG = 1$ for series *A*, $nG = 10$ for series *B* and *C*. $nG = 20$ for series *D*. Series *A* shows the orthotropic behavior of a single grain. 77

5.1 A discontinuity separating two regions. Each region can have different elastic or electric behavior. (Xiao and Bhattacharya, 2008) 115

List of Tables

3.1	Yield strength, ultimate strength and total elongation of mild steel, TRIP steels, and martensite, WorldAutoSteel.	59
-----	--	----

Chapter 1

Introduction

Solids undergo phase transformations where the crystal structure changes with temperature, chemical potential, stress, applied electric fields, or other external parameters. These occur by either long-range diffusion of atoms (diffusional phase transformation) or by some form of cooperative, homogeneous movement of many atoms that results in changes in crystal structure (displacive phase transformation). In the latter case, these movements are usually less than the interatomic distances, and the atoms maintain their coordination. The most common example of displacive phase transformations is martensitic transformation. The martensitic transformation in steel is economically very important and can result in very different behavior in the product. Other examples of martensitic transformations are shape memory alloys which are lightweight, solid-state alternatives to conventional actuators such as hydraulic, pneumatic, and motor-based systems.

The martensitic transformation usually only depends on temperature and stress and, in contrast to diffusion-based transformations, is not time dependent. In shape memory alloys the transformation is reversible. On the other hand in steel, the martensite formation from austenite by rapidly cooling carbon-steel is not reversible; so steel does not have shape memory properties.

In Chapters 2 and 3, we study the interesting yet very complicated behavior of martensitic

transformation interactions with plastic deformations. A good example here is steel, which has been known for thousands of years but still is believed to be a very complicated material. Steel can show different behavior depending on its complex microstructure. Thus understanding the formation mechanisms is crucial for the interpretation and optimization of its properties. As an example, low alloyed steels with transformation induced plasticity (TRIP), metastable austenite steels, are known for strong hardening and excellent elongation and strength. It is suggested that the strain-induced transformation of small amounts of untransformed (retained) austenite into martensite during plastic deformation is a key to this excellent behavior.

In the second chapter, we investigate the morphology of martensitic phase transformation in the presence of plasticity. Using a phase field model, we introduce the total energy of the system as a function of an order parameter which is correlated with the transformation strain, and address the effect of elasticity, volume change, nucleation barrier, and plastic deformations on the morphology of the transformation.

Our numerical simulations suggest that the volume change of the transformation is responsible for the observed fine microstructure of martensite which has been observed in lath steel. It also suggests that the interactions between plasticity and phase transformation result in pinning of the martensitic transformation and presence of untransformed regions of retained austenite. As a conclusion, in agreement with experimental observations in steel, our simulations suggest that the interactions between plasticity and the volume change are responsible for the observed fine martensite microstructure with retained austenite known as lath microstructure.

In the third chapter, we study the yielding and overall plastic behavior of orthotropic polycrys-

talline metals. There is always a tradeoff between hardness and toughness in materials. Here we show that small fractions of soft yet tough layers between hard but brittle layers can result in a hard and tough overall behavior even in the polycrystal. One example is layers of austenite between martensite layers in lath microstructure which is observed in steel. Based on Hill's anisotropic plasticity model, we use a rate-independent, strain hardening orthotropic, associate plasticity model for each single crystal and estimate the overall plastic behavior of a polycrystal. As the conclusion to the first part of this work, we identify the low-yield strength austenite and high volume changes of transformation as the underlying microstructure resulting in the hard and tough behavior of the polycrystalline observed in experiments.

In the last two chapters, we study the interactions of solid-solid phase transformations with electrochemical processes. It is suggested that electronic and ionic structures depends on lattice parameters, thus it is expected that structural transformations can lead to dramatic changes in material properties. These transformations can also change the energy barrier and hysteresis. It is known that compatible interfaces can reduce elastic energy and hysteresis, and thus may extend the life of the system. Solid-solid transformations change the crystalline structure. These geometry changes can have long range effects and cause stresses in the whole material. The generated stress field itself changes the total free energy, due to the change in elastic energy, and thus, the electrochemical potential and processes are affected. An example is olivine phosphates which are candidates for cathode material in Li-ion batteries. These materials undergo an orthorhombic to orthorhombic phase transition. Recent experiments in the literature have suggested that elastic compatibility can affect rates of charge/discharge in the battery. Our theory provides some insight into this observation.

In the fourth chapter, using asymptotic limit analysis, we study the effects of geometry and size of electrodes on elastic energy and concentration profile. We consider the state of lowest free energy of the system; although in practice, due to kinetics, defects, etc., the material may be at a metastable state of energy and may not reach its lowest free energy. Here, we use a phase-field model to estimate the behavior of the elasto-electro-chemical system. The surface energy is modeled as a function of the space gradients of the li-ion concentration, which plays an important rule in describing the concentration profile for different sizes and geometries. The electrochemical energy is modeled as a double-well function with minima near fully lithiated and delithiated states. The elastic energy, assuming coherent interfaces, is a function of the phase transformation between lithiated and delithiated phases, e.g., orthorhombic to orthorhombic phase transformation in $LiFePO_4$. It can also be a function of the applied displacement and traction boundary conditions from the charge collector and electrolyte. It is expected that the elastic energy can play an important role by making the transformation barrier higher and thus limiting the rate. It can also be a major player in the life cycle of the system. This means that one should make the crystallographic changes in electrodes as compatible as possible in order to have higher rates and more cycles. One other import issue is that, when the gradient energy term is large compared to the electrochemical energy, the system does not obey Fick's law. This could occur, for example, across an interface in inhomogeneous systems in which the concentration profile is characterized by a strongly varying curvature. In this case, one has to do a more general study to understand the system and predict its behavior.

We consider three cases:

a) Small body limit: in this limit, we prove that in very small particle limit the concentration profile should be of a single domain in each particle. This results in the elimination of the elastic energy for very small particles. The reduced energy barrier suggests higher rates as suggested by recent experiments and also possibly longer life of the battery. Our results show that for very small particles we should have only either fully lithiated or fully delithiated particles, as reported by experiments of Delmas and some other groups, thus the overall behavior of the concentration, as an averaging scheme, can show reduced miscibility gap.

b) Large body limit: in this limit we prove that we should see multiple layers of lithiated and delithiated phases adjacent to each other in a preferred direction in order to minimize the elastic energy. This is again in accordance with several experiments on large domains.

c) Thin film limit: In this limit we show that the concentration profile should be uniform in the thickness, though depending on the other dimensions of the film it can show periodic layers of lithiated and delithiated phases with a preferred normal direction. This is also consisted with recent experiments of thin films of $LiFePO_4$.

In the fifth chapter we derive a general continuum model of elasto-electro-chemistry systems. Using a continuum mechanical approach, assuming near equilibrium conditions, we consider first-order solid-solid phase transformations in addition to ionic bulk diffusions and surface reactions in elasto-electro-chemical systems. Here, effects of heat and temperature changes are skipped for simplicity. Starting from second law of thermodynamics, we use conservation of mass and Maxwell's equations and introduce space charges and ion densities as field (state) variables in addition to deformation. We derive the general continuum mechanics equations of mass transfer in the bulk and on the surface. We show that in the special cases one can simplify our equations to those

empirical ones, such as Fick's and Butler-Volmer equations. The formulation is general and allows for modeling the whole system with fixed and moving boundaries. We also derive the force acting on the phase boundary, generalized Eshelby-momentum tensor, which determines the speed of the transformation and can be a rate limiting effect in electrochemical systems.

Chapter 2

Martensitic Phase Transformation in the Presence of Plasticity

2.1 Introduction

Martensitic phase transformation is a diffusionless, solid-to-solid, structural phase transformation from a high-temperature phase, austenite, to a low-temperature phase, martensite. The resultant martensite structure shows itself as multiple symmetry-related variants of martensite which are oriented differently with respect to the austenite lattice but have identical crystal structure. This is because the high-temperature austenite phase often has greater symmetry than the low-temperature martensite phase (Bhattacharya 2003).

When martensite transformation occurs in a material that also undergoes plasticity, the dislocations that are responsible for the plasticity in the austenite structure can be inherited by the martensite. This causes an interaction between the phase transformation and plasticity. A well-known material which shows both plasticity and phase transformation is steel. Here, the transformation converts a face-centered cubic, *f.c.c.*, austenite lattice to a body-centered tetragonal, *b.c.t.*, martensite lattice. The product lattice is not unique and has many variants, each with a distinct

orientation due to fewer crystallographic symmetries after transformation. This transformation, initiated by sudden cooling (quenching), results in enormous shear strains and the product usually avoid these intolerable strains by either slipping (plastic deformation) or twinning. The combination of transformation and plasticity leads to complex microstructures. Specifically, it has been proposed that plastic accommodation causes the technologically important plate-lath morphological transition in steels (Olson and Cohen 1986). This transformation plays a critical role in the resulting hardness of steel. This is the motivation for our model.

The competition of plasticity and the phase transformation results in different types of martensite in steel. Austenite yield strength is about 2-3 times less than martensite. If plasticity can happen before the phase transformation, then we see lath martensite, which is the combination of plastic strains and transformation strains. If the yield strength of martensite is so high that plasticity doesn't happen, we see plate martensite. Yield strength depends on the carbon content, the higher the carbon content, the higher the yield strength, and so we expect to see plate martensite with very sharp and straight interface, as elasticity is scale-less; however, when there is plasticity involved, we see a very complicated interface (surprisingly enough in this case the higher the carbon the more complicated the boundary) which may be due to another mechanism of carbon atom movements. Adding more carbon not only gives more resistance to yielding, but by also strengthening austenite, it makes the transformation harder, and so we need more energy in this case, resulting in lower M_s . This might be due to the fact that more carbon results in bigger c/a , where (a, a, c) are the dimensions of the martensite unit cell, $c > a$, noting that carbon offset in the $b.c.t.$ is the cause of lengthening in one direction. It seems that growth of martensite embryos happens first by elongation until stopped by an obstacle, and then by thickening of martensite.

H.K.D.H. Bhadeshia (1979) studied the retained austenite trapped between laths/platelets

martensites in steels. That group found that twin-related martensite variants do not favor the retention of austenite. They observed that inter-martensite austenite films were most likely seen when the adjacent martensite variants were in the same crystallographic orientation. They also suggested there would be less retained austenite between twin related variants of martensite. In $Fe - 4Ni - 0.4C$, the observed retained austenite films were about 1% and rather discontinuous. In $Fe - 3.9Mo - 0.18C$ inter-martensite retained austenite films were very fine, but their quantity was considerable. In $Fe - 0.08C - 1.1Mn - 0.2Si - 5.5Ni - 14.5Cr - 2.1Mo - 0.7Nb - 1.9Cu$, they observed large quantities of heavily faulted austenite. In $Fe - 0.31C - 2.0Si$ the alternate martensite laths were twin related, and they didn't find any retained austenite.

Wayman and co-workers (1976, 1992) studied the crystallography and morphology of ferrous martensite. For plate substructure, they observed that the parallel sided plates are characterized by an internal structure consisting of a single set of twins that sometimes extends completely across the plate to the interfaces. Stronger austenite results in finer martensite twins. For $Fe - Ni$ alloys, they reported segmented and irregular plates, a central region of twins, and arrays of skew dislocations in the peripheral regions (for example in $Fe - 29Ni$ they reported no twins, however they saw fully twined $Fe - 34Ni$ alloys). Constancy of the shape change across the plate width implies that the lattice invariant strain is constant and changes from slip to twinning. They suggested the change to be due to a local temperature rise at the interface during growth.

They observed dislocations, resulting from accommodation strains, in the untwined regions of the plates which were confined to the interface. Lack of constancy was observed in the substructure, not only in different alloys but from plate to plate. Defects may be inherited from stacking faults in the austenite. Transition from twinning to slip occurred during growth. The dislocations generating the complementary strain remain in the interface and accommodate the matching of the lattices.

Growth of individual sub-plates and macroscopic plates is accompanied by intense accommodation slip in the austenite on the particular $(111)F$ plane that is nearly parallel to the habit plane.

The experimental observations suggest that at first the inclusion grows longitudinally, and then after reaching the borders of the austenite grain or any other constraint, say the borders of other inclusions, it thickens.

Maki and co-workers (2005) studied $Fe - Ni$ alloys and concluded that martensite inherits plasticity from austenite. They also observed that there is no plasticity in the mid-rib, twined plate, but the area around the lath is highly plastic, and suggested that plasticity begins after the formation of the mid-rib. They (2006) also studied $Fe - Ni - Co$ alloys and observed that for smaller volume changes, there is less dislocation density, and the M/A interface is smoother. They observed that in non-ferrous alloys, if volume change is about zero, we only have plate martensite; but in ferrous alloys, we might see lenticular too. They suggested that smaller volume change and lower M_s result in more lenticular, while more volume change and more M_s gives more lath. They measured the dislocation density in the order of $10^{15}m^{-2}$ for lath martensite.

In 1985 Grujicic et al. discussed the mobility of martensitic interfaces in thermoelastic shape memory alloys by considering the effect of point defects on the dislocations in the interface. Grujicic, et al. (1985, 1992) evaluated activation energies at various temperatures for the mobility of martensitic interfaces in thermoelastic $Cu - Al - Ni$ alloys and compared their results with estimations from empirical formulations. Ghosh and Olson (1994) applied the same procedure in an analysis of activation energy values evaluated from the rate of formation of isothermal martensite in ferrous alloys. They obtained an analytical expression for the representation of the behavior of ferrous alloys to predict the behavior of alloys with different compositions. However all of these methods were based on empirical rules. Cahn (1961, 1962, 1968, 1969) was the first who applied

the phase field method to coherent transformations in solids by considering transformation-induced coherency strain. Wang and Khachaturyan (2006) extended the early phase field model of Cahn to arbitrary microstructures with arbitrary transformation strains using the microelasticity theory of Khachaturyan and Shatalov (1967, 1969, 1983).

When the conditions for thermo-elastic growth are not met, plastic accommodation of the transformation shape strain may be substantial. In this case the interaction between a growing martensite plate and its plastic zone becomes important, determining the growth path of a martensite inclusion. Despite of the approximate treatment of the stress-strain fields, the first model of martensitic plate growth in the plastic regime (Olson and Cohen 1985, Haezebrouck 1987) studied the longitudinal growth arrest due to plastic accommodation. Marketz and Fischer (1994) did a finite-element simulation of nucleation and growth of a martensitic plate. Wen et al. (1999) obtained a finite-element solution for modeling the growth by discrete martensitic layers. They modeled the transformation in each layer by homogeneous growth of the transformation strain from zero to its final value, and proposed a PT criterion and an extremum principle to choose the next transforming layer. However, kinetic equations were not implemented in these works. Levitas and co-workers (1999, 2002) developed a mesoscopic continuum thermo-mechanical theory of martensitic phase transition in inelastic materials and studied the problem of the appearance of a martensitic plate in an elastoplastic austenitic matrix at finite strains. However they were restricted to fixed aspect ratios and neglected the inter-inclusion interactions. As many other works, they have used some empirical relations based on best fit with a reference experiment, and therefore their works are only applicable to some specific material-environment conditions.

The stored energy of ferrous martensite depends on the morphology and microstructure. The adiabatic heating and driving force at M_s for lath martensite is very small compared to that of the

plate martensite. When lath martensite is formed in $Fe - 29wt\%Ni$ at $266 - -133K$, the evolved heat corresponds to an enthalpy of transformation $\sim 1600 J/mole$ independent of transformation temperature and volume fraction (Tamura and Wayman 1992). This is similar to enthalpy change for $Fe - 30.3wt\%Ni$ transformed at $243 - -198K$. But at lower temperatures where plate martensite is formed, it is more than $2600 J/mole$. Noting that the stored energy due to the dislocations is very low, Christian (1979) suggested that the difference is due the better elastic accommodation of the plates. For an $Fe - 13.7\%Ni - 0.86\%C$ steel transformed at $297 - 188K$, as the volume fraction changes from 7 to 59%, the measured enthalpy change at $507K$ decreases from 4650 to $1600J/mole$. Christian suggested that the increase in the stored energy is due to high work-hardening and high dislocation densities in the regions of deformed austenite which have subsequently to be transformed to martensite.

Despite the detailed experimental observations, idealized theoretical models, and empirical rules in the literature, there is a lack of a complete microstructure study. There are discrepancies with different models, and the role of plasticity is not understood throughly. We seek to develop a model that describes microstructure development during quenching and to determine the criteria for the resulted microstructure change from plate to lath with retained austenite. We then study the effect of loading on the quenched system to understand the mechanism of concurrent toughening and hardening observed in some materials, such as steel. We limit ourselves to two-dimension, small strains, 2 variants of martensite.

2.2 Model

We characterize the microstructure by an order parameter, which distinguishes austenite and martensite phases by assigning different values to each of them. We introduce transformation

strains and plastic strains. We assume that there are three major contributions to the free energy. The first is the interfacial energy on interfaces separating different phases. Second is the chemical energy which prefers the martensite state to the austenite state at the temperature of interest. Finally, the third is the elastic energy. Plastic strain is governed by a Mises yield criteria and Ramberg-Osgood isotropic hardening.

2.2.1 Phase-field parameter (order parameter)

We study the austenite-martensite phase transition in the presence of plasticity by introducing a phase field model. A key model in the phase field model of our problem is to formulate the total free energy of the system as a function of the order parameter, ϕ , such that $\phi = \pm\phi_0$ stands for different martensite variants (twins), and $\phi = 0$ stands for austenite.

2.2.1.1 Chemical energy

$G(\phi)$, the chemical free energy of a homogeneous system is usually approximated by a Landau polynomial expansion with respect to the order parameter. We model it by a three-well function with minima at austenite, and 2 martensite variants. In our model austenite is assumed to be less stable than martensite due to undercooling caused by quenching.

$$G(\phi) = G(0) \frac{(3\alpha^2 - \beta^2 - 2\phi^2) (\beta^2 - \phi^2)^2}{3\alpha^2\beta^4 - \beta^6}, \quad (2.1)$$

differentiating with respect to the order parameter gives

$$\frac{\partial G(\phi)}{\partial \phi} = G(0) \frac{-12\phi(\phi^2 - \alpha^2)(\phi^2 - \beta^2)}{\beta^4(3\alpha^2 - \beta^2)}, \quad (2.2)$$

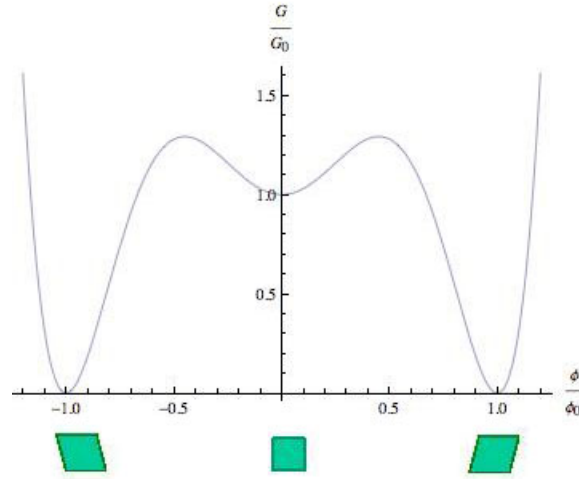


Figure 2.1: Chemical energy as a function of the order parameter. $\phi = 0$ means untransformed austenite, $\phi = \pm\phi_0$ indicates the two variants of the transformed martensite.

α and β are the local maximizer and minimizer of $G(\phi)$. $G(\phi = 0)$ is the undercooling, chemical driving force. The activation energy (barrier energy), A , is then

$$A = G(0) \left(\frac{(\alpha^2 - \beta^2)^3}{b^4(3\alpha^2 - \beta^2)} - 1 \right). \quad (2.3)$$

As we have assumed the wells to be at $\phi = 0, \pm\phi_0$, and austenite to be less stable than martensite, we have $\beta = \phi_0$ and $0 < \tilde{a} = a/\phi_0 < 0.577$ and

$$A = G(0) \left(\frac{(\tilde{a}^2 - 1)^3}{3\tilde{a}^2 - 1} - 1 \right). \quad (2.4)$$

Once we know the activation energy, and the undercooling for a specific composition and temperature, we can calculate \tilde{a} .

2.2.1.2 Interfacial energy

The gradient term, $\frac{\lambda^2}{2}|\nabla\phi|^2$ accounts for rapid changes of ϕ or the interface between different phases. Its role is to suppress any oscillation that would occur when solving for the other two terms and thus may be regarded as interface energy. This interfacial energy penalizes abrupt changes in the system by making a transition zone, however this transition zone may not be significant in reality, and we may see a sharp interface between austenite and martensite states, as in plate martensite. In this case, the introduced interfacial energy is a mathematical term to correctly connect the energies in micro scale to the continuum scale, while it does not change the overall pattern or affect the overall behavior if the computational domain is large enough. Here, the parameter λ^2 describes the length scale of the numerical simulations and is usually determined by either fitting of interfacial energies to experimental results or by using first principles.

2.2.2 Austenite-martensite phase transformation

Like all displacive transformations in steels, the growth of martensite is associated with a shape deformation which is characterized as an invariant-plane strain. The invariant plane is the habit plane of the martensite. For martensitic phase transformation in ferrous alloys, the deformation is a combination of a large shear ($s \approx 0.26$) parallel to the invariant-plane and a dilatation ($d \approx 0.03$) normal to the plane.

2.2.2.1 Transformation strain

We assume the transformation strain, a function of order parameter ϕ , as:

$$\epsilon^T = \begin{pmatrix} \gamma\phi^2 & \eta\phi \\ \eta\phi & \gamma\phi^2 \end{pmatrix}. \quad (2.5)$$

Typical values for transformation strain of steel, are 0.02 – –0.05 volumetric transformation strain and 0.20 transformation shear. Assuming the order parameter $\phi = \pm 0.2$ for martensite variants, we have γ and η of order $o(1)$.

2.2.2.2 Kinematics compatibility: prediction of A-M and M-M boundaries

Continuity of the displacement at the boundary of two different phases requires the difference in their derivatives to be of rank one. Mathematically it means that if \mathbf{F} and \mathbf{G} are the deformation gradients in two adjacent regions, there should exist vectors \mathbf{a} and $\hat{\mathbf{n}}$ such that (Bhattacharya 2003),

$$F_{ij} - G_{ij} = 2a_i n_j. \quad (2.6)$$

This requires the difference in the symmetric part of the derivatives, strain tensors, to satisfy the following equation:

$$\Delta\epsilon_{ij} = a_i n_j + a_j n_i. \quad (2.7)$$

In the case of infinitesimal strains, defining λ_i , and e_i as the eigenvalues and eigenvectors of $\Delta\epsilon$, the interface will be possible if $\lambda_1 > \lambda_2 = 0 > \lambda_3$. In this case we can find the vector \hat{n} from

$$\hat{\mathbf{n}} = \pm\sqrt{\lambda_1}\mathbf{e}_1 + \sqrt{\lambda_2}\mathbf{e}_2. \quad (2.8)$$

Consider the two dimension case of our problem. We only consider the transformation strain, as it is the major component of the strain, compared to elastic strains. For the boundary between two adjacent martensite regions we have

$$\epsilon_1^{tr} = \begin{pmatrix} \phi^2 & \eta\phi \\ \eta\phi & \phi^2 \end{pmatrix} \quad (2.9)$$

and

$$\epsilon_2^{tr} = \begin{pmatrix} \phi^2 & -\eta\phi \\ -\eta\phi & \phi^2 \end{pmatrix} \quad (2.10)$$

so we will get

$$\Delta\epsilon = \begin{pmatrix} 0 & 2\eta\phi \\ 2\eta\phi & 0 \end{pmatrix}. \quad (2.11)$$

The eigenvalues and eigenvectors of this matrix are $\lambda = 2\phi, -2\phi$ and $\mathbf{e} = (1/\sqrt{(2)}, \pm 1/\sqrt{(2)})$, so we will have $\mathbf{n} = \pm(1/\sqrt{(2)}, -1/\sqrt{(2)}) + (1/\sqrt{(2)}, 1/\sqrt{(2)})$ so $\mathbf{n} = (0, 1)$ or $(1, 0)$. So in 2D, martensite variants form right angles with each other.

Now consider the two dimension austenite/martensite interface; as austenite is strain free, we

will have

$$\Delta\epsilon = \begin{pmatrix} \phi^2 & \eta\phi \\ \eta\phi & \phi^2 \end{pmatrix} \quad (2.12)$$

which has $\lambda = \phi^2 \pm \phi$, and $\mathbf{e} = (1, \pm 1)$. If we substitute $\phi = .2$, the the austenite/martensite interface will be about ± 6 or 84° . We saw that in two dimensions A/M interface is possible. However making an austenite/martensite interface is not possible in a three dimension case. This is the reason for laboratory-observed microstructure in steels. In this case the interface will be between austenite and twinned martensite.

2.2.3 Plasticity

It is believed that plasticity plays an important role in the irreversibility of the phase transformation and also the observed hard and tough behavior of some steels. Here, we define a rate-independent isotropic hardening J_2 plasticity model.

2.2.3.1 Plastic strain

Our main assumption is that martensite is much harder than austenite, so we assume linear elastic behavior for martensite variants, and strain hardening, J_2 plasticity model for austenite. We further note that plasticity, ϵ^p , is transferred from austenite to martensite, so the total inelastic strain at each point is $\epsilon^{tr} + \epsilon^p$, as shown in Figure 2.2.

2.2.3.2 Hardening

The stored cold work energy, $W^p(\epsilon^{nl}, q)$, is the non-elastic part of the free energy which depends on irreversible plasticity strains. q is an internal variable indicating the state of work hardening.

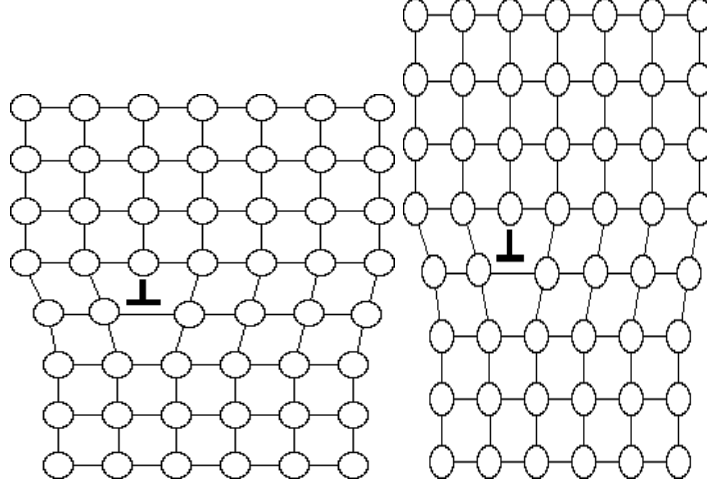


Figure 2.2: Phase transformation of a plastic region. Left shows the untransformed austenite. Right shows the transformed martensite. It is shown that plastic deformation is inherited from the old phase on left by the new phase on right.

Here we assume $q = \epsilon_M^p$ is the Mises strain. We assume a power-law form for the stored mechanical energy as follows, assuming only isotropic hardening

$$W^p(\epsilon_{ij}^p, \epsilon_M^p) = \frac{n\epsilon_0^p}{n+1} \sigma_0 \left(1 + \frac{\epsilon_M^p}{\epsilon_0^p}\right)^{\frac{n+1}{n}} \quad (2.13)$$

from which the yield stress is

$$\sigma_y = \frac{\partial W^p(\epsilon^p, \epsilon_M^p)}{\partial \epsilon_M^p} = \sigma_0 \left(1 + \frac{\epsilon_M^p}{\epsilon_0^p}\right)^{\frac{1}{n}} \quad (2.14)$$

the back stress of kinematic hardening vanishes:

$$\sigma^* = \frac{\partial W^p(\epsilon^p, \epsilon_M^p)}{\partial \epsilon^p} = 0. \quad (2.15)$$

In the limit when $n \rightarrow \infty$, we have perfect elastic-plastic behavior

$$\sigma_y \rightarrow \sigma_0 \left(1 + \frac{\epsilon_M^p}{\epsilon_0^p}\right)^0 = \sigma_0. \quad (2.16)$$

2.2.3.3 Yield criteria

The Mises yield criterion suggests that the yielding of materials begins when the second deviatoric stress invariant J_2 reaches a critical value. This implies that the yield condition is independent of hydrostatic stresses.

$$f(J_2) = \sqrt{J_2} - k = 0, \quad (2.17)$$

where k is the yield stress of the material in pure shear.

Applying a uniaxial stress, it is seen that, at the onset of yielding, the magnitude of the shear yield stress in pure shear, k , is $\sqrt{3}$ times lower than the tensile yield stress in the case of uniaxial tension, σ_y . Thus, we have

$$k = \frac{\sigma_y}{\sqrt{3}}. \quad (2.18)$$

The Mises yield criterion can be expressed as:

$$f(J_2) = \sqrt{3J_2} - \sigma_y = 0. \quad (2.19)$$

Substituting J_2 as a function of the stress tensor components

$$(\sigma_{11} - \sigma_{22})^2 + (\sigma_{22} - \sigma_{33})^2 + (\sigma_{33} - \sigma_{11})^2 + 6(\sigma_{23}^2 + \sigma_{31}^2 + \sigma_{12}^2) = 6k^2 = 2\sigma_y^2, \quad (2.20)$$

which defines the yield surface as a circular cylinder whose intersection with the deviatoric plane, is a circle with radius $\sqrt{2k}$, or $\sqrt{2/3}\sigma_y$.

We assume plane stress in our model so we have $\sigma_{33} = \sigma_{31} = \sigma_{32} = 0$.

2.2.4 Elastic energy

We assume infinitesimal elastic deformations and identical isotropic behavior by all phases; so we can write the elastic energy density as

$$W^1(\epsilon, \epsilon^{pl}, \epsilon^{pt}(\phi)) = \frac{1}{2} (\epsilon - \epsilon^{pt} - \epsilon^{pl}) : \mathbb{C} : (\epsilon - \epsilon^{pt} - \epsilon^{pl}). \quad (2.21)$$

2.2.5 Total potential energy

Putting the aforementioned energy terms together, we postulate the energy functional density as the sum of the four terms in the following form:

$$U = \frac{\lambda^2}{2} |\nabla\phi|^2 + G(\phi) + \frac{1}{2} (\epsilon - \epsilon^{pt} - \epsilon^{pl}) : \mathbb{C} : (\epsilon - \epsilon^{pt} - \epsilon^{pl}) + W^p(\epsilon^{pl}, \epsilon_M^{pl}), \quad (2.22)$$

from which the total energy of the system is

$$E = \int_{\Omega} U d\Omega. \quad (2.23)$$

2.2.6 Driving forces, equilibrium, and evolution

Here we assume that the material is always at the state of stress equilibrium, so minimizing the Lagrangian of the total free energy with respect to the strains gives

$$\nabla \cdot (\mathbb{C} : (\epsilon - \epsilon^{pt} - \epsilon^{pl})) = 0. \quad (2.24)$$

The driving force for the phase transformation, order parameter, is assumed to be the change of the total free energy with respect to the order parameter

$$d_\phi = -\frac{\partial E}{\partial \phi}. \quad (2.25)$$

The spatial evolution of ϕ , which completely defines the microstructural evolution during phase transformation is obtained by assuming a linear dependence of the rate of deformation on the driving force

$$\dot{\phi} = -\frac{\partial E}{\partial \phi}. \quad (2.26)$$

Equations in this format are widely used to study various problems of microstructure evolution.

We get the following evolution equation:

$$\dot{\phi} = \lambda^2 \Delta \phi - G'(\phi) + (\epsilon - \epsilon^{pt} - \epsilon^{pl}) : \mathbb{C} : \frac{\partial \epsilon^{pt}}{\partial \phi} - \frac{\partial W^p}{\partial \phi}. \quad (2.27)$$

Similarly we have

$$\mathbf{d}_{\epsilon^{pl}} = -\frac{\partial E}{\partial \epsilon^{pl}}, \quad (2.28)$$

so we have

$$d_{\epsilon_{ij}^{pl}} = \mathbb{C} : (\epsilon - \epsilon^{pt} - \epsilon^{pl})_{ij} - \frac{\partial W^p}{\partial \epsilon_{ij}^p} = \sigma_{ij}^{dev} - \sigma_{ij}^*, \quad (2.29)$$

where in the second equation, we have made the assumption of no volume change due to plasticity in metals, and defined the deviatoric part of the stress tensor as σ_{ij}^{dev} . σ^* is the back stress. Here for simplicity we neglect kinematic hardening, so $\sigma^* = \mathbf{0}$.

2.2.7 Time-discrete model

To study the above model numerically, we introduce a time discretization and seek an implicit formulation, (Stainier and Ortiz 1999). To this end, we introduce the incremental work function to be:

$$F_n(\epsilon_{n+1}, \epsilon_{n+1}^{pl}, \phi_{n+1}) = \int_{\Omega} f_n d\Omega, \quad (2.30)$$

where

$$f_n = U_{n+1}(\epsilon_{n+1}, \epsilon_{n+1}^{pl}, \phi_{n+1}) - U_n(\epsilon_n, \epsilon_n^{pl}, \phi_n) + \Delta t \psi^* \left(\frac{\epsilon_{n+1}^{pl} - \epsilon_n^{pl}}{\Delta t}, \frac{\phi_{n+1} - \phi_n}{\Delta t} \right), \quad (2.31)$$

where ψ^* is the dual kinetic potential.

We assume that the dual kinetic potential has an additive form, and can be separated into

plastic and internal variable dissipation:

$$\psi^* \left(\frac{\epsilon_{n+1}^{pl} - \epsilon_n^{pl}}{\Delta t}, \frac{\phi_{n+1} - \phi_n}{\Delta t} \right) = \psi^{*p} \left(\frac{\epsilon_{n+1}^{pl} - \epsilon_n^{pl}}{\Delta t} \right) + \psi^{*\phi} \left(\frac{\phi_{n+1} - \phi_n}{\Delta t} \right). \quad (2.32)$$

Given $\epsilon_n, \epsilon_n^{pl}, \phi_n$, we minimize F_n with respect to $\epsilon_{n+1}, \epsilon_{n+1}^{pl}, \phi_{n+1}$. Minimization with respect to ϵ_{n+1} gives the mentioned equilibrium equation (2.24).

Minimization of F_n with respect to the plastic strain at each state gives:

$$\delta_{\epsilon_{n+1}^{pl}} F_n = 0. \quad (2.33)$$

This can be written as

$$\frac{\partial U_{n+1}}{\partial \epsilon_{n+1}^{pl}} + \Delta t \frac{\partial \psi^*}{\partial \epsilon_{n+1}^{pl}} = -(\mathbf{Y}^p)_{n+1} + \frac{\partial \psi^{*p}}{\partial \epsilon_{n+1}^{pl}} \left(\frac{\epsilon_{n+1}^{pl} - (\epsilon_n^{pl})}{\Delta t} \right) = 0. \quad (2.34)$$

In the above formula, the driving force with respect to the plastic strain is defined as:

$$\mathbf{Y}^p = -\frac{\partial U}{\partial \epsilon^{pl}} = \mathbb{C} (\epsilon - \epsilon^{pt}(\phi) - \epsilon^{pl}) - \frac{\partial W^p}{\partial \epsilon^{pl}} = \sigma - \sigma^*, \quad (2.35)$$

and

$$\frac{\partial \psi^*}{\partial \dot{\epsilon}} = \sigma - \sigma^*, \quad (2.36)$$

where

$$\sigma^* = \frac{\partial W^p(\epsilon, \epsilon^{pl})}{\partial \epsilon^{pl}}. \quad (2.37)$$

Finally, minimization with respect to the order parameter ϕ gives:

$$\delta_{\phi_{n+1}} F_n = 0, \quad (2.38)$$

or equivalently

$$\frac{\partial U_{n+1}}{\partial \phi_{n+1}} + \Delta t \frac{\partial \psi^*}{\partial \phi_{n+1}} = - (y^\phi)_{n+1} + \frac{\partial \psi^{*\phi}}{\partial \dot{\phi}_{n+1}} \left(\frac{\phi_{n+1} - \phi_n}{\Delta t} \right) = 0, \quad (2.39)$$

where driving force for the order parameter ϕ is defined by:

$$y^\phi = - \frac{\partial U}{\partial \phi} = - \frac{\partial W^1(\epsilon, \epsilon^{pl}, \phi)}{\partial \phi_{n+1}} + \Delta \phi_{n+1} - \frac{\partial G_c(\phi_{n+1})}{\partial \phi_{n+1}}. \quad (2.40)$$

This can be further simplified as

$$\begin{aligned} y^\phi &= - \frac{\partial W^1(\epsilon, \epsilon^{pl}, \epsilon^{pt}(\phi))}{\partial \epsilon^{pt}(\phi)_{n+1}} \frac{\partial \epsilon^{pt}(\phi_{n+1})}{\partial \phi_{n+1}} + \Delta \phi_{n+1} - \frac{\partial G(\phi_{n+1})}{\partial \phi_{n+1}} \\ &= \sigma_{n+1} \frac{\partial \epsilon^{pt}(\phi_{n+1})}{\partial \phi_{n+1}} + \Delta \phi_{n+1} - \frac{\partial G(\phi_{n+1})}{\partial \phi_{n+1}}. \end{aligned} \quad (2.41)$$

Now, assume there exists a kinetic potential ψ^ϕ , such that we can write its dual potential as:

$$\psi^{*\phi}(\dot{\phi}) = \frac{1}{2} \dot{\phi}^2. \quad (2.42)$$

Differentiating with respect to the rate of change of the order parameter gives

$$\frac{\partial \psi^{*\phi}}{\partial \dot{\phi}_{n+1}} \left(\frac{\phi_{n+1} - \phi_n}{\Delta t} \right) = \frac{\phi_{n+1} - \phi_n}{\Delta t}, \quad (2.43)$$

which shows that the suggested dual potential satisfies the assumed material kinetics rule

$$\frac{\phi_{n+1} - \phi_n}{\delta t} = \sigma \frac{\partial (\epsilon^{\text{tr}}(\phi))_{n+1}}{\partial \phi_{n+1}} + \Delta \phi - \frac{\partial G_c(\phi_{n+1})}{\partial \phi_{n+1}} \quad (2.44)$$

which is the implicit form.

Note that the dual potentials are derived from applying the backward-Euler algorithm to the following kinetic relations:

$$\frac{\epsilon_{n+1}^p - \epsilon_n^p}{\Delta t} = \frac{\partial \psi^p}{\partial \mathbf{Y}^p} ((\mathbf{Y}^p)_{n+1}) \quad (2.45)$$

and

$$\frac{\phi_{n+1} - \phi_n}{\Delta t} = \frac{\partial \psi^\phi}{\partial y^\phi} ((y^\phi)_{n+1}). \quad (2.46)$$

Now, considering the dual kinetic potential of the plastic dissipation, we have

$$\sigma - \sigma^* = \frac{\partial \psi^{*p}(\dot{\epsilon}^{pl})}{\partial \dot{\epsilon}^{pl}}. \quad (2.47)$$

Define an effective (Mises) plastic strain as

$$\epsilon_M^p = \sqrt{\frac{2}{3} \epsilon_{ij}^p \epsilon_{ij}^p} \quad 3 - \text{dimension}, \quad \epsilon_M^p = \sqrt{\epsilon_{ij}^p \epsilon_{ij}^p} \quad 2 - \text{dimension}. \quad (2.48)$$

It can be shown that a rate dependent plastic dual potential can be written as

$$\psi^{*p}(\dot{\epsilon}^{pl}) = \begin{cases} \infty, & \dot{\epsilon}_M^p < 0 \\ g^*(\dot{\epsilon}^{pl}), & \dot{\epsilon}_M^p \geq 0 \end{cases}, \quad (2.49)$$

where g^* is a function of the plasticity invariants $(J_1(\dot{\epsilon}^{pl}), J_2(\dot{\epsilon}^{pl}), J_3(\dot{\epsilon}^{pl}))$. Now, if we assume that we are interested in J_2 plasticity this simplifies as

$$g^*(\dot{\epsilon}^{pl}) = g^*(J_2(\dot{\epsilon}^{pl})). \quad (2.50)$$

Let's assume a power-law rate dependent plasticity model

$$g^*(\dot{\epsilon}^{pl}) = \frac{km\dot{\epsilon}_0^p}{m+1} \sigma_y \left(\frac{\dot{\epsilon}_M^p}{\dot{\epsilon}_0^p} \right)^{\frac{m+1}{m}}. \quad (2.51)$$

Then, for $\dot{\epsilon}_M^p > 0$ we will get

$$\sigma - \sigma^* = \frac{\partial g^{*p}(\dot{\epsilon}^p)}{\partial \dot{\epsilon}^p} = k\sigma_y \left(\frac{\dot{\epsilon}_M^p}{\dot{\epsilon}_0^p} \right)^{\frac{1}{m}} \quad (2.52)$$

which is equivalent to

$$\dot{\epsilon}_M^p = \dot{\epsilon}_0^{pl} \left(\frac{\sigma - \sigma^*}{k\sigma_y} \right)^m. \quad (2.53)$$

Finally we assume the stored energy of the cold work

$$W^p = W^p(\epsilon_{ij}^{pl}, q) \quad (2.54)$$

where the dependence of W^p on ϵ_{ij}^{pl} gives the kinematic hardening, and its dependence on q gives the isotropic hardening behavior in which q is an internal variable. A suitable choice for q can be

$$q = \int \dot{\epsilon}_M^p dt \quad \text{or} \quad q = \epsilon_M^p. \quad (2.55)$$

So, we have shown that the proposed variational form satisfies all kinetics rules. In the numerical experiment section we use the incremental formulation described here with the energies and plasticity models described earlier. We further use a rate-independent plastic dissipation model. We use the values defined in the following section.

2.3 Parameters

2.3.1 Nucleation barrier

To understand the effect of nucleation barrier and deciding on the range of it in our model (Figures 2.3 and 2.5), we do a simple one-dimension model, and then extend the results to two dimensions.

2.3.1.1 One- dimension two-well model

We seek to understand the interfacial energy and interfacial width. For simplicity assume we work in one- dimension and neglect elastic energy comparing to the other terms. We idealize and assume to have

$$G(\varphi) = \frac{\kappa}{4} (\varphi^2 - \varphi_0^2)^2 = \frac{\kappa}{4} \varphi_0^4 (\tilde{\varphi}^2 - 1)^2 \quad (2.56)$$

where $\tilde{\varphi} = \varphi/\varphi_0$. Adding the gradient term,

$$f = \frac{\lambda^2}{2}\varphi_{,x}^2 + G(\varphi) = \frac{\lambda^2}{2}\varphi_{,x}^2 + \frac{\kappa}{4}(\varphi^2 - \varphi_0^2)^2 = \varphi_0^2 \frac{\lambda^2}{2}\tilde{\varphi}_{,x}^2 + \frac{\kappa}{4}\varphi_0^4(\tilde{\varphi}^2 - 1)^2 \quad (2.57)$$

we get

$$\dot{\varphi} = \lambda^2\varphi_{,xx} - \kappa\varphi(\varphi^2 - \varphi_0^2) \quad \text{or} \quad \varphi_0\dot{\tilde{\varphi}} = \varphi_0^2\lambda^2\tilde{\varphi}_{,xx} - \varphi_0^3\kappa\tilde{\varphi}(\tilde{\varphi}^2 - 1). \quad (2.58)$$

The stationary solution of this ODE is obtained by setting $\dot{\varphi} = 0$. Assume the solution to be of the form

$$\varphi = a \tanh\left(\frac{x}{x_0}\right). \quad (2.59)$$

So

$$\varphi_{,xx} = -2a \frac{\sinh\left(\frac{x}{x_0}\right)}{x_0^2 \cosh^3\left(\frac{x}{x_0}\right)}, \quad (2.60)$$

or

$$-2a\lambda^2 \frac{\sinh\left(\frac{x}{x_0}\right)}{x_0^2 \cosh^3\left(\frac{x}{x_0}\right)} - \kappa a \frac{\sinh\left(\frac{x}{x_0}\right)}{\cosh\left(\frac{x}{x_0}\right)} \left(a^2 \frac{\sinh^2\left(\frac{x}{x_0}\right)}{\cosh^2\left(\frac{x}{x_0}\right)} - \varphi_0^2 \right) = 0, \quad (2.61)$$

and

$$\frac{-2\lambda^2}{x_0^2} - k \left(a^2 \sinh^2\left(\frac{x}{x_0}\right) - \varphi_0^2 \cosh^2\left(\frac{x}{x_0}\right) \right) = 0. \quad (2.62)$$

Using $\cosh^2 x - \sinh^2 x = 1$ we get

$$a = \varphi_0 \quad \text{and} \quad \frac{2\lambda^2}{x_0^2} = k\varphi_0^2 \rightarrow x_0 = \frac{1}{\varphi_0} \sqrt{\frac{2\lambda^2}{k}}, \quad (2.63)$$

and

$$\varphi = \varphi_0 \tanh \left(\frac{\varphi_0 x}{\sqrt{\frac{2\lambda^2}{\kappa}}} \right). \quad (2.64)$$

The energy is

$$E_0 = \int_{-\infty}^{\infty} f(\varphi(x)) dx = \varphi_0^2 \frac{2}{3} \sqrt{\frac{2\lambda^2}{\kappa\varphi_0}} (2\lambda^2 + \kappa\varphi_0^2). \quad (2.65)$$

This energy is associated with an interface of the approximate width of

$$L \simeq 4\varphi_0 \sqrt{\frac{2\lambda^2}{\kappa}}. \quad (2.66)$$

2.3.1.2 Two-dimension axi-symmetric three-well model

The required energy for the growth of a nuclei of radius r is the surface energy minus the change in the chemical potential:

$$E = 2\pi r\gamma - \pi r^2 G(0) \quad (2.67)$$

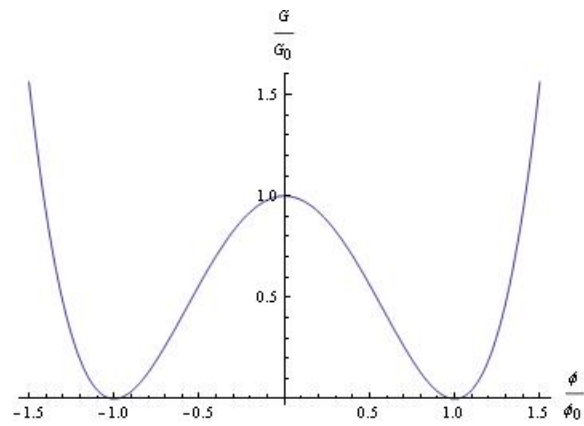


Figure 2.3: Simple two-well model. Normalized energy as a function of the normalized order parameter

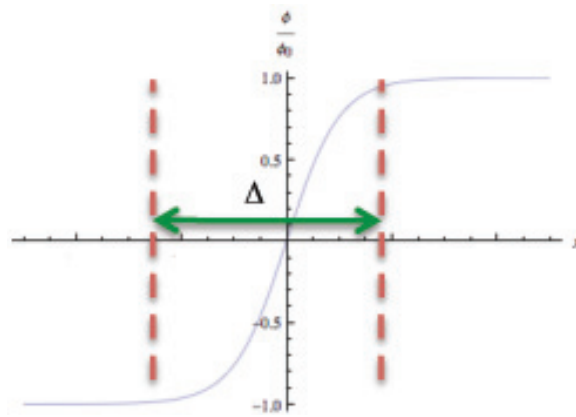


Figure 2.4: Transition zone is defined as the width of the region between $\phi = 0$ and $\phi = \pm\phi_0$. Transition length depends on the coefficient of the interfacial energy and defined the physical length scale of the problem.

where γ is the surface energy. To find the critical value of r

$$\frac{dE}{dr} = \gamma - r^* G(0) = 0 \implies r^* = \frac{\gamma}{G(0)}. \quad (2.68)$$

Approximating with the aid of the simple $1 - D$ problem, if the radius is large enough compared to the transition zone in the $1 - D$ two-well calculation, $r \gg L$, we can assume $\gamma \sim E_0$ as calculated previously, ($1 - D$ two-well model) such that

$$r^* = \frac{E_0}{G(0)}. \quad (2.69)$$

We may also assume that going from the less stable well to one of the more stable ones in the three-well model can be approximated by the same behavior as going from one well to the other one in the two-well model:

$$\frac{\kappa}{4} \varphi_0^4 = G^* - G(0) = E_a \quad (2.70)$$

where G^* is the local maximum of $G(\varphi)$, and E_a is the energy barrier (activation energy).

Comparing the two-well and the three-well model we see that the adjacent wells are separated by $2\varphi_0$ in two-well model, and by β in three-well model, so we have $\beta = 2\varphi_0$, so

$$\kappa = \frac{2^2 E_a}{\varphi_0^4} = \frac{2^6 E_a}{\beta^4} \quad (2.71)$$

which results in

$$E_0 = \frac{1}{12} \sqrt{\frac{\lambda^2 \beta}{E_a}} \beta^3 \left(\lambda^2 + \frac{2^3}{\beta^2} E_a \right). \quad (2.72)$$

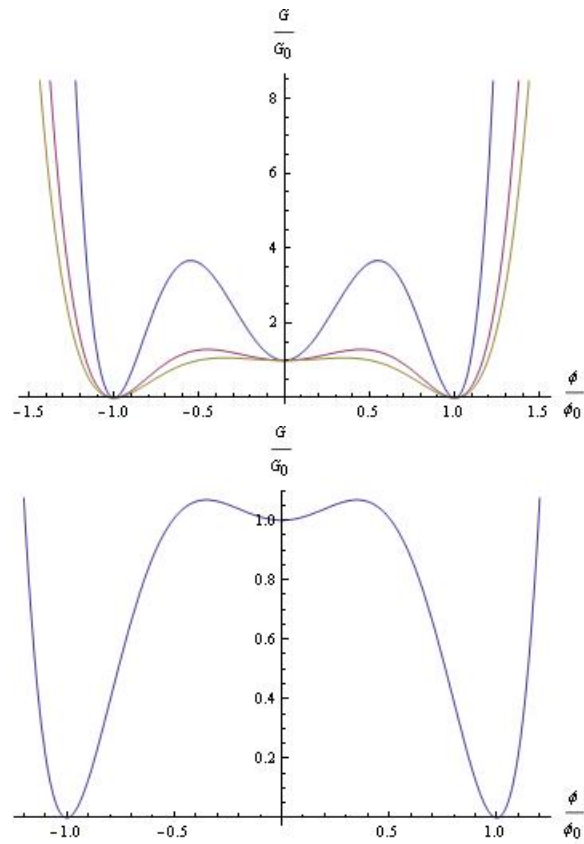


Figure 2.5: A three-well model. Left: Normalized energy as a function of the normalized order parameter for different values of $\alpha = 0.55, 0.45, 0.35$. Right: A closer look at the chemical energy function for $\alpha = 0.35$

The thickness of the transition zone would be

$$L = 2\beta \sqrt{\frac{2\lambda^2 \beta^4}{2^6 E_a}} = \frac{\beta^3}{4} \sqrt{\frac{2\lambda^2}{E_a}}. \quad (2.73)$$

Now, let us insert a length scale in the model, assume that h is the grid distance in our model and we want the transition zone to be n grids, $L = nh$, in our model we get

$$nh = \frac{\beta^3}{4} \sqrt{\frac{2\lambda^2}{E_a}} \rightarrow \frac{2\lambda^2}{E_a} = \left(\frac{4nh}{\beta^3}\right)^2. \quad (2.74)$$

Now assume $G(0) = \theta E_a$, then

$$\frac{\lambda^2 \beta^2}{h^2 G(0)} = \frac{2^3}{\theta} \left(\frac{n}{\beta^2}\right)^2. \quad (2.75)$$

From equation (2.72),

$$r^* = \frac{E_0}{G(0)} = \frac{1}{12\theta} \sqrt{\frac{\lambda^2 \beta}{E_a}} \beta^3 \left(\frac{\lambda^2}{E_a} + \frac{2^3}{\beta^2}\right). \quad (2.76)$$

From equation (2.74),

$$r^* = \frac{2^3}{3\theta} \frac{nh}{\sqrt{2\beta^3}} \left(\frac{n^2 h^2}{\beta^4} + 1\right). \quad (2.77)$$

For typical values of $\beta \sim 0.2$, we have

$$r \sim \frac{60n h}{\theta}. \quad (2.78)$$

For a transition zone of $L = nh = 1 - 10 \text{ nm}$, we have

$$r \sim \frac{50 - 500}{\theta}. \quad (2.79)$$

In our simulations, we choose $r = D/100$ where D is the domain size. For a domain of few hundreds by few hundreds grids, r is only a few grids long, so we need $\theta \sim 20$, which corresponds to $\alpha = 0.35$ in the chemical energy formulation.

2.3.2 Physical range of parameters and scaling

Recall our incremental work function,

$$\begin{aligned} f_n = & \frac{\lambda^2}{2} |\nabla \phi_{n+1}|^2 + G(\phi_{n+1}) \\ & + \frac{1}{2} \left(\epsilon_{n+1} - \epsilon_{n+1}^{pt} - \epsilon_{n+1}^{pl} \right) : \mathbb{C} : \left(\epsilon_{n+1} - \epsilon_{n+1}^{pt} - \epsilon_{n+1}^{pl} \right) \\ & + \sigma_y \left(\frac{\epsilon_{n+1}^{pl} - \epsilon_n^{pl}}{\Delta t} \right) \Delta t + \frac{k}{2} \left(\frac{\phi_{n+1} - \phi_n}{\Delta t} \right)^2 \Delta t \end{aligned} \quad (2.80)$$

where we assume an isotropic power law hardening for plasticity. Normalizing with respect to the chemical energy, we get

$$\begin{aligned} f_0 \tilde{f}_n = & \frac{\lambda^2}{x_0^2} \phi_0^2 \frac{1}{2} |\nabla_{\tilde{x}} \tilde{\phi}_{n+1}|^2 + f_0 \tilde{G}(\tilde{\phi}_{n+1}) \\ & + \frac{1}{2} \phi_0^2 \mu_0 \left(\tilde{\epsilon}_{n+1} - \tilde{\epsilon}_{n+1}^{pt} - \tilde{\epsilon}_{n+1}^{pl} \right) : \tilde{\mathbb{C}} : \left(\tilde{\epsilon}_{n+1} - \tilde{\epsilon}_{n+1}^{pt} - \tilde{\epsilon}_{n+1}^{pl} \right) \\ & + \phi_0^2 \mu_0 \tilde{\sigma}_y \left(\frac{\tilde{\epsilon}_{n+1}^{pl} - \tilde{\epsilon}_n^{pl}}{\Delta \tilde{t}} \right) \Delta \tilde{t} + \frac{\phi_0^2 k}{t_0} \frac{1}{2} \left(\frac{\tilde{\phi}_{n+1} - \tilde{\phi}_n}{\Delta \tilde{t}} \right)^2 \Delta \tilde{t} \end{aligned} \quad (2.81)$$

which can be written as

$$\begin{aligned}
\tilde{f}_n = & A_1 \frac{1}{2} |\nabla_{\tilde{x}} \tilde{\phi}_{n+1}|^2 + \tilde{G}(\tilde{\phi}_{n+1}) \\
& + A_2 \frac{1}{2} \left(\tilde{\epsilon}_{n+1} - \tilde{\epsilon}_{n+1}^{pt} - \tilde{\epsilon}_{n+1}^{pl} \right) : \tilde{\mathbb{C}} : \left(\tilde{\epsilon}_{n+1} - \tilde{\epsilon}_{n+1}^{pt} - \tilde{\epsilon}_{n+1}^{pl} \right) \\
& + A_2 \tilde{\sigma}_y \left(\frac{\tilde{\epsilon}_{n+1}^{pl} - \tilde{\epsilon}_n^{pl}}{\Delta \tilde{t}} \right) \Delta \tilde{t} + A_3 \frac{1}{2} \left(\frac{\tilde{\phi}_{n+1} - \tilde{\phi}_n}{\Delta \tilde{t}} \right)^2 \Delta \tilde{t}
\end{aligned} \tag{2.82}$$

where

$$A_1 = \frac{\lambda^2 \phi_0^2}{x_0^2 f_0} \tag{2.83}$$

$$A_2 = \frac{\phi_0^2 \mu_0}{f_0} \tag{2.84}$$

$$A_3 = \frac{\phi_0^2 k}{t_0 f_0}. \tag{2.85}$$

We choose t_0 such that $A_3 = 1$. For martensitic transformation in steel we choose $\phi_0 = \epsilon_{shear}^{pt} = 0.2$. Using $\mu_0 \sim 100 \text{ GPa}$, $f_0 \sim 1000 \text{ cal/mole} \sim 0.5 \text{ GPa}$, $\sigma_y \sim 200 - 500 \text{ MPa}$, we get $A_2 \sim 10$ and $\tilde{\sigma}_y \sim 0.010 - 0.025$. Finally the surface energy is about $0.01 - 0.1 \text{ J/m}^2$. Using a Cahn-Hilliard model, Olson and Cohen (1982) suggested that $\lambda^2 \sim 10^{-11} - 10^{-12} \text{ J/m}$ which results in $A_1 \sim 10^{-18}/x_0^2$, so if we take $A_1 \sim [0.01 - 1]$ we would have $x_0 \sim [1 - 10] \text{ nm}$, which means that our calculation periodic cell is on the order of $1 \text{ } \mu\text{m}^2$.

2.4 Numerical Exploration

We discretize space using finite difference and explore the evolution in two dimensions. We assume temperature does not change during the process, and consider periodic boundary conditions to study the effects of volume change, and plastic deformations on the morphology of a single crystal.

A typical result is shown in Figure 2.6. The color bar shows the order parameter. We observe that the stress field due to the neighboring nuclei plays a key role on how a nucleus grows into a plate of a specific thickness dictated by minimizing the sum of the elastic energy and surface energy.

2.4.1 Effect of material parameters on the morphology during the quenching process

2.4.1.1 Role of transformation barrier

We define the transformation barrier as the maximum height in the chemical energy curve between austenite and martensite wells. We have verified that transformation barrier has a major role in allowing the transformation, but beyond that it doesn't change the morphology once the transformation has occurred. Figure 2.7 shows that when the transformation barrier is too high (right figure) the elastic energy barrier can get too high and the material would prefer to stay at the metastable austenite phase although it has higher chemical energy.

2.4.1.2 Role of surface energy

We find that very high surface energies can stop the transformation, but surface energy doesn't play any major role in the morphology. Furthermore, increasing surface energy makes nucleation harder, but the phase growth faster once we are past the nucleation. Figure 2.7 shows that when the surface energy coefficient is very high (right figure) the elastic energy barrier can get too high and the material would prefer to stay at the metastable austenite phase although it has higher chemical energy.

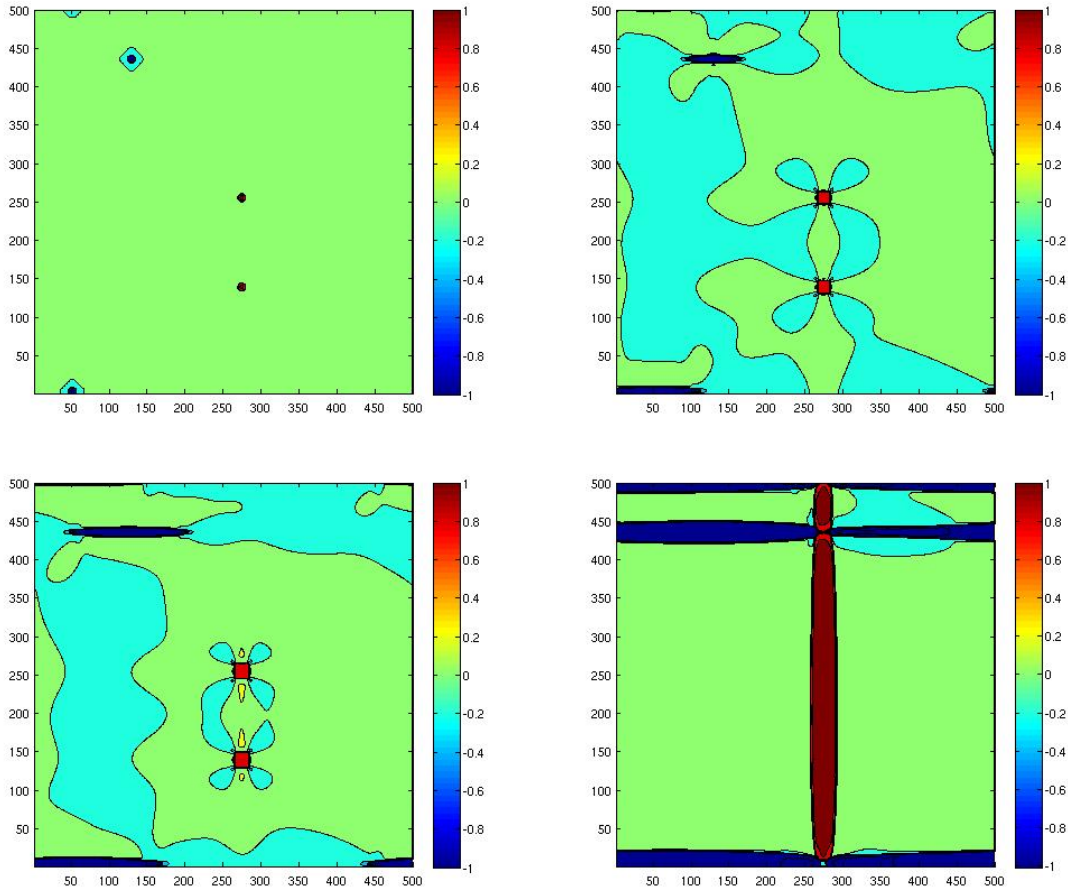


Figure 2.6: Martensitic transformation upon quenching. Volume change=0, average strain=0. Here we show some middle time steps, $t = 0, 16, 20, 30$ and not the final morphology. The color bar shows the order parameter. We observe that the stress field due to the neighboring nuclei plays a key role on how a nucleus grows into a plate of a specific thickness dictated by minimizing the sum of the elastic energy and surface energy.

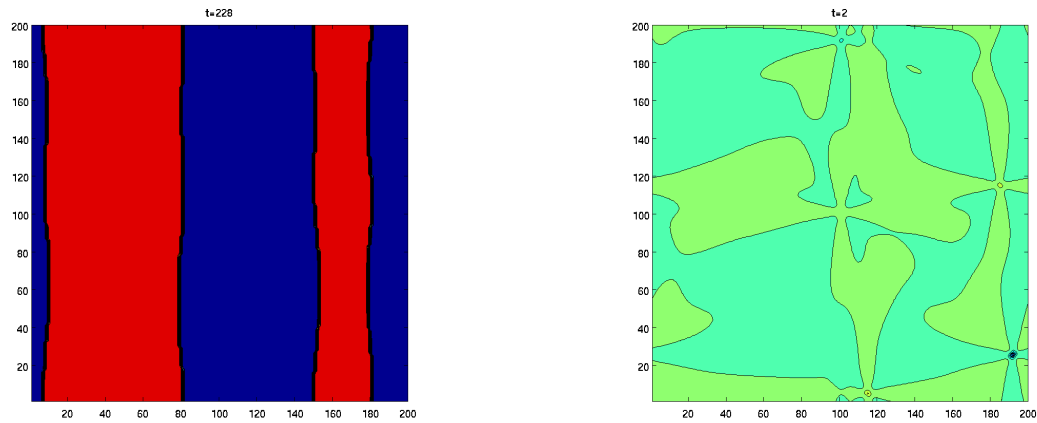


Figure 2.7: Martensitic transformation upon quenching. Volume change=0.08, average strain=0. When the transformation barrier or the coefficients of surface energy or elastic energy are very high (right figure) the energy barrier can get too high and the material would prefer to stay at the metastable austenite phase (green) instead of the twined martensite structure (red and blue).

2.4.1.3 Role of elastic moduli

Elastic energy plays a very crucial role in the transformation, however as the minimum elastic energy attains by long stripes, we won't see a morphology change due to the elastic energy variation once martensite is formed. Higher elastic modulus makes nucleation harder, but the phase growth faster, once we are past the nucleation. However its variation has small effect on changing morphology. If there are two adjacent embryos of different types, we will see that they first grow along the length, and then thicken, but we won't see any retained austenite between them, as their stress fields lessen each other. Figure 2.7 shows that when the elastic energy coefficient is very high (right figure) the elastic energy barrier can get too high and the material would prefer to stay at the metastable austenite phase although it has higher chemical energy.

2.4.1.4 Role of volume change

We observe that volume change makes finer microstructure path (compare Figures 2.6 and 2.8), but has little effect on the final morphology in the elastic case. In short, volume change is identified as the cause of the autocatalytic nucleation as observed in Figure 2.8. This is due to the higher volumetric stress caused by the diagonal term in the transformation tensor. When the phase transformation can be stopped, say by plasticity, the resultant morphology gets finer with the increase of the volume change. We will later show that the volume change plays an important role in the morphology of the lath martensite.

2.4.1.5 Role of plastic deformation

We observed that plasticity can change the morphology of the microstructure only if there is also volume change involved. This is in agreement with experimental observations in steels, in what is called as lath martensite (Figure 2.9).

2.4.1.6 Role of under-cooling

We observe that for large values of ΔG corresponding to higher values of $T - M_s$, the material can overcome the elastic energy barrier and transforms as a plate microstructure. However for lower values of under-cooling, the combined effect of volume change and plasticity make the volumetric stress high enough to stop the phase growths which results in the formation of lath martensite and untransformed regions of austenite. This is in agreement with result from experiments (see Umemoto (1983) for example).

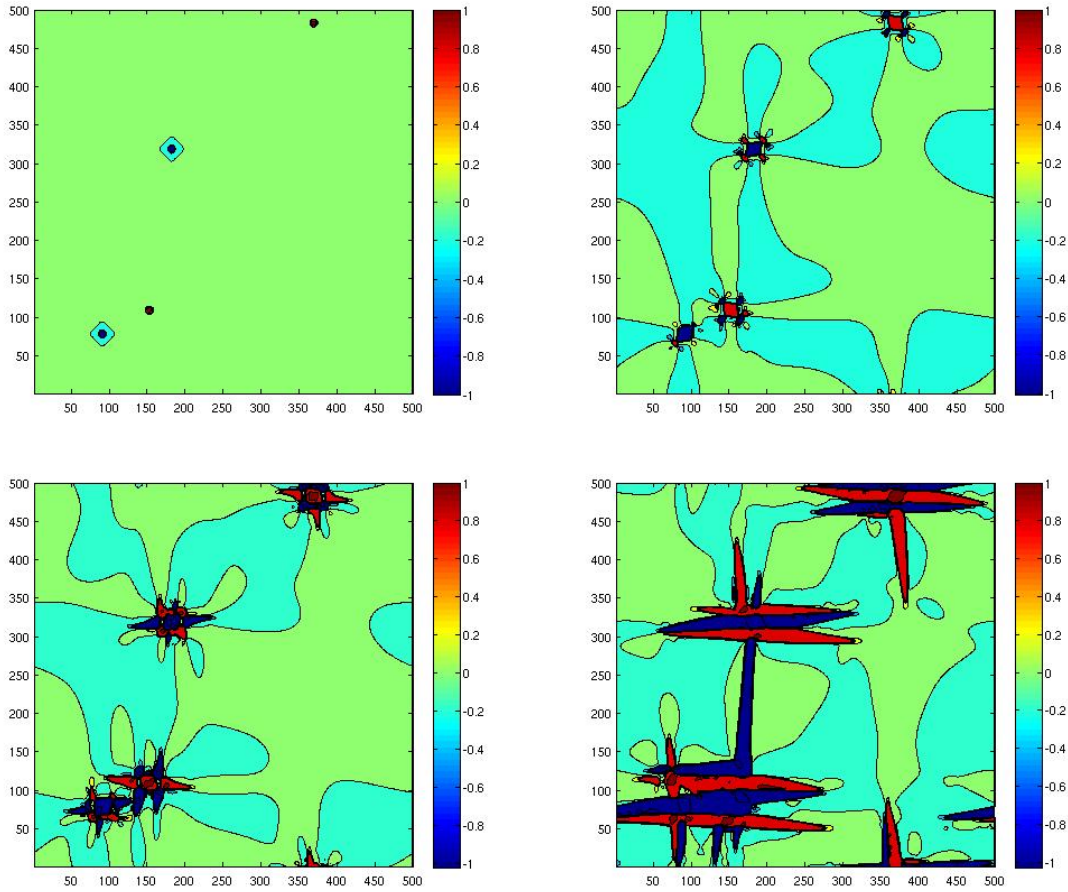


Figure 2.8: Martensitic transformation upon quenching. Volume change=0.08, average strain=0. Here we show some middle time steps, $t = 0, 16, 20, 30$ and not the final morphology. The color bar shows the order parameter. Here we observe that the stress field due to one nucleus results in the nucleation of the other variant. We further observe the twined plates which grow together and nucleate more plates.

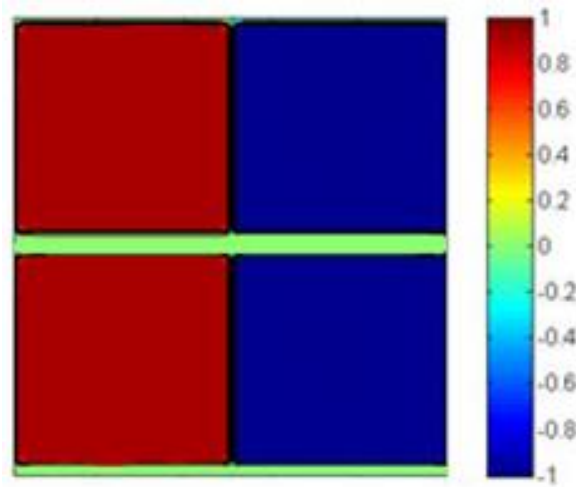


Figure 2.9: Effect of plasticity: Observed twinning and retained austenite in the final morphology, a simple cartoon

2.4.2 Lath microstructure and retained austenite: combined role of volume change and plasticity

To better understand the complicated effect of volume change and plasticity, we tried some different numerical experiments. Figure 2.10 shows the morphology when there is no plasticity and no volume change. Figure 2.11 shows the morphology when there is no volume change but there is plasticity. Figure 2.12 shows the morphology when there is no plasticity but there is a volume change; here we observe that where increasing the stress field, volume change can reduce the driving force and even stop the growth of the martensite. Finally, Figure 2.13 shows the morphology when there is volume change and plasticity. Here we observe that plasticity, by reducing the deviatoric stresses, can lower the energy barrier, and thus help the phase transformation which leads to the observation of the retained austenite in a complicated lath microstructure. All of these were done by applying $average\ strain = 0$ and for a domain size 200×200 . Next we tried the last two simulations for

average stress = 0 boundary condition. As the stresses are lower in this case, volume change could not stop the phase transformation and we only observed the plate microstructure regardless of the plasticity situation. In order to understand the effect of surface energy in this case, we tried the plastic experiments with a larger domain size, 400×400 , so we could reduce the surface energy coefficients without numerical problems. Here we observed that for small enough surface energy density, we can observe a fine lath microstructure with retained austenite regardless of the boundary conditions. So we identify the combined effect of plasticity and volume change as the key to the experimentally observed lath microstructure with the retained austenite. Thus the amount of the retained austenite is a function of the volume change and yield stress for a given undercooling, which is in agreement with experiments (see for example Maki et. al. (2005, 2006)).

2.4.3 Effect of loading on the morphology of the quenched microstructure

Here, we study the effect of external displacement loading on the final morphology from the quenching. We observe that upon applying far-field strain, the material tries to accommodate it by increasing the volume fraction of the preferred martensite variant at the expense of reduction of the other variant. We also see that some of the retained austenite transforms to the preferred martensite variant (Figure 2.18). This is clearly in agreement with the experimental observations in the literature.

2.5 Discussions and experimental verifications

We observe that:

- 1— At first a circular nucleus deforms to a thin long plate with some characteristic width, then

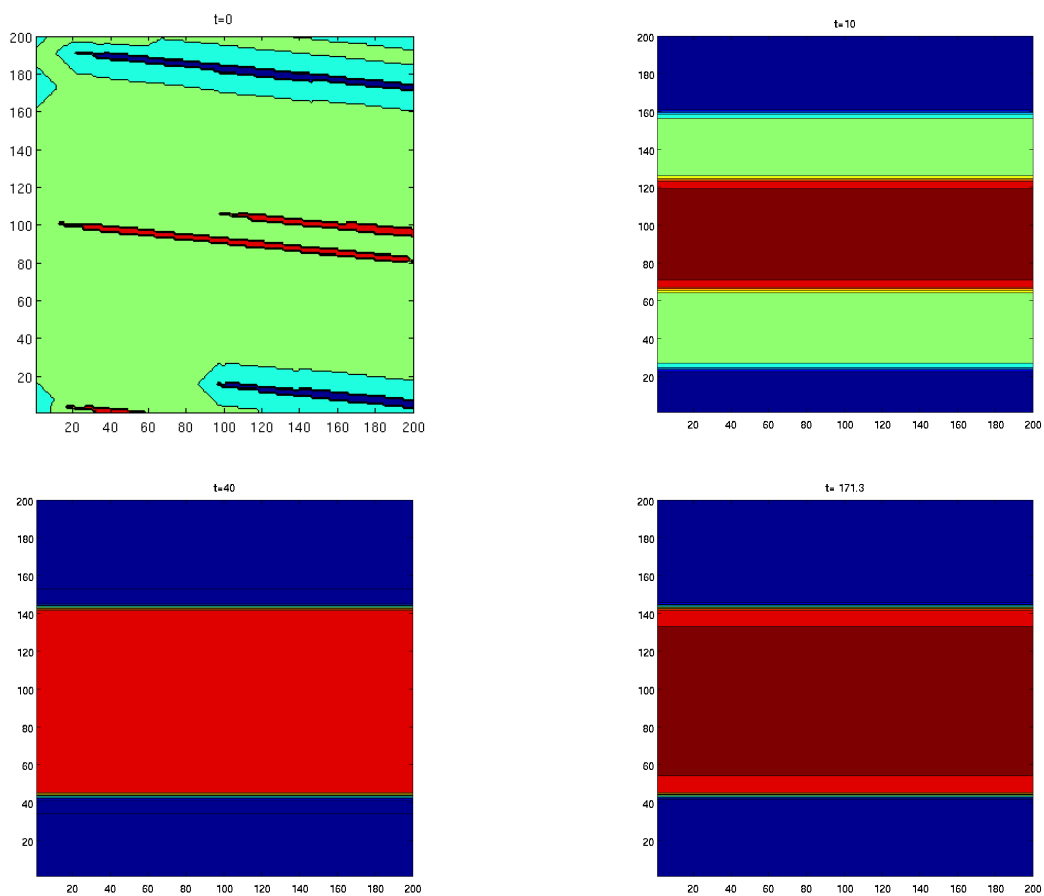


Figure 2.10: Martensitic transformation with no volume change, average strain=0, no plasticity, average surface energy. In the absence of volume change and plasticity, the material makes long twined plates of martensite to minimize the total elastic energy. The surface energy forces the morphology to be a coarse one.

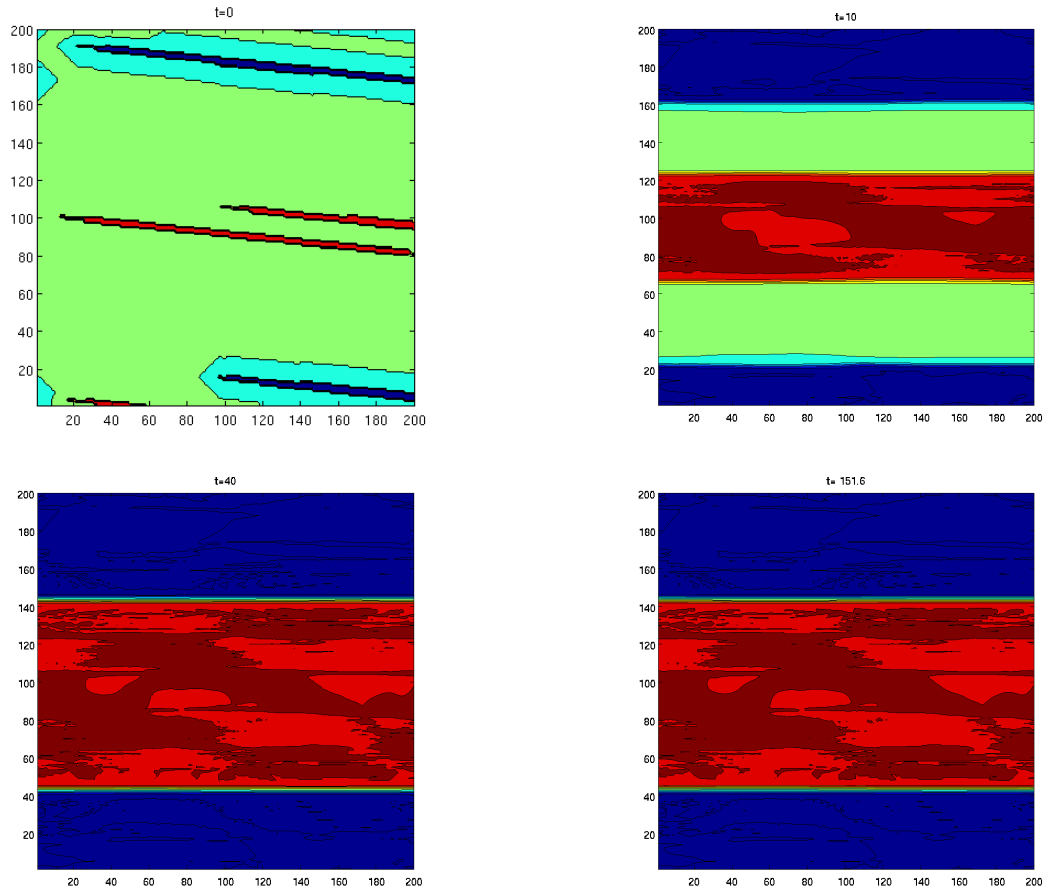


Figure 2.11: Martensitic transformation with no volume change, average strain=0, $\sigma_y = 200$ MPa, average surface energy. In the absence of volume change, the plasticity reduces the deviatoric and total stresses and thus reduces the elastic energy barrier to transformation, and thus makes the transformation easier. The material still makes long twined plates of martensite to minimize the total elastic energy. The surface energy forces the morphology to be a coarse one.

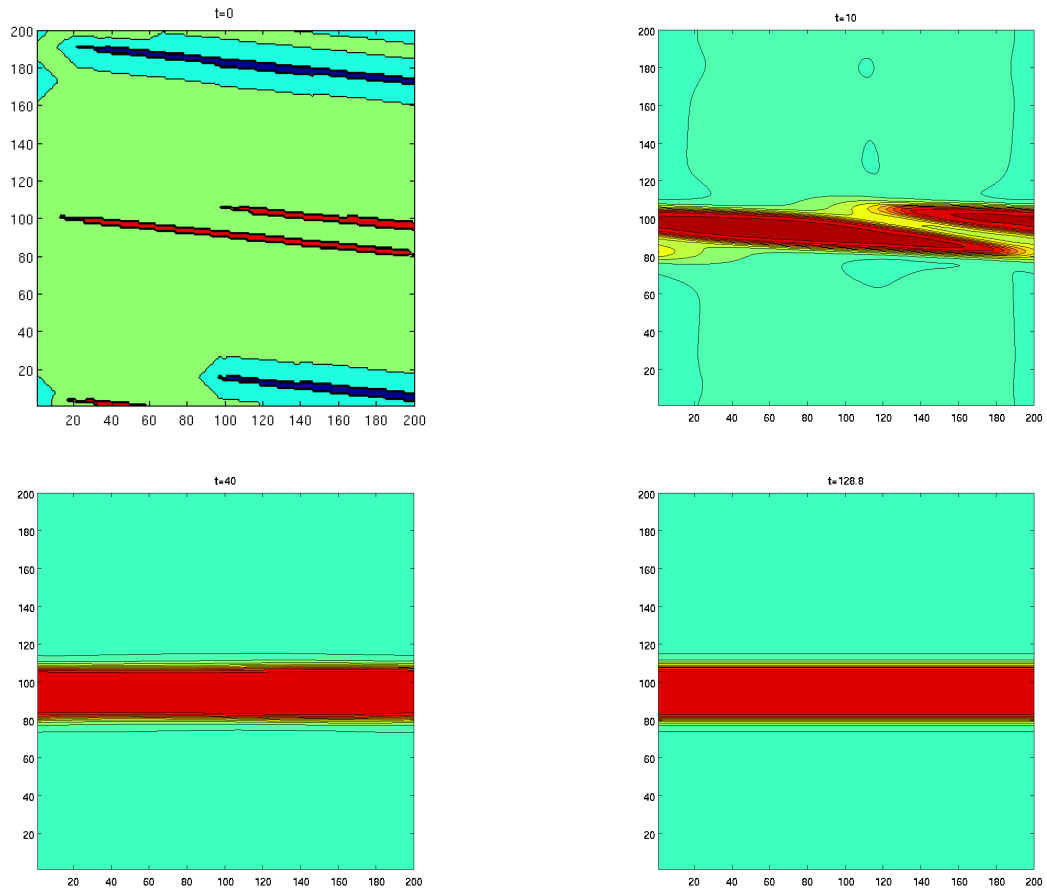


Figure 2.12: Martensitic transformation with volume change=0.08, average strain=0, no plasticity, average surface energy. Volume change causes higher stresses and thus higher elastic energy barrier in the material, and thus makes the phase transformation slower. The boundary conditions, average strain=0, results in higher stresses in general, and thus the phase transformation stops as the driving force from the chemical energy difference between the austenite and martensite is not enough to overcome the elastic energy barrier.

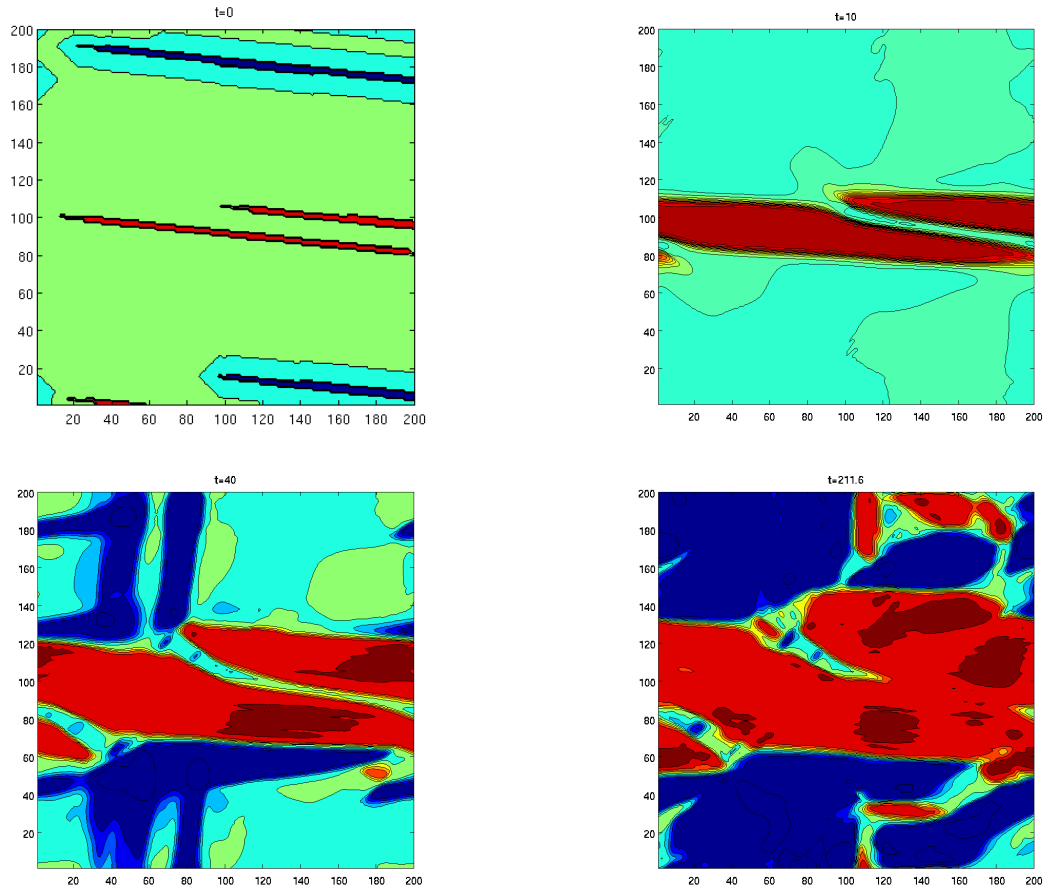


Figure 2.13: Martensitic transformation with volume change=0.08, average strain=0, $\sigma_y = 200$ MPa, average surface energy. Volume change causes higher stresses and thus higher elastic energy barrier in the material, and thus makes the phase transformation slower. On the other hand plastic deformation reduces the deviatoric stresses and thus makes the transformation easier. The boundary conditions, average strain=0, results in higher stresses in general. In this case the competition between lower deviatoric stress due to plastic deformation and higher volumetric stresses due to volume change results in a complex morphology with regions of retained austenite.

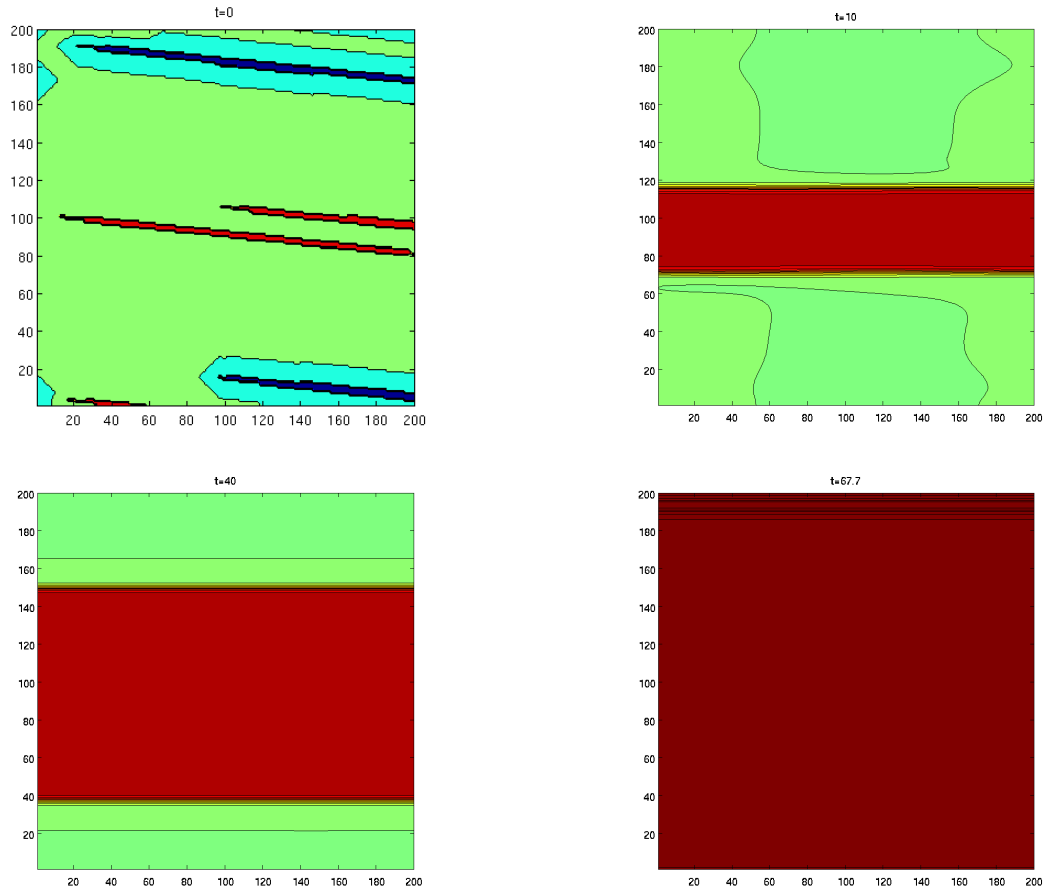


Figure 2.14: Martensitic transformation with volume change=0.08, average stress=0, no plasticity, average surface energy. Volume change causes higher stresses and thus higher elastic energy barrier in the material, and thus makes the phase transformation slower.

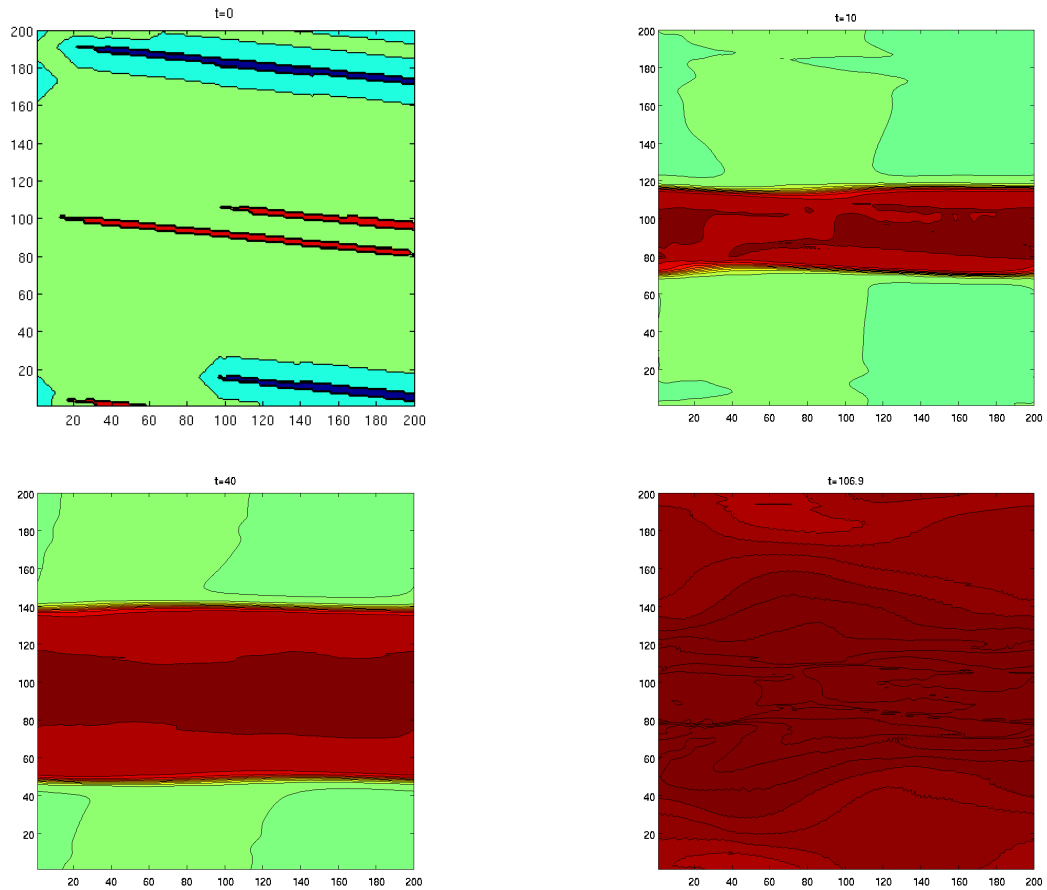


Figure 2.15: Martensitic transformation with volume change=0.08, average stress=0, $\sigma_y=200$ MPa, average surface energy. Volume change causes higher stresses and thus higher elastic energy barrier in the material, and thus makes the phase transformation slower. On the other hand plastic deformation reduces the deviatoric stresses and thus makes the transformation easier. The boundary conditions, average stress=0, results in lower stresses in general. The phase transformation completes.

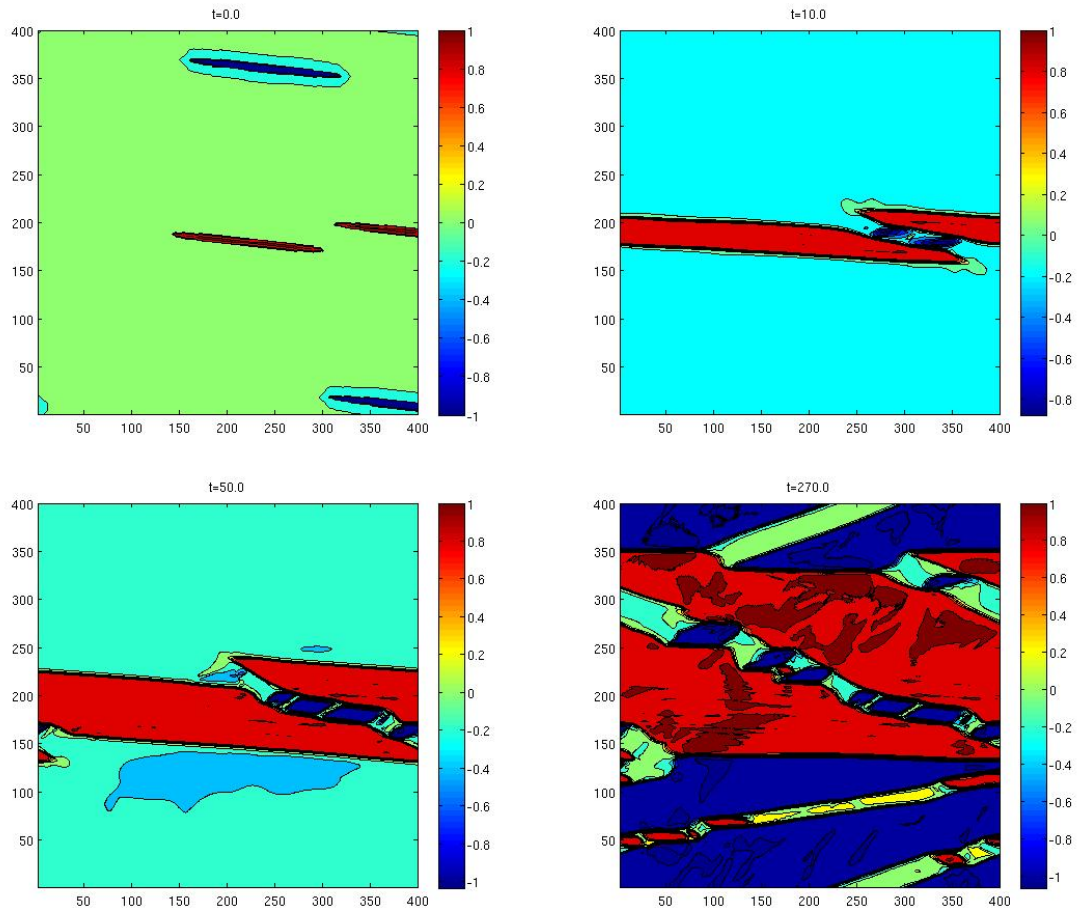


Figure 2.16: Martensitic transformation with volume change=0.08, average strain=0, $\sigma_y = 200$ MPa, average surface energy. It is observed that the combination of the volume change at plastic deformation results in a complex morphology including regions of twinning and retained austenite). Due to plastic deformation the preferred angle between austenite and martensite differs from that of the no plastic case $\sim 6^\circ$.

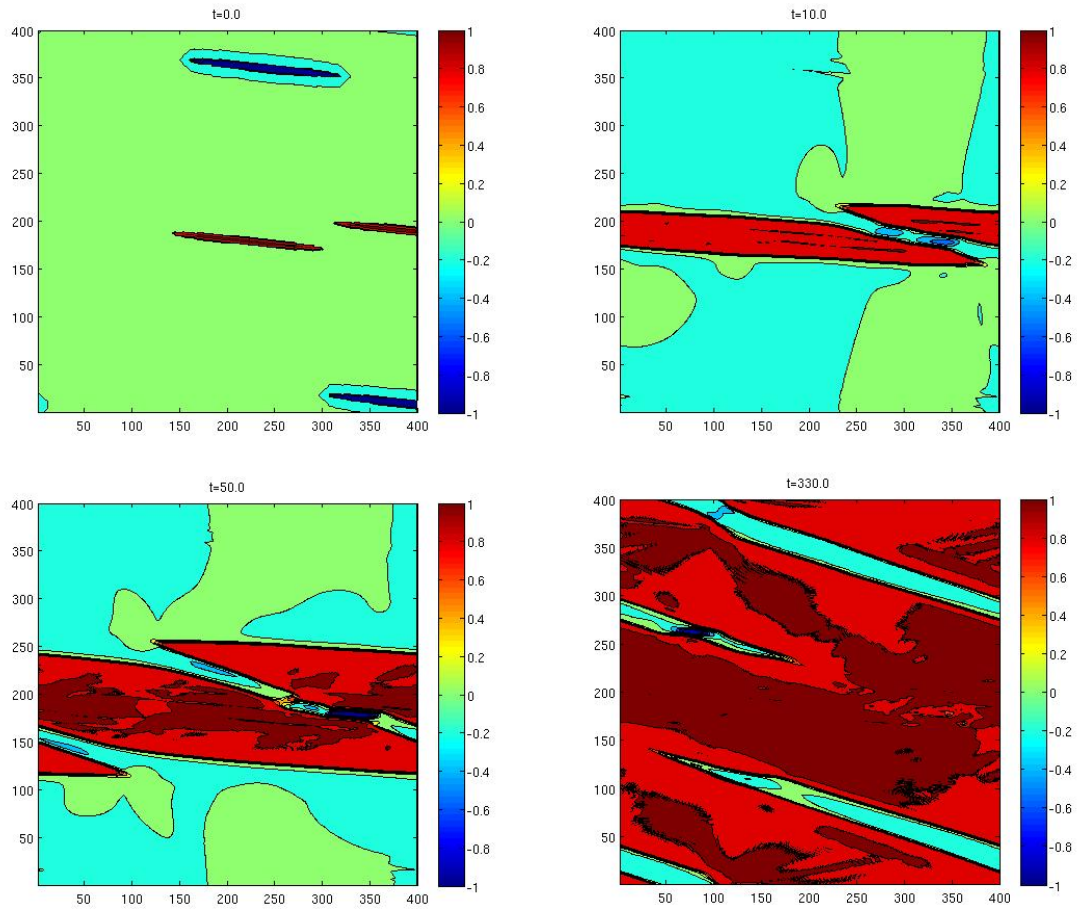


Figure 2.17: Martensitic transformation with volume change=0.08, average stress=0, $\sigma_y = 200$ MPa, low surface energy. It is observed that the combination of the volume change at plastic deformation results in the presence of some untransformed regions of austenite (retained austenite). Due to plastic deformation the preferred angle between austenite and martensite, $\sim 15^\circ$ here, differs from that of the no plastic case $\sim 6^\circ$.

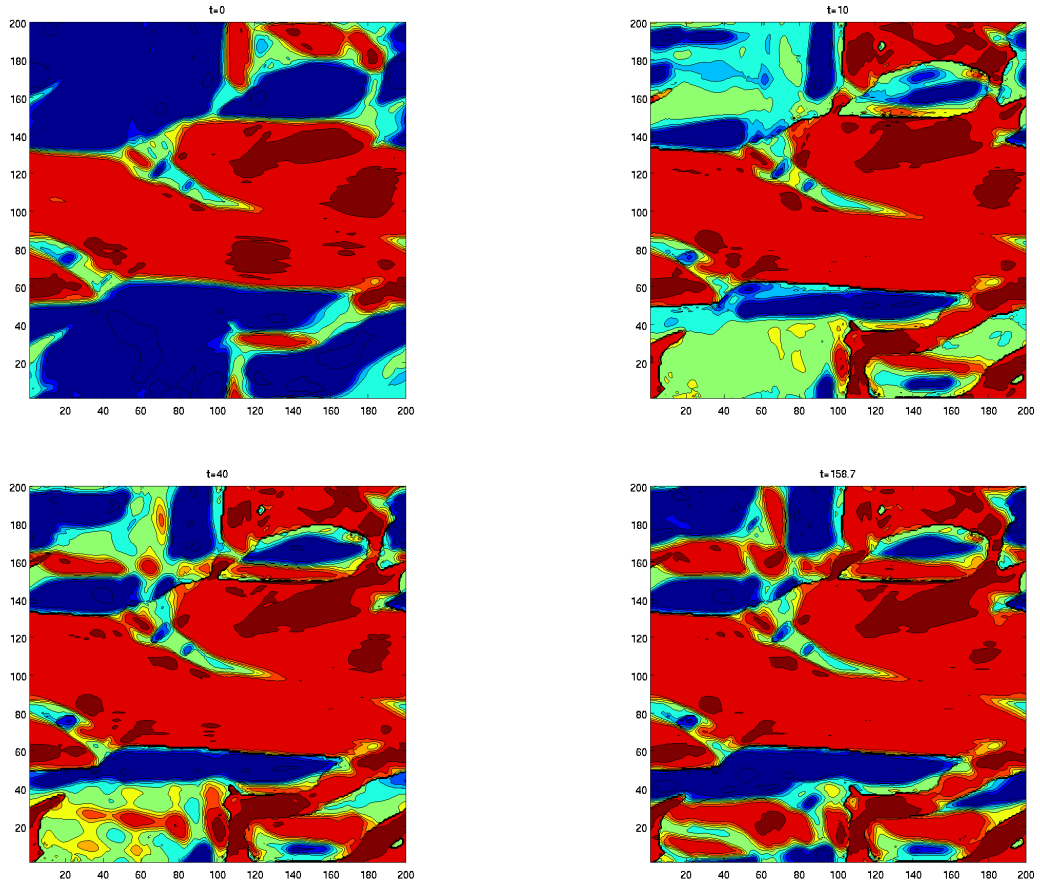


Figure 2.18: Martensitic transformation with volume change=0.08, average strain=0, $\sigma_y = 200$ MPa, low surface energy. With applied $\epsilon_{12}^0 = 0.1$. It's observed that upon applying far-field strain, the material tries to accommodate it by increasing the volume fraction of the preferred martensite variant at the expense of reduction of the other variant. We also see that some of the retained austenite transforms to the preferred martensite variant.

it make twins on its sides, then it grows faster. When there is no room no grow in length it widens. After all the austenite is gone, it fixes to the correct angle which is 6 degrees for 0.04 and 0.2 diagonal and off diagonal elements of transformation strain matrix.

2— Volume change is identified as the cause of the autocatalytic nucleation.

3— After we add plasticity to the model we observe pinning of the phase transformation and thus lath martensite instead of plate martensite.

4— Based on our simulations we observed that the rate of plastic deformation is higher at the beginning of the transformation and decreases as transformation progresses.

5— When there is no volume change the stresses are much lower than the cases with high volume changes. The resultant stress field thus can make more nucleation and may be a reason to explain the finer microstructure seen in the case of large volume changes.

6— Plasticity reduces the deviatoric stress, σ^{dev} and thus makes the phase transformation easier. This is why for a small driving force we observe more transformation when the yield stress is lower. On the other hand the combination of volume change, ΔV in steel, and plasticity results in a geometry different from that of a minimum elastic energy, long plate; thus the volumetric stress, σ^{vol} , increases. This increase of the volumetric stress adds to the resisting force of the transformation, $\int_{\Omega} \sigma^{vol} \Delta V d\Omega$, and thus can stop the phase transformation and results in retained austenite.

In conclusion, as has been observed by experiments by Wayman, Olson, Maki, Bhadeshia, and many others, volume change and plasticity interactions with the phase transformation play a key role in dictating the complicated lath martensite with the retained austenite over the plate martensite. Here for the first time, by studying the microstructure, we described the mechanism which is a combination role of both plasticity and volumetric stress increase due to volume change. This is a

point that was missed in previous works and can answer the discrepancies found by previous models on the effect of plastic deformation on phase transformation.

For the future work we suggest 3-D modeling (which will have difficulties with A/M boundaries in 3-D as mentioned earlier) and also studying the effect of composition on the studied parameters, and from there, on the morphology.

2.6 References

1. J.W. Cahn, Acta Metall. 9 (1961) 795801.
2. J.W. Cahn, Acta Metall. 10 (1962) 907913.
3. J.W. Christian, The theory of transformations in metals and alloys, Pergamon Press, Oxford (1965) 815.
4. A.G. Khachaturyan, Sov. Phys. Solid State 8 (1967) 2163.
5. J.W. Cahn, Trans. Metall. Soc. MIME 242 (1968) 166180.
6. J.W. Cahn, The Mechanism of Phase Transformations in Crystalline Solids, The Institute of Metals, London, 1969, pp. 15.
7. A.G. Khachaturyan, G.A. Shatalov, Sov. Phys. Solid State 11 (1969) 118.
8. C.L. Magee, Phase Transformation, ASM (1970) 115-156.
9. G.B. Olson, M. Cohen, Met. Trans. A7 (1976) 1897-1904.
10. G.B. Olson, M. Cohen, Met. Trans. A7 (1976) 1905-1914.
11. G.B. Olson, M. Cohen, Met. Trans. A7 (1976) 1915-1923.

12. C.M. Wayman, New Aspects of Martensite Transformation, Trans. JIM Suppl., 17 (1976), 159.
13. A.G. Khachaturyan and A.F. Rumynina, Phys. Stat. Sol. 45a, 1978, 393.
14. J.W. Christian, Thermodynamics and kinetics of martensite, ICOMAT, 1979.
15. H. Bhadeshia, Ph.D. thesis, University of Cambridge, 1979.
16. E.M. Lifshitz, L.P. Pitaevskii, Part 1, Landau and Lifshitz Course of Theoretical Physics, vol. 5, third ed., Pergamon Press, Oxford, 1980.
17. M. Cohen, C.M. Wayman, in: J.K. Tien, J.F. Elliott (Eds.), Metallurgical Treatises, TMS-AIME, 1981, 445468.
18. G.B. Olson, M. Cohen, Metallurgical and Materials Transactions A, Springer, 1982.
19. A.G. Khachaturyan, Theory of Structural Transformations in Solids, John Wiley and Sons, New York, 1983.
20. M. Umemoto, E. Yoshitake, I. TAMURA, "The morphology of martensite in Fe-C, Fe-Ni-C and Fe-Cr-C alloys", JOURNAL OF MATERIALS SCIENCE 18 (1983) 2893-2904
21. M. Grujicic, G.B. Olson, W.S. Owen, Metall. Trans. 16A (1985), 1713.
22. M. Grujicic, G.B. Olson, W.S. Owen, Metall. Trans. 16A (1985), 1723.
23. G. B. Olson, M. Cohen, in Frontiers in Materials Technologies, M. A. Meyers and O.T. Inal, Ed., Elsevier, 1985, 43.
24. G. B. Olson, M. Cohen, in Dislocations in Solids, edited by F. R. N. Nabarro Elsevier Science Publishers, Amsterdam, 1986, Vol. 7, 297407.

25. Olson, G.B., Cohen, M., 1986. In: Nabarro, F.R.N. (Ed.), *Dislocation in Solids*, vol. 7, NorthHolland, 295.
26. D. M. Haezebrouck, Doctoral thesis, MIT, 1987.
27. Y.A. Izyumov, V.N. Syromoyatnikov, *Phase Transitions and Crystal Symmetry*, Kluwer Academic Publishers, Boston, 1990.
28. Grujcic, M., Ling, H. C., Haezebrouck, D. M., and Owen, W. S. (1992). In G. B. Olson and W. S. Owen (Eds.). *Martensite - A Tribute to Morris Cohen* (p. 175). ASM International.
29. I. Tamura and C.M. Wayman, *Martensite transformations and mechanical effects*, *Martensite*, Edited by G.B. Olson and W.S. Owen, ASM 1992.
30. G. Ghosh and G.B. Olson *Acta Metall. Mater.* 42 (1994) 3371.
31. Marketz, F., and Fischer, F. D., 1994a, *Comput. Mater. Sci.*, 3, 307; 1994b, *Modelling Simulation Mater.Sci. Engng.*, 2, 1017.
32. P. Toledano, V. Dmitriev, *Reconstructive Phase Transitions*, World Scientific, New Jersey, 1996.
33. Wen, Y. H., Denis, S., and Gautier, E., 1999, *Proceedings of the IUTAM Symposium on Micro- and Macrostructural Aspects of Thermoplasticity*, Bochum, Germany, 2529 August 1997, edited by O. T. Bruhns and E. Stein (Dordrecht: Kluwer), 335-344.
34. Idesman A.V., Levitas V.I., Stein E. *Comp. Meth. in Appl. Mech. and Eng.*, 1999, Vol. 173, No. 1-2, 71-98.
35. A.C.E. Reid, G.B. Olson, *Mater. Sci. Eng.* A309A310 (2001) 370376.

36. Levitas V.I., Idesman A.V., Olson G.B. and Stein E. Philosophical Magazine, A, 2002, Vol. 82, No. 3, 429-462.
37. K. Bhattacharya, microstructure of martensite, Oxford, 2003.
38. Idesman A.V., Levitas V.I., Preston D.L., and Cho J.-Y. J. Mechanics and Physics of Solids, 2005, Vol. 53, No. 3, 495-523.
39. Maki, Scripta Materilia 2005.
40. Maki, Mat. Scs. Eng. 2006.
41. Y. Wang, A. G. Khachaturyan, Mat Sci Eng, 2006,
42. L. Stainier, M. Ortiz, Study and validation of a variational theory of thermo-mechanical coupling in finite visco-plasticity, International Journal of Solids and Structures, 2010,

Chapter 3

Yielding and Overall Plastic Behavior of Orthotropic Polycrystalline Metals

3.1 Introduction

Metal industry is very dependent on developing materials which can answer the ever increasing needs for mixed superior behavior. It is seen that some types of steel, e.g., TRIP steel, can show hard yet tough behavior.

Specifically, TRIP steels show high-strength and also exhibit better ductility at a given strength level. The enhanced formability is due to the transformation of retained austenite (ductile, high temperature phase of iron) to martensite (tough, non-equilibrium phase) during plastic deformation. The microscopy of these metals shows lath martensite with plates of austenite between them. As the result of the increased formability, TRIP steels are very appealing to the automotive industry and are used to produce more complicated parts than other high-strength steels while optimizing weight and structural performance.

In this chapter, we seek to study whether lath microstructure can lead to enhanced ductility.

Steel grade	YS(MPa)	UTS(MPa)	Tot. EL(%)
Mild 140/270	140	270	42-48
TRIP 350/600	350	600	24-30
TRIP 450/800	450	800	26-32
MS 950/1200	950	1200	5-7
MS 1250/1520	1250	1520	3-6

Table 3.1: Yield strength, ultimate strength and total elongation of mild steel, TRIP steels, and martensite, WorldAutoSteel.

Parallel plate of hard and soft material lead to highly anisotropic yield behavior. So we describe the behavior of a single crystal using anisotropic plasticity.

Hill (1947, 1948, 2000), introduced a general anisotropic plasticity. Lubliner (1975, 1990) studied a non-smooth dissipation function and derived the plastic behavior based on thermodynamics of plasticity. Ortiz and Stainier (1999) introduced a general variational formulation for the plastic behavior of a single crystal. We follow them to postulate a single crystal plastic law. We then use this to study the effective behavior of a polycrystal. To study the polycrystal behavior, we treat the plastic strain in each grain as an eigenstrain (Mura 1982) and estimate the overall elastic behavior with the similar concepts used by Shodja and Roumi (2005, 2006) and Roumi and Shodja (2007) for the overall elastic behavior of composites.

3.2 Anisotropic plastic behavior of a single crystal

We find a general formulation for orthotropic plasticity, and implicitly, as implicit models are unconditionally stable, implement the model as a part of our effective behavior model to find overall elastoplastic behavior of a two-phase material.

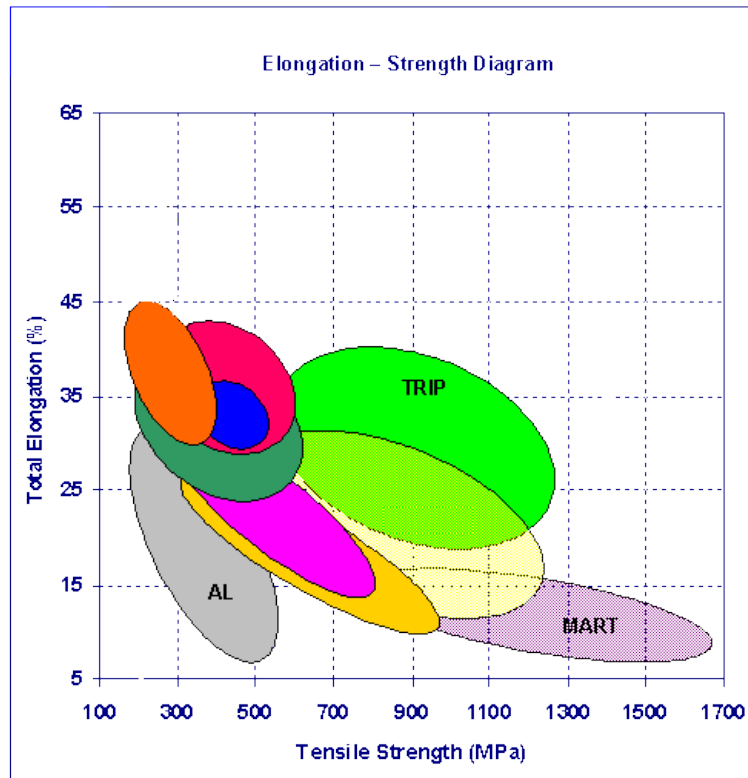


Figure 3.1: Stress-strain curve for different steels compared to aluminum according to United States Steel Corporation

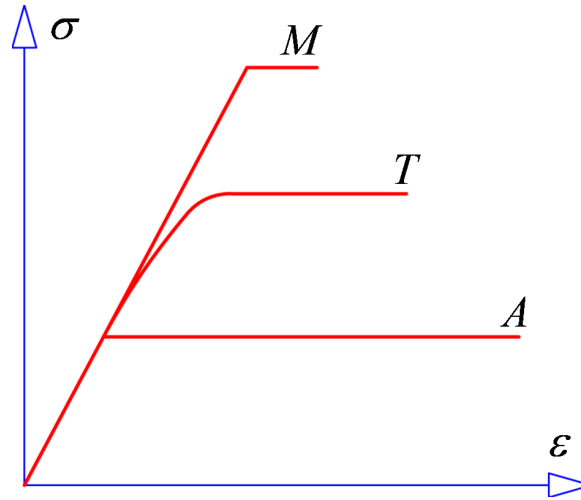


Figure 3.2: Stress-strain curve for martensite, TRIP steel, and austenite

3.2.1 Yield criteria

The von Mises yield criterion is one of the simplest and most widely used yield criteria for metals. It suggests that the yielding of materials begins when the second deviatoric stress invariant J_2 reaches a critical value. This implies that the yield condition is independent of hydrostatic stresses:

$$f(J_2) = \sqrt{J_2} - k = 0, \quad (3.1)$$

where k is the yield stress of the material in pure shear. In analogy with the Mises criteria, Hill (1948) suggested an associated flow rule for anisotropic metals. He considered both volumetric and deviatoric stress and introduced a general yield criterion as

$$2f = F(\sigma_{yy} - \sigma_{zz})^2 + G(\sigma_{zz} - \sigma_{xx})^2 + H(\sigma_{xx} - \sigma_{yy})^2 + 2L\sigma_{yz}^2 + 2M\sigma_{zx}^2 + 2N\sigma_{xy}^2 = 1, \quad (3.2)$$

for suitable values of coefficients F, \dots, N . Postulating on general grounds similar in form to the Mises criterion, he claimed that

$$d\epsilon_{ij} = \frac{\partial f}{\partial \sigma_{ij}} d\lambda, \quad (3.3)$$

where $d\lambda$ is a positive scalar factor of proportionality. For plane strain the yield condition simplifies as

$$2f = \left(\frac{FG + GH + HF}{F + G} \right) (\sigma_{xx} - \sigma_{yy})^2 + 2N\sigma_{xy}^2 = 1. \quad (3.4)$$

For orthotropic material, due to the rotational symmetry of the anisotropy in an element about z axis, there is a relation between the coefficients:

$$F = G, \quad N = G + 2H. \quad (3.5)$$

In a 2 – D case, one can define the stress tensor with the following vectors

$$x = \frac{\sigma_{11} - \sigma_{22}}{\sqrt{2}}, \quad y = \frac{\sigma_{11} + \sigma_{22}}{\sqrt{2}}, \quad z = \sqrt{2}\sigma_{12}. \quad (3.6)$$

From here the yield surface can be expressed as $\Phi(x, y, z) = 1$; for a twice differentiable and convex function. The assumption of orthotropic behavior makes a constraint that $\Phi(x^2, y^2, z^2) = 1$, Hill (2000).

Based on Hill's work, for the specific case of 2 – D orthotropic metal, (volume-preserving), we

consider a yield criteria as

$$2f = H'(\sigma_{xx} - \sigma_{yy})^2 + 2N' \sigma_{xy}^2 = 1, \quad (3.7)$$

or equivalently

$$\left(\frac{S_x - S_y}{2\tau_1}\right)^2 + \frac{S_{xy}^2}{\tau_2^2} = 1. \quad (3.8)$$

We emphasize the main purpose of this work is to understand the qualitative behavior of a metal with easy and hard directions, so we stick with a simple model.

3.2.2 Flow rule

In analogy with Mises plasticity, Lubliner (1975) suggested a general anisotropic model of rate-independent plasticity based on a non-smooth dissipation function

$$\psi^* = \dot{q}_\alpha \sqrt{M_{\alpha\beta}} \dot{q}_\beta \geq 0, \quad (3.9)$$

where \mathbf{M} is a positive definite, symmetric tensor, and q is some internal variable. Assuming plastic incompressibility condition puts a constraint on the

$$C_{i\beta} \dot{q}_\beta = 0 \quad i = 0, \dots, k. \quad (3.10)$$

Using the thermodynamic foundation described earlier, he showed that the yield criterion can be written as

$$Y_\alpha M_{\alpha\beta}^{-1} Y_\beta = 1, \quad (3.11)$$

where

$$Y_\alpha = \frac{1}{\psi^*} M_{\alpha\beta} \dot{q}_\beta \quad (3.12)$$

is the driving force for plasticity.

Now we need to find the tensor \mathbf{M} for our 2 – D orthotropic model. We showed that the yield surface is defined by

$$\left(\frac{S_x - S_y}{2\tau_1}\right)^2 + \frac{S_{xy}^2}{\tau_2^2} = 1. \quad (3.13)$$

Notice that in 2 – D :

$$(S_x + S_y)^2 = 0 \quad (3.14)$$

$$S_x^2 + S_y^2 = -2S_x S_y \quad (3.15)$$

$$(S_x - S_y)^2 = S_x^2 + S_y^2 + S_x^2 + S_y^2 = 2(S_x^2 + S_y^2), \quad (3.16)$$

so we have

$$\frac{S_x^2 + S_y^2}{2\tau_1^2} + \frac{S_{xy}^2}{\tau_2^2} = 1 \quad (3.17)$$

$$\frac{S_x^2 + S_y^2}{2} + \frac{\tau_1^2}{\tau_2^2} S_{xy}^2 = \tau_1^2 \quad (3.18)$$

$$S_x^2 + S_y^2 + 2\kappa^2 S_{xy}^2 = 2\kappa^2 \tau_2^2, \quad (3.19)$$

where $\kappa = \frac{\tau_1}{\tau_2}$ is assumed to be constant and doesn't change with the loading or hardening.

The yield criterion can be written as

$$\begin{pmatrix} S_x & S_y & S_{xy} & S_{yx} \end{pmatrix} \begin{pmatrix} 1 & 0 & 0 & 0 \\ 0 & 1 & 0 & 0 \\ 0 & 0 & \kappa^2 & 0 \\ 0 & 0 & 0 & \kappa^2 \end{pmatrix} \begin{pmatrix} S_x \\ S_y \\ S_{xy} \\ S_{yx} \end{pmatrix} = 2\kappa^2 \tau_2^2, \quad (3.20)$$

which results in

$$M = 2\kappa^2 \tau_2^2 \begin{pmatrix} 1 & 0 & 0 & 0 \\ 0 & 1 & 0 & 0 \\ 0 & 0 & \frac{1}{\kappa^2} & 0 \\ 0 & 0 & 0 & \frac{1}{\kappa^2} \end{pmatrix}. \quad (3.21)$$

3.2.3 Hardening

The stored cold work energy, $W^p(\epsilon^p, q)$ is the non-elastic part of the free energy which depends on irreversible plasticity strains. q is an internal variable indicating the state of work hardening. Here we assume $q = \epsilon_{eff}^p = \sqrt{(\epsilon_{11}^p)^2 + (\epsilon_{22}^p)^2 + 2(\frac{\epsilon_{12}^p}{\kappa})^2}$ the effective strain. We assume a power-law form

for the stored mechanical energy as follows, assuming only isotropic hardening

$$W^p(\epsilon_{ij}^p, \epsilon_{eff}^p) = \frac{n\epsilon_0^p}{n+1} \sigma_0 \left(1 + \frac{\epsilon_{eff}^p}{\epsilon_0^p}\right)^{\frac{n+1}{n}}, \quad (3.22)$$

where σ_0 is the yield stress. The yield stress is

$$\sigma_y = \frac{\partial W^p(\epsilon^p, \epsilon_{eff}^p)}{\partial \epsilon_{eff}^p} = \sigma_0 \left(1 + \frac{\epsilon_{eff}^p}{\epsilon_0^p}\right)^{\frac{1}{n}}. \quad (3.23)$$

We assume no kinetic hardening, so the back stress of kinematic hardening vanishes:

$$\sigma^* = \frac{\partial W^p(\epsilon^p, \epsilon_{eff}^p)}{\partial \epsilon^p} = 0. \quad (3.24)$$

For our 2 – D orthotropic model we have

$$\kappa\tau_2 = \kappa\tau_2^0 \left(1 + \frac{\sqrt{(\epsilon_{11}^p)^2 + (\epsilon_{22}^p)^2 + 2(\frac{\epsilon_{12}^p}{\kappa})^2}}{\epsilon_0^p}\right)^{\frac{1}{n}}. \quad (3.25)$$

Note that when only shear σ_{12} is applied for a single crystal we have:

$$\sigma_y = \kappa\tau_2 \left(1 + \frac{\sqrt{2(\epsilon_{12}^p)^2}}{\kappa\epsilon_0^p}\right)^{\frac{1}{n}} \neq \tau_2 \left(1 + \frac{\sqrt{2(\epsilon_{12}^p)^2}}{\epsilon_0^p}\right)^{\frac{1}{n}}. \quad (3.26)$$

3.2.4 Orthotropic behavior: Two slip systems

In this section we try to give physical meaning to the yield values, τ_1, τ_2 , described earlier. For an orthotropic 2 – D composite material the behavior is estimated by the relation between the average stress and strain for each specific loading. As an example for the linear behavior, assuming that

direction the normal between the two layers is along the '2' axis, one finds that

$$\sigma_{11} = f_M \sigma_{11}^M + f_A \sigma_{11}^A \quad ; \quad \epsilon_{11} = \epsilon_{11}^M = \epsilon_{11}^A, \quad (3.27)$$

$$\sigma_{22} = \sigma_{22}^M = \sigma_{22}^A \quad ; \quad \epsilon_{22} = f_M \epsilon_{22}^M + f_A \epsilon_{22}^A, \quad (3.28)$$

$$\sigma_{12} = \sigma_{12}^M = \sigma_{12}^A \quad ; \quad \epsilon_{12} = f_M \epsilon_{12}^M + f_A \epsilon_{12}^A, \quad (3.29)$$

and from there the Secant moduli are

$$E_1^* = f_A E_1^A + f_M E_1^M, \quad (3.30)$$

$$\frac{1}{E_2^*} = \frac{f_A}{E_2^A} + \frac{f_M}{E_2^M}, \quad (3.31)$$

$$\frac{1}{G_{12}^*} = \frac{f_A}{G_{12}^A} + \frac{f_M}{G_{12}^M}. \quad (3.32)$$

As we are considering dilute volume fractions, $f_A \sim 1 - 5\%$, of the weak material, austenite, we will have

$$\sigma_{11} \sim \sigma_{11}^M, \quad (3.33)$$

$$\sigma_{22} = \sigma_{22}^A, \quad (3.34)$$

$$\sigma_{12} = \sigma_{12}^A. \quad (3.35)$$

And so we can estimate the yield stress for the hard, and easy directions, respectively, as

$$\tau_1 \sim \tau_1^M, \quad \text{for} \quad \frac{\epsilon_{11}^0 - \epsilon_{22}^0}{2} \text{ loading}; \quad (3.36)$$

$$\tau_2 = \tau_2^A, \quad \text{for} \quad \epsilon_{12}^0 \text{ loading}, \quad (3.37)$$

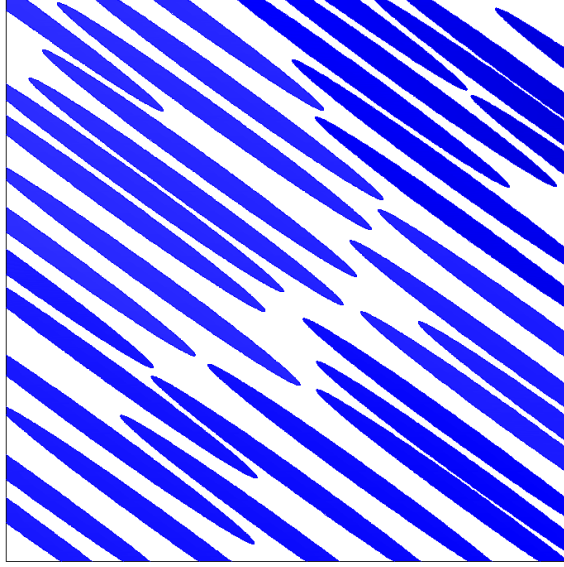


Figure 3.3: A schematic figure showing lath microstructure: martensitic layers (blue), with retained austenite (white) between them

where the yield surface is defined by

$$\left(\frac{S_{11} - S_{22}}{2\tau_1^2}\right)^2 + \frac{S_{12}^2}{\tau_2^2} = 1. \quad (3.38)$$

3.2.5 Incremental work function

In general to find the elastoplastic behavior of a system, given the previous state of the system and the applied loading, one can introduce an incremental work function as (Ortiz and co-workers 1999, 2010)

$$F_n(\epsilon_{n+1}, \epsilon_{n+1}^p) = \int_{\Omega_0} f_n(\epsilon_{n+1}, \epsilon_{n+1}^p) d\Omega, \quad (3.39)$$

where

$$f_n(\epsilon_{n+1}, \epsilon_{n+1}^p) = A_{n+1}(\epsilon_{n+1}, \epsilon_{n+1}^p) - A_n(\epsilon_n, \epsilon_n^p) + \Delta t \psi_{n+1}^*. \quad (3.40)$$

A is the stored energy in the material as stated earlier, and q is the hardening parameter. The plasticity driving force is then obtained by minimizing f with respect to ϵ_{n+1}^p :

$$\mathbf{Y} = -\frac{\partial A_{n+1}}{\partial \epsilon_{n+1}^p} = \sigma_{n+1} - \sigma_{n+1}^c = \frac{\partial \Delta t \psi_{n+1}^*}{\partial \epsilon_{n+1}^p}, \quad (3.41)$$

where $\sigma = \frac{\partial W^e}{\partial \epsilon^e}$ is the equilibrium stress, and $\sigma^c = \frac{\partial W^p}{\partial \epsilon^p}$ is the back stress. For infinitesimal deformation we have linear elasticity

$$A_{n+1} = (\epsilon_{n+1} - \epsilon_{n+1}^p) : \mathbb{C} : (\epsilon_{n+1} - \epsilon_{n+1}^p) + W^p(\epsilon_{n+1}^p, q_{n+1}). \quad (3.42)$$

Assuming only isotropic strain hardening, the incremental work function can be written as

$$\min_{\epsilon_{n+1}^p} f_n(\epsilon_{n+1}, \epsilon_{n+1}^p) \implies \min_{\epsilon_{n+1}^p} \left\{ \frac{\kappa}{2} (\theta_{n+1})^2 + \mu |e_{n+1} - \epsilon_{n+1}^p|^2 + \Delta t \frac{\partial t \psi_{n+1}^*}{\partial \epsilon_{n+1}^p} \right\}. \quad (3.43)$$

Further assuming volume preserving plasticity, the driving force for plasticity is

$$\mathbf{Y} = -\frac{\partial F_n}{\partial \epsilon_{n+1}^p} = \sigma^{dev} \quad \text{and} \quad \mathbf{Y} = \frac{\partial \psi^*}{\partial \epsilon_{n+1}^p}. \quad (3.44)$$

From here we have

$$\sigma_{n+1}^{Pre} - 2\mu \Delta \epsilon^p = \sigma_{n+1}^c + \frac{\partial t \psi_{n+1}^*}{\partial \epsilon_{n+1}^p} \quad (3.45)$$

where

$$\sigma_{n+1}^{Pre} = \mathbb{C} : (\epsilon_{n+1} - \epsilon_n^p). \quad (3.46)$$

For the special case of rate-independent plasticity

$$\psi^* = \sigma_y \dot{\epsilon}_{eff}^p \quad (3.47)$$

$$\mathbf{Y} = \frac{\partial \psi^*}{\partial \dot{\epsilon}_{n+1}^p} = \sigma_y \mathbf{M} \frac{\dot{\epsilon}^p}{\dot{\epsilon}_{eff}^p}. \quad (3.48)$$

From here we have the flow rule as

$$\dot{\epsilon}_{ij}^p = M_{ijkl} \dot{\epsilon}_{eff}^p \frac{\sigma_{kl}^{dev}}{\sigma_y} \quad (3.49)$$

where $\mathbf{M} = 3/2\mathbf{I}$ for 3 - D and $\mathbf{M} = \mathbf{I}$ for 2 - D for Mises plasticity, and \mathbf{I} is the unit tensor. For our orthotropic model, the plastic dissipation is

$$\psi^* = \sqrt{2\kappa\tau_2} \Delta(\epsilon_{eff}^p)^2 \quad (3.50)$$

where

$$\Delta\epsilon_{eff}^p = \sqrt{(\Delta\epsilon_{11}^p)^2 + (\Delta\epsilon_{22}^p)^2 + \left(\frac{\Delta\epsilon_{12}^p}{\kappa}\right)^2 + \left(\frac{\dot{\epsilon}_{21}^p}{\kappa}\right)^2} \quad (3.51)$$

so the driving force for the plastic strain is

$$Y_{11} = \sqrt{2\kappa\tau_2} \frac{\Delta\epsilon_{11}^p}{\Delta\epsilon_{eff}^p}, \quad Y_{22} = \sqrt{2\kappa\tau_2} \frac{\Delta\epsilon_{22}^p}{\Delta\epsilon_{eff}^p}, \quad Y_{12} = \sqrt{2\kappa\tau_2} \frac{\Delta\epsilon_{12}^p}{\kappa^2 \Delta\epsilon_{eff}^p} \quad (3.52)$$

which also satisfies the yield condition as expected:

$$Y_{11}^2 + Y_{22}^2 + 2\kappa^2 Y_{12}^2 = 2\kappa\tau_2 \frac{(\Delta\epsilon_{11}^p)^2 + (\Delta\epsilon_{22}^p)^2 + 2(\Delta\epsilon_{12}^p)^2 \frac{\kappa^2}{\kappa^4}}{(\Delta\epsilon_{eff}^p)^2} = 2\kappa\tau_2. \quad (3.53)$$

From equation (3.52)

$$Y_{11} - \sqrt{2\kappa\tau_2} \frac{\Delta\epsilon_{11}^p}{\Delta\epsilon_{eff}^p} = 0, \quad Y_{22} - \sqrt{2\kappa\tau_2} \frac{\Delta\epsilon_{22}^p}{\Delta\epsilon_{eff}^p} = 0, \quad Y_{12} - \sqrt{2\kappa\tau_2} \frac{\Delta\epsilon_{12}^p}{\kappa^2 \Delta\epsilon_{eff}^p} = 0 \quad (3.54)$$

defining

$$S_{ij}^{pre} = Y_{ij} + 2\mu\Delta\epsilon_{ij}^p \quad (3.55)$$

we can write

$$S_{11}^{pre} - 2\mu\Delta\epsilon_{11}^p - \sqrt{2\kappa\tau_2} \frac{\Delta\epsilon_{11}^p}{\Delta\epsilon_{eff}^p} = 0, \quad (3.56)$$

$$S_{22}^{pre} - 2\mu\Delta\epsilon_{22}^p - \sqrt{2\kappa\tau_2} \frac{\Delta\epsilon_{22}^p}{\Delta\epsilon_{eff}^p} = 0, \quad (3.57)$$

$$S_{12}^{pre} - 2\mu\Delta\epsilon_{12}^p - \sqrt{2\kappa\tau_2} \frac{\Delta\epsilon_{12}^p}{\kappa^2 \Delta\epsilon_{eff}^p} = 0. \quad (3.58)$$

By solving this equations, say by Newton-Raphson method, we can have the incremental plastic stress for a given loading, $\epsilon^0, \mathbf{S}^{pre}$.

3.3 Overall plastic behavior of a polycrystal

In this section we analyze a polycrystalline metal by modeling the random grain structure and calculation of strain/stress field. Overall properties of the polycrystalline metals depend on the

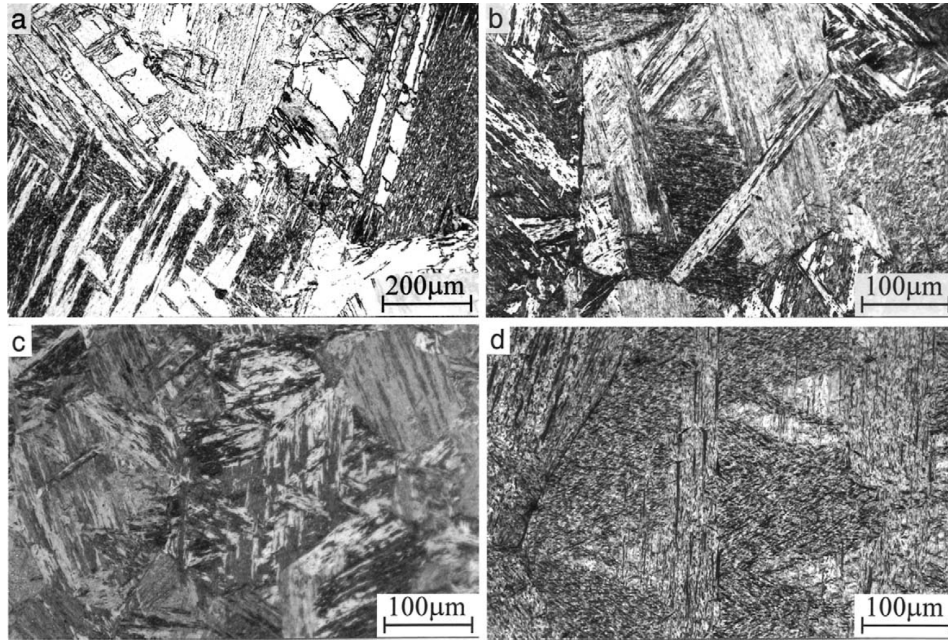


Figure 3.4: Optical micrographs of lath martensite in (a) Fe-0.0026C, (b) Fe-0.18C, (c) Fe-0.38C and (d) Fe-0.61C alloys. Etching solution: 3% nital. Morito et al. (2005)

properties of randomly shaped and oriented grains and are defined by the properties of, and interaction between, the crystal grains. Here, using Voronoi tessellation we assign random polycrystalline structure (random orientation of crystal lattice) to each of the grains. We assume that each grain is a monocrystal with anisotropic plastic behavior. Our plasticity model assumes that plastic deformation is caused by crystalline slip on either of the two predefined slip directions of crystal lattice. Slip direction is defined by orientation of crystal lattice, which differs from grain to grain (random orientation). Crystal plasticity assumes that plastic deformation is a result of crystalline slip only and therefore strongly depends on orientation of crystal lattice. Rate-independent plasticity with isotropic hardening law, as described in the previous section, is used in our model. Periodic finite difference method is used to obtain numerical solutions of strain and stress fields.

Following Mura, we treat plastic strains as eigenstrains and solve for the overall mechanical behavior (see Shodja and Roumi (2005, 2006) and Roumi and Shodja (2007)). The stress at any point of any of the grains is defined as

$$\boldsymbol{\sigma} = \mathbb{C} : (\boldsymbol{\epsilon} - \boldsymbol{\epsilon}^p) \quad (3.59)$$

equilibrium requires that

$$\nabla (\mathbb{C} : (\boldsymbol{\epsilon} - \boldsymbol{\epsilon}^p)) = 0 \implies \nabla (\mathbb{C} : \boldsymbol{\epsilon}) = \nabla (\mathbb{C} : \boldsymbol{\epsilon}^p). \quad (3.60)$$

We decompose the stress and strain fields into two parts: one due to the applied loading at the boundary and the other due to the anisotropy made by the rotations of the grains with respect to each other.

$$\boldsymbol{\epsilon}(\mathbf{x}) = \boldsymbol{\epsilon}^0 + \tilde{\boldsymbol{\epsilon}}(\mathbf{x}) \quad (3.61)$$

$$\nabla (\mathbb{C} : \tilde{\boldsymbol{\epsilon}}) = \nabla (\mathbb{C} : \boldsymbol{\epsilon}^p) \quad (3.62)$$

from the plasticity model we will have

$$\boldsymbol{\epsilon}^p = \boldsymbol{\epsilon}^p(\boldsymbol{\epsilon}) = \boldsymbol{\epsilon}^p(\boldsymbol{\epsilon}^0 + \tilde{\boldsymbol{\epsilon}}(\mathbf{x})) \quad (3.63)$$

from which we can estimate the strain at each point of any grain due to the anisotropy made by the rotations of the grains with respect to each other as

$$\tilde{\boldsymbol{\epsilon}}(\mathbf{x}) = \tilde{\boldsymbol{\epsilon}}(\boldsymbol{\epsilon}^0, \mathbf{x}). \quad (3.64)$$

After finding the strain/stress field for each of the grains, the constitutive equations can be written as

$$\bar{\sigma} = \langle \sigma \rangle = f(\langle \epsilon \rangle) = f(\epsilon^0) \quad (3.65)$$

which is based on the following lemmas:

a) Average stress theorem, Nemat-Nasser and Hori (1993) states that: "When a body is subjected to traction boundary condition with σ^0 a constant stress tensor, the stress averaged over the entire body is the same as σ^0 regardless of the complexity of the stress field within the domain."

b) Hill's lemma (1963, 1993): Consider an RVE (statistically homogeneous) with volume V and surface S . Assume equilibrium condition is satisfied (no body forces exist). Then for linear displacement or uniform traction boundary conditions we have the following lemma:

"For any stress and strain fields σ, ϵ at a given point in the RVE under prescribed boundary traction or boundary displacement condition:

$$\overline{\sigma_{ij}\epsilon_{ij}} - \bar{\sigma}_{ij}\bar{\epsilon}_{ij} = \frac{1}{|\Omega|} \int_S (u_i - x_j\bar{\epsilon}_{ij})(\sigma_{ik}n_k - \overline{\sigma_{ik}n_k})dS, \quad (3.66)$$

where the *overline* stands for volume average. It says, for statically admissible stress field or kinematically admissible displacement field the average of the product $\overline{\sigma\epsilon} = \bar{\sigma}\bar{\epsilon}$."

3.3.1 Voronoi tessellation

Voronoi tessellation is a kind of decomposition of a metric space determined by distances to a specified discrete set of objects in the space, e.g., by a discrete set of points. In the simplest case, we are given a set of points S in the plane, which are the Voronoi sites. Each sites has a Voronoi

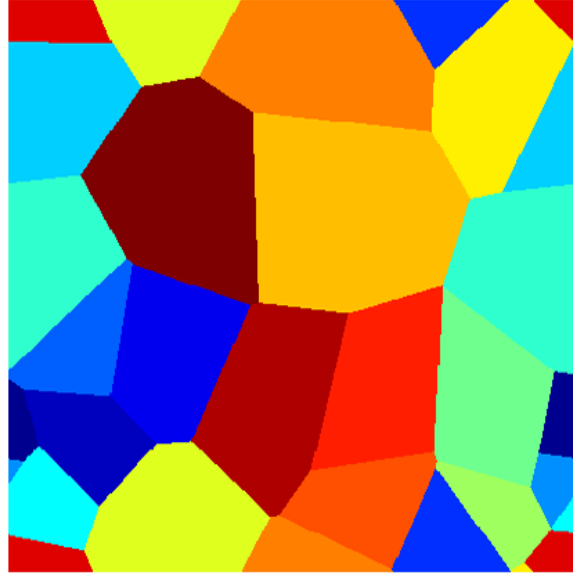


Figure 3.5: Voronoi tessellation

cell, also called a Dirichlet cell, $V(s)$ consisting of all points closer to s than to any other site. The segments of the Voronoi diagram are all the points in the plane that are equidistant to the two nearest sites. The Voronoi nodes are the points equidistant to three (or more) sites.

3.3.2 Algorithm to estimate overall plastic behavior of a polycrystal

For each loading ϵ^0 follow this algorithm:

0— Knowing the previous state of the material ϵ_n^p , for a given applied uniform displacement loading at the boundary, ϵ_{n+1}^0 , assume that $\delta \mathbf{e}_0^p(\mathbf{x}) = \epsilon_{n+1}^p(\mathbf{x}) - \epsilon_n^p(\mathbf{x}) = 0$.

1— $i = i + 1$, then $\delta \mathbf{e}_i^p(\mathbf{x}) = \delta \mathbf{e}_{i-1}^p(\mathbf{x})$.

2— Calculate $\tilde{\epsilon}_{n+1}(\mathbf{x})$ from the equilibrium equation as stated earlier.

3— Calculate global stress field $\sigma_{n+1}(\mathbf{x}) = \mathbb{C} : (\epsilon_{n+1}^0 + \tilde{\epsilon}_{n+1}(\mathbf{x}) - \epsilon_{n+1}^p(\mathbf{x}))$.

4— Calculate local stress field $\Sigma_{n+1}(\mathbf{X}) = \mathbf{R}^T(\theta)\sigma_{n+1}(\mathbf{x})\mathbf{R}(\theta)$ for each grain.

- 5— Calculate the local plastic strain field $\mathbf{E}_{i+1}^p(\mathbf{X})$ from $\Sigma_{n+1}(\mathbf{X})$ for each grain based on our single crystal anisotropic model.
- 6— Calculate the global plastic strain field $\epsilon^p(\mathbf{x}) = \mathbf{R}(\theta)\mathbf{E}^p\mathbf{R}^t(\theta)$.
- 7— Continue 1 – 4 until $norm(\mathbf{e}_{i+1}^p(x) - \mathbf{e}_i^p(\mathbf{x})) < error$.
- 8— Calculate the average stress in the polycrystal.
- 9— Go back to 0, and increase the load.

3.3.3 Numerical results and discussion

To estimate the overall behavior of the material, we apply boundary conditions as linear displacement loadings. Here we examine two different loadings:

- a) $\epsilon_{11}^0 = -\epsilon_{22}^0 = \epsilon^0$; $\epsilon_{12}^0 = 0$.
- b) $\epsilon_{11}^0 = -\epsilon_{22}^0 = 0$; $\epsilon_{12}^0 = \epsilon^0$.

Figure 3.6 shows our results. The domain size is a periodic cell as shown in Figure 3.5. As can be seen, the anisotropy reduces once we increase our domain size, and we see that the polycrystal tends to show an isotropic hard and tough behavior. This is in agreement with the experiments on TRIP steels as shown in Figure 3.2, and thus our formulation describes this interesting behavior of TRIP steels.

To conclude, we see that very small amount of weak layers between the layers of a hard material, can significantly change the plastic behavior of the metal by reducing the hardness and increasing the toughness. In conclusion, using a simple plasticity model to study the qualitative behavior of 2 – D orthotropic polycrystals, we showed that retained austenite is crucial for the ductility of the polycrystalline metal.

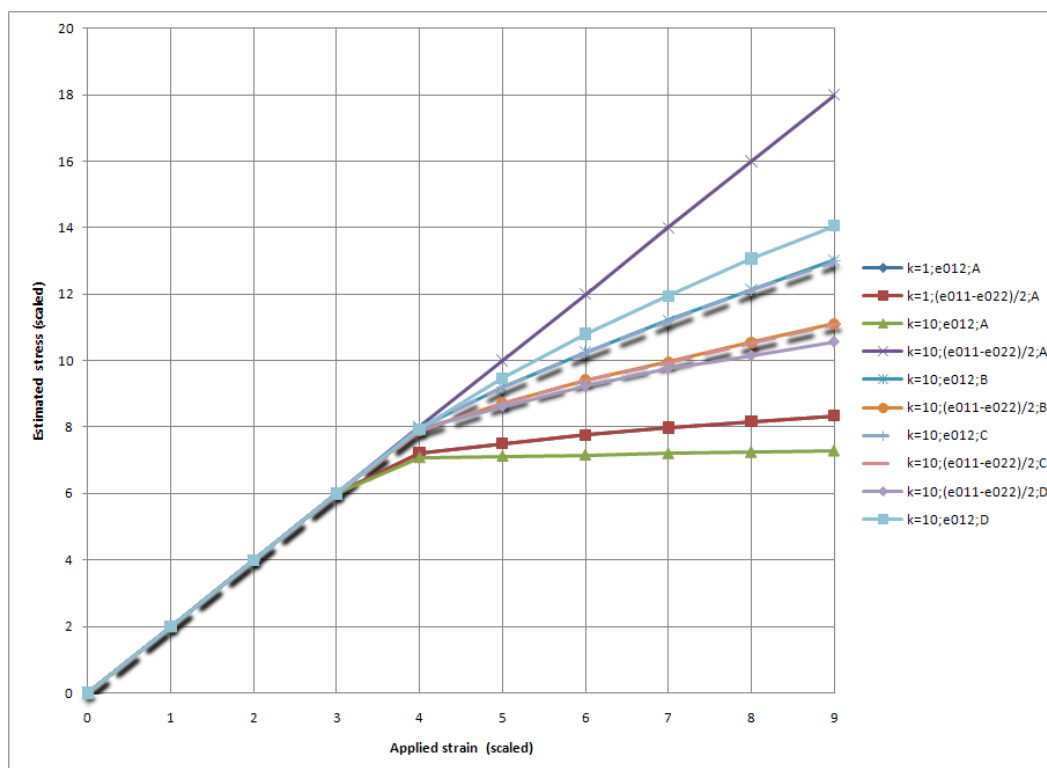


Figure 3.6: Estimated mechanical behavior of the polycrystal for different values of domain sizes, $n \times n$, and number of grains nG . $n = 200$ for series *A* and *B*, $n = 400$ for series *C* and *D*. $nG = 1$ for series *A*, $nG = 10$ for series *B* and *C*. $nG = 20$ for series *D*. Series *A* shows the orthotropic behavior of a single grain.

3.4 References

1. R. Hill , "A theory of the yielding and plastic flow of anisotropic materials", (3rd edn. ed.), Proc. R. Soc. A193 (1947).
2. R. Hill, "A theory of the yielding and plastic flow of anisotropic metals", Proc. Royal Soc. London, Series A, Math. Physical sciences, Vol 193, No. 1033. 1948, 281-297
3. R. Hill, 1963. Elastic properties of reinforced solids: some theoretical principles. J. Mech. Phys. Solids 11, 357-372.
4. J. Lubliner, Acta Mech. 22, (1975), 289-293.
5. T. Mura, 1982. Micromechanics of Defects in Solids, first ed. Martinus Nijhoff Publishers, The Hague-Boston.
6. M. Zyckowski, T. Kurtyka, Acta Mech. 52, (1984), 1-13.
7. J. Lubliner, 1990, Plasticity Theory, Macmillan Publishing Company.
8. G. A. Maugin, 1992, The Thermodynamics of Plasticity and Fracture, Cambridge university Press.
9. S. Nemat-Nasser, M. Hori, 1993. Micromechanics: Overall Properties of Heterogeneous Materials. Elsevier, North-Holland, Amsterdam.
10. R.V. Kohn ,and T.D. Little, 59, no. 1, (1998), SIAM Journal on Applied Mathematics.
11. M.V. Nebozhyn, P. Castaneda, 1999, IUTAM Symposium on Micro- and Macrostructural Aspects of Thermoplasticity, Kluwer Academic Publishers.

12. M. Ortiz, L. Stainier, The variational formulation of viscoplastic constitutive updates, COMPUT METHOD APPL M 171 (3-4): 419-444 APR 9 1999.
13. R. Hill, "Plastic anisotropy and the geometry of yield surfaces in stress space", JMPS, Vol 48 (2000) 1093-1106.
14. G.H. Goldsztein, vol 457, no. 2015, (2001), Proc. R. Soc. Lond. A.
15. S. Morito, H. Tanaka H. R. Konishi, T. Furuhashi, T. Maki, Acta Materialia, Volume 51, Number 6, 2 April 2003, 1789-1799(11).
16. Kachanov, 2004, Fundamentals of the theory of Plasticity, Dover Publications.
17. K. Bhattacharya, P. M. Suquet, Proc. Royal Society London A, 461:2797-2816, 2005.
18. H.M. Shodja, F. Roumi, Overall behavior of composites with periodic multi-inhomogeneities. Mech. Mater. 37, 343-353 (2005).
19. Q. Yang, L. Stainier, M. Ortiz, JMPS, 54, (2006), 401-424.
20. H. M. Shodja, F. Roumi, Effective moduli of coated particulate composites with BCC structure at high concentration. ASCE August, 882-888 (2006).
21. F. Roumi, H.M. Shodja, Elastic solids with high concentration of arbitrarily oriented multiphase particles. Acta Mech. 189, 125-139 (2007).
22. L. Stainier, M. Ortiz, Study and validation of a variational theory of thermo-mechanical coupling in finite visco-plasticity, INT J SOLIDS STRUCT 47: 705-715, 2010.

Chapter 4

The Role of Size, Geometry, and Mechanical Compatibility in Diffusive Phase Transformations

4.1 Introduction

A common feature of electrochemical systems is a significant voltage hysteresis between the charge and discharge curve. The existence of the hysteresis even in very small current regimes suggests that there may be some mechanical energy barriers. Batteries are among the widely used electrochemical systems. In classical batteries, the electrodes operate by ion insertion/de-insertion processes, which in addition to chemical reactions in the electrodes can apply deformations and forces on the electrode materials that change the performance. Lithium-ion rechargeable batteries are extensively used in our everyday life. In a typical Li-ion battery, the anode can be made of carbon, and the electrolyte can be an organic lithium salt. Different materials have been proposed as the cathode. It has been suggested that cathodes made of $FePO_4$ (triphylite) promise safe, inexpensive, high-power rechargeable batteries.

When used as a cathode in rechargeable batteries triphylite undergoes a solid-to-solid phase

transformation involving a change of crystal structure. Although the equilibrium structure of $FePO_4$ is rodolicoite, lithium can be electrochemically removed from $FePO_4$ without changing the orthorhombic olivine structure of $LiFePO_4$. Despite no change in the orthorhombic structure, the crystalline dimensions change, which causes a misfit strain between the two phases. This transformation can limit the rate at which the battery can charge/discharge.

Nano-sized $Li_{1-x}FePO_4$ and $Li_{1-x}MnPO_4$ have shown different electrochemical, solid solution behavior compared to coarser-grained $LiFePO_4$, which exhibits a conventional two-phase reaction. Chiang and co-workers (2008) found that when cathode particles are of very small size, the batteries charge faster. They claimed that this improvement in the performance is due to the faster first-order phase transformation between $LiFePO_4$ and $FePO_4$ due to changes in surface area and stress field. They observed that when lattice misfits are smaller they see more strain compared to the case with more misfit, and they concluded that this should be due to the formation of coherent interface in the small misfit case, compared to the incoherent interface in the larger misfit case. Experiments by Yet-Ming Chiang and co-workers suggested that nanoscale ($< 50\text{ nm}$) $Li_{1-x}FePO_4$ has a size-dependent, reduced miscibility gap compared to coarser-grained materials. It has also been seen that the discharge capacity reduces more for large particles than for nanoparticles.

Chen and Richardson (2006), studied the mechanism of $LiFePO_4$ transformation into $FePO_4$. They concluded that the movement of lithium ions in the highly anisotropic $LiFePO_4$ and $FePO_4$ is confined to channels along the [010]-axis. In addition, there is a layered character to the $FePO_4$ host parallel to the (100) plane. The observation of the highly restricted Li motion within the bulk solids, with no assistance toward homogeneity, suggests that Li is extracted/inserted only at the phase boundary, with Li ions moving parallel to the boundary instead of diffusing through the crystal. This mechanism has been confirmed for the case of $LiMnPO_4$ as well. They observed

ordered domains of $FePO_4$ spaced between the parent $LiFePO_4$ domains, a morphology induced by the stress fields due to the lattice parameter mismatch. The transformation proceeded in the direction of the [100]-axis at dislocation lines running parallel to the [001]-axis. Chen and Richardson conclude that: "The ideal particle shape is small thin plates of $LiFePO_4$, as thin as possible, to minimize the distance of Li movement." They observed domains separated by a boundary zone form within the crystal.

We study the interactions of solid-solid phase transformations with electrochemical processes. It is suggested that electronic and ionic structures depend on lattice parameters, thus it is expected that structural transformations can lead to dramatic changes in material properties. These transformations can also change the energy barrier and hysteresis. It is known that compatible interfaces can reduce elastic energy and hysteresis (Kohn 1991, Bhattacharya 2003, James 2009) and thus may extend the system's life. Solid-solid transformations change the crystalline structure. These geometry changes can have long-range effects and cause stresses in the whole material. The generated stress field itself changes the total free energy, due to the change in elastic energy, and thus, the electrochemical potential and processes are affected. An example is olivine phosphates which are candidates for cathode material in Li-ion batteries. These materials undergo an orthorhombic-to-orthorhombic phase transition. Experiments by Yet-Ming Chiang and co-workers suggested that elastic compatibility can affect rates of charge/discharge in the battery.

Using asymptotic limit analysis, we study the effects of geometry and size of electrodes on elastic energy and concentration profile. We consider the state of lowest free energy of the system; although in practice due to kinetics, defects, etc., the material may be at a metastable state of energy and may not reach its lowest free energy. Here, we use a phase-field model to estimate the behavior of the

elasto-electro-chemical system. The surface energy is modeled as a function of the space gradients of the li-ion concentration, which plays an important rule in describing the concentration profile for different sizes and geometries. The electrochemical energy is modeled as a double-well function with minima near fully lithiated and delithiated states. The elastic energy, assuming coherent interfaces, is a function of the phase transformation between lithiated and delithiated phases, e.g., orthorhombic-to-orthorhombic phase transformation in $LiFePO_4$. It can also be a function of the applied displacement and traction boundary conditions from the charge collector and electrolyte. It is expected that the elastic energy can play an important role by making the transformation barrier higher and thus limit the rate. It can also be a major player in the life cycle of the system. This means that one should make the crystallographic changes in electrodes as compatible as possible in order to have higher rates and more cycles. One other import issue is that, when the gradient energy term is large compared to the electrochemical energy, the system does not obey Fick's law. This could occur, for example, across an interface in inhomogeneous systems in which the concentration profile is characterized by a strongly varying curvature. In this case, one has do a more general study to understand the system and predict its behavior. We consider three cases:

a) Small body limit: in this limit, we prove that in very small particle limit the concentration profile should be of a single domain in each particle. This results in the elimination of the elastic energy for very small particles. The reduced energy barrier suggests higher rates as suggested by experiments of Yet-Ming Chiang and coworkers and also possibly longer life of the battery. Our results show that for very small particles we should have only either fully lithiated or fully delithiated particles, as reported by experiments of Delmas et al. (2008), thus the overall behavior of the concentration, as an averaging scheme, can show reduced miscibility gap.

b) Large body limit: in this limit we prove that we should see multiple layers of lithiated and

delithiated phases adjacent to each other in a preferred direction in order to minimize the elastic energy. This is again in accordance with several experiments on large domains.

c) Thin film limit: in this limit we show that the concentration profile should be uniform in thickness. Though depending on the other dimensions of the film it can show periodic layers of lithiated and delithiated phases with a preferred normal direction. This is also verified experimentally for thin films of $LiFePO_4$ by Chen and Richardson (2006) and also another group.

In the following work, for simplicity, we neglect anisotropy in elastic constants of the two phases. We also assume that the two materials have the same elastic constants. However, we do not neglect the anisotropic nature of diffusion and surface reactions.

4.2 Model

Consider a bounded Lipschitz domain $\Omega \subset \mathbb{R}^3$ occupied by a body in the reference configuration. Let $0 \leq c(\mathbf{x}) \leq 1$ denote the normalized chemical concentration and $\mathbf{u}(\mathbf{x})$ the mechanical displacement at a point $x \in \Omega$. The infinitesimal strain is $\epsilon = \frac{1}{2}(\nabla \mathbf{u} + \nabla \mathbf{u}^T)$. The stress-free state can change with concentration. Therefore, we introduce a transformation strain,

$$\epsilon^t(c) = c\eta, \quad \eta \in \mathbb{M}_{sym}^{3 \times 3} \tag{4.1}$$

that depends linearly with concentration.

We postulate that the Gibbs free energy of the system is the following functional of the concen-

tration c and the displacement u :

$$E[c, u] = \int_{\Omega} \left\{ f(c) + \frac{1}{2} (\nabla c \cdot \mathbf{K} \nabla c) + \frac{1}{2} (\epsilon(\mathbf{u}) - \epsilon^t) \cdot \mathbb{C} (\epsilon(\mathbf{u}) - \epsilon^t) \right\} dx \quad (4.2)$$

where f is the chemical free energy density, \mathbf{K} is a positive-definite matrix representing interfacial energy, and \mathbb{C} is the elastic modulus. The first term about represents the chemical free energy. Thus, f is convex in miscible systems and non-convex in immiscible systems. We shall mostly consider the case where f is non-convex with two wells. We assume without loss of generality psi is non-negative. The second term penalizes gradients of composition, and thus the phase boundary in immiscible systems. The final term is the elastic energy of the system.

We are interested in finding the ground-state of the system for a given average concentration c_0 . Therefore, we minimize the energy above over c and \mathbf{u} subject to the constraint

$$\int_{\Omega} (c - c_0) d\Omega = 0. \quad (4.3)$$

Assuming that the chemical energy density f has a quadratic growth¹, we introduce the following admissible class of functions

$$\mathcal{A} := \{ \{c, \mathbf{u}\} : c \in H^1(\Omega, \mathbb{R}), \mathbf{u} \in H^1(\Omega, \mathbb{R}^3), \langle c \rangle = c_0, \langle \mathbf{u} \rangle = 0, \langle \nabla \mathbf{u} - \nabla \mathbf{u}^T \rangle = 0 \} \quad (4.4)$$

where $\langle \cdot \rangle$ denotes the volume average. Thus, the problem we study is:

(P) Given c_0 , minimize $E[c, \mathbf{u}]$ on \mathcal{A} .

¹We ignore for now the constraint that $0 \leq c \leq 1$ for mathematical convenience.

We note in passing that we can also study the problem of the body immersed in a bath with fixed electro-chemical potential by replacing f with $f - \mu_{ext}c$ in the functional and dropping the constraint $\langle c \rangle = c_0$ from the admissible class of functions.

The following theorem assures us of the existence of minimizers of (P).

Theorem 4.2.1 (Existence of minimizers) *Given any c_0 , there is a minimizer $\{c, \mathbf{u}\}$ of E in \mathcal{A} .*

Proof. The proof follows standard techniques of the direct method of the calculus of variations (see for example, Dacorogna). We note that the functional E is bounded uniformly from below, and is finite for each element in \mathcal{A} . Thus, we may choose a minimizing sequence $\{c^k, \mathbf{u}^k\}$.

Now observe that for each c , $E[c, \cdot]$ is convex and $\min_{\mathbf{u}} E[c, \mathbf{u}]$ has an unique solution u_c such that

$$\nabla \cdot \mathbb{C}(\epsilon(\mathbf{u}_c) - \epsilon^t) = 0 \text{ in } \Omega, \quad \mathbb{C}(\epsilon(\mathbf{u}_c) - \epsilon^t)\hat{\mathbf{n}} = 0 \text{ on } \partial\Omega, \quad (4.5)$$

$$\int_{\Omega} \frac{1}{2}(\epsilon(\mathbf{u}_c) - \epsilon^t(c)) \cdot \mathbb{C}(\epsilon(\mathbf{u}_c) - \epsilon^t(c)) \, dx \leq \frac{1}{2} \int_{\Omega} \epsilon^t(c) \cdot \mathbb{C}\epsilon^t(c) \, dx. \quad (4.6)$$

The last inequality follows by taking $u = 0$ as the test function.

Now returning to our minimizing sequence,

$$E(c^k, \mathbf{u}_{c^k}) \leq E(c^k, \mathbf{u}^k) \leq C \quad (4.7)$$

so that

$$\int \frac{1}{2} \nabla c^k \cdot K \nabla c^k \, dx \leq C'. \quad (4.8)$$

It follows that there exists a subsequence (relabelled)

$$\nabla c^k \rightharpoonup \nabla c \text{ in } W^{1,2}. \quad (4.9)$$

Similarly,

$$\int_{\Omega} f(c^k) dx \leq C' \quad (4.10)$$

so that there exists a subsequence (relabelled)

$$c^k \rightharpoonup c \text{ in } L^2. \quad (4.11)$$

Together, we conclude that

$$c^k \rightarrow c \text{ in } L^r, \quad 1 \leq r < 6. \quad (4.12)$$

Recall that $\epsilon^t = \eta c$, and so trivially $\epsilon^t(c^k) \rightarrow \epsilon^t(c)$ in L^2 . Therefore, we can recall the equilibrium condition (4.5) and invoke Hill's lemma or the div-curl lemma of Tartar to conclude that

$$\int (\epsilon(\mathbf{u}_{c_k}) - \epsilon^t(c_k)) \cdot \mathbb{C}(\epsilon(\mathbf{u}_{c_k}) - \epsilon^t(c_k)) dx \rightarrow \int (\epsilon(\mathbf{u}_c) - \epsilon^t(c)) \cdot \mathbb{C}(\epsilon(\mathbf{u}_c) - \epsilon^t(c)) dx. \quad (4.13)$$

We combine this with the convexity of the interfacial energy and the growth condition on f to conclude that

$$E[c, \mathbf{u}_c] \leq \lim E[c^k, \mathbf{u}_{c_k}] \leq \lim E[c^k, \mathbf{u}^k]. \quad (4.14)$$

We conclude that $\{c, \mathbf{u}_c\}$ is a minimizer of E in \mathcal{A} .

4.3 Small and large body limit

Consider a sequence of bodies $\Omega = \lambda\Omega_0$ for $\lambda \in (0, \infty)$, $\text{Vol. } \Omega_0 = 1$ and define

$$E^\lambda[c, \mathbf{u}] = \frac{1}{\lambda^3} E[c, \mathbf{u}] = \frac{1}{\lambda^3} \int_{\lambda\Omega_0} \left\{ \frac{\alpha^2}{2} |\nabla c|^2 + f(c) + \frac{1}{2} (\epsilon - \epsilon^t) \cdot \mathbb{C}(\epsilon - \epsilon^t) \right\} dx \quad (4.15)$$

where we have assumed that $K = \alpha^2 I$ is isotropic. We define $\mathbf{x}_0, C, \mathbf{U}$ through the following scaling relations

$$\mathbf{x} = \lambda\mathbf{x}_0, \quad C(\mathbf{x}_0) = c(\mathbf{x}) = c(\lambda\mathbf{x}_0), \quad \mathbf{U}(\mathbf{x}_0) = \frac{1}{\lambda} \mathbf{u}(\lambda\mathbf{x}_0). \quad (4.16)$$

Thus,

$$E^\lambda = \int_{\Omega_0} \left\{ \frac{\alpha^2}{2\lambda^2} |\nabla_{x_0} C|^2 + f(C) + \frac{1}{2} (\epsilon - \epsilon^t) \cdot \mathbb{C}(\epsilon - \epsilon^t) \right\} dx_0. \quad (4.17)$$

From now we drop the subscript 0 and use \mathbf{x} instead of \mathbf{x}_0 .

It follows from the existence theorem above that for each λ we have a minimizer C^λ, U^λ of E^λ . We seek to understand how these minimizers behave in the limits $\lambda \rightarrow 0$ (small body) and $\lambda \rightarrow \infty$ (large body). Since $\mathbf{U}^\lambda = \mathbf{U}_{C^\lambda}$, we occasionally abuse notation to describe C^λ to be the minimizer of E^λ .

4.3.1 Small particle limit

We show that in the limit of small particles, $\min E^\lambda \rightarrow f(c_0)$. Roughly, the interfacial energy dominates and thus we have uniform composition, and this has to be equal to the imposed average. Further, since the composition is uniform, the elastic energy is zero.

We have the following theorem. The ideas and the statement are similar to those of DeSimone.

Theorem 4.3.1 *For E^λ defined in (4.17),*

$$\lim_{\lambda \rightarrow 0} \min_{\mathcal{A}} E^\lambda = f(c_0) \quad (4.18)$$

Further, for any sequence C^λ of minimizers of E^λ , there exists a subsequence that converges in H^1 to c_0 .

Proof. For any λ , we have

$$E^\lambda[C^\lambda, U_{C^\lambda}] \leq E^\lambda[c_0, U_{c_0}] \quad (4.19)$$

for a minimizer C^λ . Since each term in the energy is non-negative, it follows that

$$\int_{\Omega_0} |\nabla C^\lambda|^2 dx \leq \frac{2\lambda^2}{\alpha^2} \int_{\Omega_0} f(c_0) dx = \lambda^2 D \quad (4.20)$$

for constant D independent of λ . Clearly

$$\nabla C^\lambda \rightarrow 0 \text{ in } L^2. \quad (4.21)$$

Similarly,

$$\int_{\Omega_0} f(C^\lambda) dx \leq D' \quad (4.22)$$

which implies that for a subsequence,

$$C^\lambda \rightharpoonup c_0 \text{ in } L^2. \quad (4.23)$$

Together, they imply that,

$$C^\lambda \rightarrow c_0 \text{ in } H^1. \quad (4.24)$$

This proves one of the statements of the theorem.

We now revisit (4.19) in light of the convergence above. We can use the dominated convergence theorem to conclude that

$$\lim_{\lambda \rightarrow 0} \int_{\Omega} \left\{ \frac{\alpha^2}{2\lambda^2} |\nabla C^\lambda|^2 + \frac{1}{2} (\epsilon_{\mathbf{U}_{C^\lambda}} - \epsilon^t(C^\lambda)) \cdot \mathbf{C}(\epsilon_{\mathbf{U}_{C^\lambda}} - \epsilon^t(C^\lambda)) \right\} dx \leq 0. \quad (4.25)$$

Since the terms on the left are non-negative, the rest of the theorem follows.

4.3.2 Large body limit

In this section we consider the limit of a large body. We make the additional assumption that f is the minimum of two quadratic wells with equilibrium concentrations c_1 and c_2 ,

$$f(c) = \frac{D}{2} \min \{ |c - c_1|^2, |c - c_2|^2 + f_0 \}. \quad (4.26)$$

Further we take $D = 1$ by renormalization.

We have the following theorem.

Theorem 4.3.2 For E^λ defined in (4.17) and for f as in (4.26),

$$\lim_{\lambda \rightarrow \infty} \min_{\mathcal{A}} E^\lambda = \min_{c_1^*, c_2^*, \theta} \left(\theta f(c_1^*) + (1 - \theta) f(c_2^*) + \frac{1}{2} \theta (1 - \theta) H(\epsilon^t(c_1^*) - \epsilon^t(c_2^*)) \right) \quad (4.27)$$

where the minimization is carried out over all variables that satisfy $\theta c_1^* + (1 - \theta) c_2^* = c_0$ and where

$$H(\eta) = \eta \cdot \mathbb{C} \eta - G(\eta) \quad (4.28)$$

$$G(\eta) = \dots \quad (4.29)$$

Proof. First we find an **upper bound** by construction. For any given λ and for any given θ, c_1^*, c_2^* that satisfy the constraint, we divide Ω into parallel stripes S_1, S_2, S_3, S_4 of width $\lambda^{-1}, \theta \lambda^{-1/2}, \lambda^{-1}, (1 - \theta) \lambda^{-1/2}$ with normal \mathbf{k} and repeated periodically. Note that this is like a laminate of width $\lambda^{-1/2}$ and volume fraction θ where the layers are separated by interpolation layers of thickness λ^{-1} . We construct a test function c^λ that takes the value c_1^* and c_2^* in the stripes S_2 and S_4 , respectively, while interpolating linearly in the stripes S_1 and S_3 . Note that $c^\lambda \in H^1$, ∇c^λ vanishes on S_2 and S_4 and $\nabla c^\lambda = O(\lambda)$ on S_1 and S_3 . We can easily verify that

$$\int_{\Omega} \frac{\alpha^2}{2\lambda^2} |\nabla c^\lambda|^2 dx = O\left(\frac{1}{\lambda^2} \cdot \lambda^2 \cdot \frac{\lambda^{1/2}}{\lambda}\right) = O(\lambda^{-1/2}) \rightarrow 0. \quad (4.30)$$

Similarly,

$$\int_{\Omega} f(c^\lambda) dx \rightarrow \theta f(c_1^*) + (1 - \theta) f(c_2^*). \quad (4.31)$$

Finally, the elastic energy tends to that of a laminate of materials with eigenstrain $c_1^*\eta$ and $c_2^*\eta$.

The energy of such a laminate is given by Kohn (1991) to be

$$\frac{1}{2}\theta(1-\theta)(c_1^* - c_2^*)^2 h(\eta, \mathbf{k}) \quad (4.32)$$

where

$$h(\eta, \mathbf{k}) = \eta \cdot \mathbb{C} \eta - g(\eta, \mathbf{k}) \quad (4.33)$$

$$g(\eta, \mathbf{k}) = \dots \quad (4.34)$$

Putting these together, we have shown that

$$\min_{\mathcal{A}} E^\lambda \leq E^\lambda[c^\lambda, U_{c^\lambda}] \rightarrow \theta f(c_1^*) + (1-\theta)f(c_2^*) + \frac{1}{2}\theta(1-\theta)(c_1^* - c_2^*)^2 h(\eta, \mathbf{k}). \quad (4.35)$$

We obtain the desired upper bound by optimizing over θ, c_1^*, c_2^* , and \mathbf{k} .

We now turn to the **lower bound**. Given the non-negativity of the interfacial energy as well as the fact that increasing the admissible function makes a lower bound, we see

$$\lim_{\lambda \rightarrow \infty} \min_{\mathcal{A}} E^\lambda \geq \inf_{\mathcal{A}'} \int_{\Omega} \left\{ f(C) + \frac{1}{2}(\epsilon - \epsilon^t) \cdot \mathbb{C}(\epsilon - \epsilon^t) \right\} dx_0 =: L \quad (4.36)$$

where

$$\mathcal{A}' := \{ \{c, \mathbf{u}\} : c \in L^2(\Omega, \mathbb{R}), \mathbf{u} \in H^1(\Omega, \mathbb{R}^3), \langle c \rangle = c_0, \langle \mathbf{u} \rangle = 0, \langle \nabla \mathbf{u} - \nabla \mathbf{u}^T \rangle = 0 \}. \quad (4.37)$$

Since f is the minimum of two quadratic wells, we can follow Kohn and rewrite the right-hand side

of (4.36) as

$$L = \inf_{c, \mathbf{u}, \chi} \int_{0, T} \frac{1}{2} |c(\mathbf{x}) - \chi(\mathbf{x})c_1 - (1 - \chi(\mathbf{x}))c_2|^2 + \frac{1}{2} (\mathbf{e}(\mathbf{u}(\mathbf{x})) - c(\mathbf{x})\eta) \cdot \mathbb{C}(\mathbf{e}(\mathbf{u}(\mathbf{x})) - c(\mathbf{x})\eta). \quad (4.38)$$

Taking the Fourier transform of c, \mathbf{u}, χ and using Plancherel's formula, the problem of our interest may be rewritten as

$$\begin{aligned} L = \inf_{\hat{c}, \hat{\mathbf{u}}, \hat{\chi}} \sum_{\mathbf{k}} \frac{1}{2} & |\hat{c}(\mathbf{k}) - \hat{\chi}(\mathbf{k})c_1 - (\delta(\mathbf{k}) - \hat{\chi}(\mathbf{k}))c_2|^2 \\ & + \frac{1}{2} (i\mathbf{k} \odot \hat{\mathbf{u}}(\mathbf{k}) - \hat{c}(\mathbf{k})\eta) \cdot \mathbb{C}(i\mathbf{k} \odot \hat{\mathbf{u}}(\mathbf{k}) - \hat{c}(\mathbf{k})\eta). \end{aligned} \quad (4.39)$$

Minimizing with respect to $\hat{\mathbf{u}}(\mathbf{k})$ for each $\mathbf{k} \neq 0$,

$$\hat{\mathbf{u}}(\mathbf{k}) = i\hat{c}(\hat{\mathbf{G}}^{-1}, \mathbf{s}\mathbf{k}) \quad \text{or} \quad \hat{\mathbf{u}}_p(\mathbf{k}) = i\hat{c} \hat{G}_{pj}^{-1} s_{jl} k_l, \quad (4.40)$$

so

$$\hat{u}_{p,q}(\mathbf{k}) = -\hat{c} \hat{G}_{pj}^{-1} s_{jl} k_l k_q \quad (4.41)$$

where $\hat{G}_{pj} = \mathbb{C}_{pmjn} k_m k_n$, $s_{jl} = -\mathbb{C}_{jlmn} \eta_{mn}$. The case $k = 0$ is simple. Substituting this back,

$$\begin{aligned} L = \min_{\theta} \frac{D}{2} & |c_0 - \theta c_1 - (1 - \theta)c_2|^2 \\ & + \inf_{\hat{\chi}} \sum_{\mathbf{k} \neq 0} \inf_{\hat{c}(\mathbf{k})} \frac{1}{2} |\hat{c}(\mathbf{k}) - \hat{\chi}(\mathbf{k})c_1 - (\delta(\mathbf{k}) - \hat{\chi}(\mathbf{k}))c_2|^2 + \frac{1}{2} \hat{c}^2(\eta \mathbb{C} \eta - A(\mathbf{k})) \end{aligned} \quad (4.42)$$

where $\theta = \hat{\chi}(0)$ and

$$A(\mathbf{k}) = (\mathbf{s}\mathbf{k}, \hat{\mathbf{G}}^{-1}\mathbf{s}\mathbf{k}) = (\mathbf{k}, \mathbf{s}\hat{\mathbf{G}}^{-1}\mathbf{s}\mathbf{k}) = s_{ij}k_j \hat{G}_{ip}^{-1} s_{pt} k_t. \quad (4.43)$$

We note that $A(\mathbf{k}) = A(\frac{\mathbf{k}}{|\mathbf{k}|})$ as all matrix elements of the operator $\hat{\mathbf{G}}^{-1}(\mathbf{k})$ are proportional to \mathbf{k}^{-2} .

Next we minimize with respect to $\hat{c}(\mathbf{k})$ for each \mathbf{k} . To this end, by differentiation,

$$\hat{c}(\mathbf{k}) - \hat{\chi}(\mathbf{k})c_1 - (\delta(\mathbf{k}) - \hat{\chi}(\mathbf{k}))c_2 + \hat{c}(\mathbf{k})B(\mathbf{k}/|\mathbf{k}|) = 0 \quad (4.44)$$

where

$$B(\mathbf{k}/|\mathbf{k}|) = \eta\mathbf{C}\eta - A(\mathbf{k}/|\mathbf{k}|). \quad (4.45)$$

We conclude

$$\hat{c}(\mathbf{k}) = \frac{\hat{\chi}(c_1 - c_2) + c_2\delta(\mathbf{k})}{1 + B(\mathbf{k}/|\mathbf{k}|)} \quad (4.46)$$

and

$$L = \min_{\theta} \frac{1}{2} |c_0 - \theta c_1 - (1 - \theta)c_2|^2 \quad (4.47)$$

$$\begin{aligned} & + \inf_{\hat{\chi}} \sum_{\mathbf{k}} \frac{1}{2} \left| \frac{\hat{\chi}(c_1 - c_2) + c_2\delta(\mathbf{k})}{1 + B(\mathbf{k}/|\mathbf{k}|)} - \hat{\chi}c_1 - (\delta(\mathbf{k}) - \hat{\chi}(\mathbf{k}))c_2 \right|^2 \\ & \quad \quad \quad + \frac{1}{2} \left| \frac{\hat{\chi}(c_1 - c_2) + c_2\delta(\mathbf{k})}{1 + B(\mathbf{k}/|\mathbf{k}|)} \right|^2 B(\mathbf{k}/|\mathbf{k}|) \\ & = \min_{\theta} \frac{1}{2} |c_0 - \theta c_1 - (1 - \theta)c_2|^2 \quad (4.48) \\ & \quad \quad \quad + \inf_{\hat{\chi}} \sum_{\mathbf{k}} \frac{1}{2} |\hat{\chi}(c_1 - c_2) + c_2\delta(\mathbf{k})|^2 \frac{B(\mathbf{k}/|\mathbf{k}|)}{1 + B(\mathbf{k}/|\mathbf{k}|)}. \end{aligned}$$

We obtain a lower bound, by optimizing over \mathbf{k} :

$$L \geq \min_{\theta} \frac{1}{2} |c_0 - \theta c_1 - (1 - \theta)c_2|^2 \quad (4.49)$$

$$+ \min_{\mathbf{k} \neq 0} \left(\frac{B(\mathbf{k}/|\mathbf{k}|)}{1 + B(\mathbf{k}/|\mathbf{k}|)} \right) \inf_{\tilde{\chi}} \sum_{\mathbf{k}} \frac{1}{2} |\hat{\chi}(c_1 - c_2) + c_2 \delta(\mathbf{k})|^2.$$

Now use Plancherel's formula again. We obtain,

$$L \geq \frac{1}{2} |c_0 - \theta c_1 - (1 - \theta)c_2|^2 \quad (4.50)$$

$$+ \min_{\mathbf{k} \neq 0} \left(\frac{B(\mathbf{k}/|\mathbf{k}|)}{1 + B(\mathbf{k}/|\mathbf{k}|)} \right) \frac{1}{2} \theta (1 - \theta) (c_1 - c_2)^2.$$

We use the identity

$$|c_0 - \theta c_1 - (1 - \theta)c_2|^2 = \theta (c_0 - c_1)^2 + (1 - \theta)(c_0 - c_2)^2 - \theta(1 - \theta)(c_1 - c_2)^2, \quad (4.51)$$

and rewrite the lower bound as

$$L \geq \min_{\theta} \left(\frac{\theta}{2} (c_0 - c_1)^2 + \frac{1 - \theta}{2} (c_0 - c_2)^2 \right. \quad (4.52)$$

$$\left. + \frac{1}{2} \theta (1 - \theta) (c_1 - c_2)^2 \left(\min_{\mathbf{k} \neq 0} \left(\frac{B(\mathbf{k}/|\mathbf{k}|)}{1 + B(\mathbf{k}/|\mathbf{k}|)} \right) - 1 \right) \right).$$

The result follows by an identity of Kohn.

4.4 Thin film limit

Consider $\Omega_h := S \times (0, h)$ where $h \ll 1$ is a measure of the film thickness, which we assume constant, and S is a suitable domain in R^2 with area A .

$$E = \int_{\Omega_h} \left\{ \frac{\alpha^2}{2} |\nabla c|^2 + f(c) + \frac{1}{2} (\epsilon - \epsilon^t) \cdot \mathbb{C}(\epsilon - \epsilon^t) \right\} d\Omega_h \quad (4.53)$$

Let L denote the diameter of the cross section S . We have different length scales as:

- 1— Intrinsic scales (i.e., depending only on the material): α .
- 2— Extrinsic scales (i.e., depending only on the sample geometry): h and L .

A rich behavior and pattern formation on intermediate scales is expected due to the multi-scale, non-convex, and nonlocal nature of the problem.

We can study different regimes:

- a) Thin film: $h \rightarrow 0$, $\alpha = \text{fixed}$.
- b) Thin but relatively large film: $h \rightarrow 0$, $\alpha \rightarrow 0$.

Here, we only consider the first case. Our goal is to recover a reduced theory which reproduces the following gross features of experimental observations: $(c(\mathbf{x}), \epsilon(\mathbf{u}(\mathbf{x})))$ does not depend on the thickness direction x_3 , $\epsilon(\mathbf{u}(\mathbf{x}))$ has no out-of-plane component, and $\sigma(x) = \mathbb{C}(\epsilon - \epsilon^t)(\mathbf{x})$ is divergence-free in the absence of an external field.

We rescale the thin film Ω_h into a reference body Ω wherein all characteristic dimensions are of order 1. Without loss of generality we choose the reference domain to be a cylinder of unit height

and cross-section S of area $A = 1$, $\Omega := S \times (0, 1)$.

$$X_1 = x_1, \quad X_2 = x_2, \quad X_3 = \frac{1}{h}x_3 \quad (4.54)$$

$$C(X) = c(x) \quad (4.55)$$

$$\nabla c(x) = C_{,\alpha}(X) \otimes e^p + \frac{1}{h}C_3 \otimes e^3, \quad \alpha = 1, 2 \quad (4.56)$$

Energy per unit thickness is

$$E^h = \frac{E}{h} = \frac{1}{h} \int_{h\Omega} \left\{ \frac{\alpha^2}{2} (|\nabla_p C|^2 + \frac{1}{h^2} |C_{,3}|^2) + f(C) + W(\epsilon(u), C) \right\} h d\Omega \quad (4.57)$$

$$E^h = \int_{\Omega} \left\{ \frac{\alpha^2}{2} (|\nabla_p C|^2 + \frac{1}{h^2} |C_{,3}|^2) + f(C) + W(\epsilon(u), C) \right\} d\Omega. \quad (4.58)$$

Theorem 4.4.1 *If $c^h \rightarrow c$ in L^2 then $W(c^h, \mathbf{u}_{c^h}) \rightarrow W(c, \mathbf{u}_c)$.*

Proof.

This is proved as part of the existence Theorem 1.1. Here we only specialize it to the thin film limit. Consider the equilibrium equations:

$$\nabla \cdot \mathbb{C}(\epsilon - \epsilon^t) = 0, \quad (4.59)$$

or equivalently, defining $\sigma(r) = \mathbb{C}(\epsilon(r) - \epsilon^t(r))$, $\mathbf{r} = (x, y, z)$, in the scaled domain Ω , for every

$[c^h, \epsilon(u_{c_h})]$ we have

$$\sigma_{xx,x}^h + \sigma_{xy,y}^h + \frac{1}{h}\sigma_{xz,z}^h = 0 \quad (4.60)$$

$$\sigma_{yx,x}^h + \sigma_{yy,y}^h + \frac{1}{h}\sigma_{yz,z}^h = 0 \quad (4.61)$$

$$\sigma_{zx,x}^h + \sigma_{zy,y}^h + \frac{1}{h}\sigma_{zz,z}^h = 0 \quad (4.62)$$

as $h \rightarrow 0$ this set of equations requires that

$$\sigma_{xz,z}^h \rightarrow 0 \quad \sigma_{yz,z}^h \rightarrow 0 \quad \sigma_{zz,z}^h \rightarrow 0 \quad (4.63)$$

$$\frac{1}{h}\sigma_{xz,z}^h \rightarrow d_1 \quad \frac{1}{h}\sigma_{yz,z}^h \rightarrow d_2 \quad \frac{1}{h}\sigma_{zz,z}^h \rightarrow d_3 \quad (4.64)$$

where in the case of stress free boundary conditions

$$\sigma_{xz}^h(\mathbf{r}) \rightarrow 0 \quad \sigma_{yz}^h(\mathbf{r}) \rightarrow 0 \quad \sigma_{zz}^h(\mathbf{r}) \rightarrow 0. \quad (4.65)$$

So we see that our elastic energy will be of a plane stress form. This will result in:

$$c^h(\mathbf{x}) \rightarrow c(\mathbf{x}) \quad \text{with } c_{,3} = 0 \implies W(c^k, \mathbf{u}_{c^k}) \rightarrow W_{2D}(c, \mathbf{u}_c) \quad (4.66)$$

where

$$\sigma^{2D} = \mathbb{C}_{pl\ stress}^{2D}(\epsilon - \epsilon^t)^{2D} \quad (4.67)$$

$$W_{2D}(c, \mathbf{u}_c) = (\epsilon(\mathbf{u}_c) - \epsilon^t(c))_{\alpha\beta}^{2D} \sigma_{\alpha\beta}^{2D} \quad \alpha, \beta \in \{1, 2\}. \quad (4.68)$$

For plates which are very large in two directions and very thin in the third direction, a calculation similar to the one for the 3D case of laminates shows that, $g(\eta)$ for the isotropic case can be simplified as

$$g(\eta) = (\kappa - \mu)(\eta_1 + \eta_2)^2 + 2\mu(\eta_1^2 + \eta_2^2); \quad \text{if } \eta_1\eta_2 \leq 0 \quad (4.69)$$

$$g(\eta) = \frac{\mu^2}{\kappa + \mu} \left(\frac{\kappa}{\mu} |\eta_1 + \eta_2| + |\eta_1 - \eta_2| \right)^2; \quad \text{otherwise} \quad (4.70)$$

where η_1, η_2 are the in-plane eigenvalues of η .

Theorem 4.4.2 *Let c^h, \mathbf{u}^h be a minimizer of $E^h(c, \mathbf{u})$:*

$$E^h(c, \mathbf{u}) = \int_{\Omega} \left\{ \frac{\alpha^2}{2} (|\nabla_p c|^2 + \frac{1}{h^2} |c_{,3}|^2) + f(c) + W(\epsilon(\mathbf{u}), c) \right\} d\Omega. \quad (4.71)$$

Then

$$\lim_{h \rightarrow 0} \min_{\mathcal{A}} E^h = \min_{c, u} \int_{\Omega} \left\{ \frac{\alpha^2}{2} (|\nabla_p c|^2 + f(c) + W_{2D}(c, u_c)) \right\} \quad (4.72)$$

where $c(x_1, x_2, x_3) = c(x_1, x_2)$, i.e., $c_{,3} = 0$, and $u_1(x_1, x_2, x_3) = u_1(x_1, x_2)$, $u_2(x_1, x_2, x_3) = u_2(x_1, x_2)$, $u_3(x_1, x_2, x_3) = 0$.

Proof.

We first note that for a minimizing sequence

$$E^h[c^h, \mathbf{u}^h] \leq C \quad (4.73)$$

so that

$$\int |\nabla_p c^h|^2 \leq C, \quad \int \left| \frac{1}{h} c_{,3}^h \right|^2 \leq C, \quad \int f(c^h) \leq C, \quad (4.74)$$

so

$$\nabla_p c^h \rightharpoonup \nabla_p c, \quad \frac{1}{h} c_{,3}^h \rightharpoonup d, \quad c^h \rightharpoonup c \quad \text{in } L^2. \quad (4.75)$$

From here we have

$$c_{,3}^h \rightarrow c_{,3} = 0 \quad \text{in } L^2, \quad c^h \rightarrow c \quad \text{in } H^1. \quad (4.76)$$

From the weak convergence of gradients

$$\nabla_p c^h = \nabla_p c + a_p^h, \quad a_p^h \rightharpoonup 0 \quad \text{in } L^2 \quad (4.77)$$

$$\frac{1}{h} c_{,3}^h = d + a_p^{(3)}, \quad a_p^{(3)} \rightharpoonup 0 \quad \text{in } L^2. \quad (4.78)$$

Next, we want to make these two weak convergences strong. To do this we compare the energy of $E[c^h, \mathbf{u}^h]$ to $E[c, \mathbf{u}]$. [We note that if $c(\mathbf{x})$ is not smooth enough we can introduce $\tilde{c}_\delta(\mathbf{x}) \in C^\infty$, independent of x_3 , with $\tilde{c}_\delta(\mathbf{x}) \rightarrow c(\mathbf{x})$ in L^2 . Then doing the following calculations for an arbitrary δ and passing $\delta \rightarrow 0$ at the end we can get the results.]

Using that c^h is a minimizing sequence and $c_{,3}(\mathbf{x}) = 0 \implies c_{,3}/h = 0$, we have

$$\int_{\Omega} \left\{ \frac{\alpha^2}{2} (|\nabla_p c^h|^2 + \frac{1}{h^2} |c_{,3}^h|^2) + f(c^h) + W(c^h, \mathbf{u}_{c^h}) \right\} \leq \int_{\Omega} \left\{ \frac{\alpha^2}{2} |\nabla_p c|^2 + f(c) + W(c, \mathbf{u}_c) \right\}. \quad (4.79)$$

First, we note that as $c^h \rightarrow c$ we have $\int f(c^h) \rightarrow \int f(c)$.

Second, in the proof of existence theorem we showed that for every given $c^h(\mathbf{x})$ we can find $u^h(\mathbf{x})$ as a function of $c^h(\mathbf{x})$ by minimizing the elastic energy. Now, from the previous theorem, if $c^h \rightarrow c$ then $W(c^k, \mathbf{u}_{c^k}) \rightarrow W_{2D}(c, \mathbf{u}_c)$, so we can write

$$\int_{\Omega} \left\{ \frac{\alpha^2}{2} (|\nabla_p c^h|^2 + \frac{1}{h^2} |c_{,3}^h|^2) \right\} \leq \int_{\Omega} \left\{ \frac{\alpha^2}{2} |\nabla_p c|^2 + O(h) \right\}, \quad (4.80)$$

so

$$\int_{\Omega} \left\{ \frac{\alpha^2}{2} (|\nabla_p c + a_p^h|^2 + \frac{1}{h^2} |c_{,3}^h|^2) \right\} \leq \int_{\Omega} \left\{ \frac{\alpha^2}{2} |\nabla_p c|^2 + O(h) \right\}, \quad (4.81)$$

then

$$\int_{\Omega} \left\{ (|\nabla_p c|^2 + |a_p^h|^2 + 2\nabla_p c a_p^h + \frac{1}{h^2} |c_{,3}^h|^2) \right\} \leq \int_{\Omega} \left\{ |\nabla_p c|^2 + O(h) \right\}. \quad (4.82)$$

Note that $a_p^h \rightarrow 0$ in L^2 , so $\int \nabla_p c a_p^h \rightarrow 0$. So we get

$$\int_{\Omega} |a_p^h|^2 + \frac{1}{h^2} |c_{,3}^h|^2 \rightarrow 0, \quad (4.83)$$

that is

$$\int_{\Omega} |a_p^h|^2 \rightarrow 0, \quad \int_{\Omega} \frac{1}{h^2} |c_{,3}^h|^2 \rightarrow 0, \quad (4.84)$$

and

$$a_p^h \rightarrow 0 \implies \nabla_p c^h \rightarrow \nabla_p c \text{ in } L^2 \quad (4.85)$$

$$\frac{1}{h} c_{,3}^h \rightarrow 0 \text{ in } L^2. \quad (4.86)$$

From there we can write

$$E^h \rightarrow E_{thin} = \int_{\Omega} \left\{ \frac{\alpha^2}{2} (|\nabla_p c|^2 + f(c) + W_{2D}(c, \mathbf{u}_c)) \right\}, \quad (4.87)$$

where $c(\mathbf{x})$ only depends on the plane coordinates, $c_{,3} = 0$.

4.4.1 Transition layers in the thin film limit

Upper bound

To construct an upper bound, consider a film Ω_h of thickness h and width L , bisected by a transition layer of width s^h . We're going to study the dependence of s^h on h . Let c_1, c_2 be two concentrations that minimize the total of electrochemical and elastic energies, that is the large body limit case, further assume ϵ_1 and ϵ_2 are two 3×3 matrices that minimize the elastic energy density corresponding to the c_1, c_2 , $W(\mathbf{G}) \geq W(\epsilon_1) = W(\epsilon_2) = 0$ for all $\mathbf{G} \in M^{3 \times 3}$. Assign $\epsilon = \epsilon_1$ on $\{\mathbf{x} \cdot \mathbf{n} < 0\} \cap \Omega_h$ and $\epsilon = \epsilon_2$ on $\{\mathbf{x} \cdot \mathbf{n} > s^h\} \cap \Omega_h$. Recall the condition of compatibility for a thin film [Bhattacharya, James, 1999]

$$\epsilon_2 - \epsilon_1 = \mathbf{a} \otimes \mathbf{n} + \mathbf{b} \otimes \mathbf{e}_3 \quad \mathbf{n} \cdot \mathbf{e}_3 = 0, \quad |\mathbf{n}| = 1 \quad (4.88)$$

where if $\mathbf{a} \parallel \mathbf{b}$ then there is a continuous but not-smooth interpolation of the deformation which makes the elastic energy in the bulk identically zero, by using a suitable choice of \mathbf{b} and extending the deformations into the transition layer up to an inclined plane in the layer. However if $\mathbf{a} \not\parallel \mathbf{b}$ then every interpolation of layer has a positive elastic energy. Here, we make no assumptions on the compatibility of strains.

A simple interpolation gives

$$c(\mathbf{x}) = \lambda c_I + (1 - \lambda) c_{II} \quad (4.89)$$

and

$$\mathbf{y}(\mathbf{x}) = \lambda(\mathbf{x} \cdot \mathbf{n}) \epsilon_1 \mathbf{x} + (1 - \lambda(\mathbf{x} \cdot \mathbf{n})) (\epsilon_2 \mathbf{x} + \mathbf{D}) \quad (4.90)$$

where $\lambda(s)$ is a smooth transition function,

$$\lambda(s) = 1 \quad s \leq 0 \quad (4.91)$$

$$\lambda(s) = 0 \quad s \geq s^h. \quad (4.92)$$

Further, for upper bound test function, we assume

$$|\lambda'| \leq M_1/s^h. \quad (4.93)$$

We have

$$\nabla c(\mathbf{x}) = \lambda' (c_I - c_{II}). \quad (4.94)$$

By using the thickness of the interface as predicted earlier, we will have

$$\int_{\Omega_h} \frac{\alpha}{2} |\nabla c(x)|^2 dx = \frac{\alpha}{2} (c_I - c_{II})^2 \int_{\Omega_h} |\lambda'|^2 dx \leq \frac{\alpha}{2} (c_I - c_{II})^2 \frac{M_1^2}{(s^h)^2} \int_{\Omega_h} dx = M_2 \alpha L \frac{h}{s^h}. \quad (4.95)$$

The electrochemical energy

$$\begin{aligned} \int_{\Omega_h} f(c) dx &\leq \int_{\Omega_h} d_1 |c(\mathbf{x})|^q + d_2 dx = \int_{\Omega_h} d_1 |c(\mathbf{x})|^q dx + \int_{\Omega_h} d_2 dx \\ &\leq d_1 c_2^q h s^h L + d_2 h s^h L = d_3 h s^h L \end{aligned} \quad (4.96)$$

where we have assumed $c_2 > c(\mathbf{x}) > c_1$ without loss of generality.

The elastic energy of the test function

$$\begin{aligned} \int_{\Omega_h} W dx &= \int_{\Omega_h} \frac{1}{2} (\epsilon(\mathbf{x}) - c(\mathbf{x})\eta) \cdot \mathbb{C} (\epsilon(\mathbf{x}) - c(\mathbf{x})\eta) dx \leq \frac{1}{2} \eta \cdot \mathbb{C} \eta \int_{\Omega_h} c^2(\mathbf{x}) dx \\ &\leq \frac{c_2^2}{2} \eta \cdot \mathbb{C} \eta \int_{\Omega_h} dx = \frac{c_2^2}{2} \eta \cdot \mathbb{C} \eta \quad h s^h L. \end{aligned} \quad (4.97)$$

The total energy will be

$$E \leq M_2 \alpha L \frac{h}{s^h} + d_3 h s^h L + \frac{c_2^2}{2} \eta \cdot \mathbb{C} \eta \quad h s^h L. \quad (4.98)$$

Now, optimizing the right-hand side with respect to s^h , we see that s^h is independent of h for

$h \ll 1$.

$$s^h = \sqrt{\alpha} \sqrt{\frac{2M_2}{2d_3 + c_2^2 \eta \cdot \mathbb{C} \eta}} \quad (4.99)$$

Substituting for s^h , we get the following upper bound on the energy of the transition layer

$$E \leq 2hL\sqrt{\alpha}\sqrt{M_2}\sqrt{d_3 + \frac{1}{2}c_2^2 \eta\mathbb{C}\eta}. \quad (4.100)$$

We note that transition layer has energy no less than order h , we do this by finding a lower bound as follows

$$E = \int_{\Omega_h} \frac{\alpha}{2} |\nabla c(\mathbf{x})|^2 + g(c, \mathbf{u}_c) dx \geq \int_{\Omega_h} \frac{\alpha}{2} \left| \frac{\partial c(\mathbf{x})}{\partial x_1} \right|^2 + g(c, \mathbf{u}_c) dx \quad (4.101)$$

$$\geq \int_{\Omega_h} \sqrt{\alpha} \left| \frac{\partial c(x)}{\partial x_1} \right| \sqrt{g(c, \mathbf{u}_c)} dx = hL \int_c \sqrt{\alpha} \sqrt{g(c, \mathbf{u}_c)} dc, \quad (4.102)$$

where we have used $a^2 + b^2 \geq 2ab$, and $c_2 \geq c(x) \geq c_1 \implies \frac{\partial c(\mathbf{x})}{\partial x_1} \geq 0$.

$$E \geq \sqrt{\alpha}hL \int_c \sqrt{g(c, \mathbf{u}_c)} dc \geq \sqrt{\alpha}hL \int_c \sqrt{f(c)} dc \quad (4.103)$$

$$\geq \sqrt{\alpha}hL \int_c \sqrt{b_1|c|^p + b_2} dc \geq \sqrt{\alpha}\sqrt{b_2}hL(c_2 - c_1) \quad (4.104)$$

That is

$$E \geq hL\sqrt{\alpha}\sqrt{b_2}(c_2 - c_1). \quad (4.105)$$

4.5 Conclusion

1— Our results show that in the small particle limit the material should be of uniform concentration in the whole particle. This means that nano particles smaller than a critical size should

show be completely lithiated, $Li_{1-y}FePO_4$, $y \sim 1$, or completely delithiated, Li_xFePO_4 , $x \sim 0$, and as the elastic energy barrier and interfacial energy barrier are zero, any reaction, including the unwanted secondary reactions, should happen very fast. Our results are consisted with the experiments of Delmas (2008). We think the solid solution behavior, as reported by Yet-Ming Chinag and co-workers and other groups, can be due to the fact that at each stage they are many particles whit $x \sim 0$, $y \sim 1$, which results in the overall behavior of any combination of them, and this explains the confusion of mistaking the behavior with the the false solid solution in any particle.

2— In the large body limit, our study suggests that the material should show laminates of completely lithiated or delithiated phases, which is observed experimentally, by Chen and Richardson (2006), and other groups.

3— For thin flat films, the concentration profile in each particle is constant in the thickness, which is observed experimentally, by Chen and Richardson (2006), and other groups. In this case the elastic and surface energy barriers are less than the large body limit, however are higher than that of nano-particles, and show good rate of charge/discharge, as observed experimentally.

4.6 References

1. R. O. Williams, Long-Period superlattices in the copper-gold system as two-phase mixtures. Metall. Trans. 11 A (1980) 247-253.
2. Larche, J. W. Cahn, 1984, The Interactions of Composition and Stress in Crystalline Solids.
3. R. O. Williams : The calculation of coherent phase equilibria. CALPHAD 8 (1984) 1-14.

4. R.V. Kohn, The relaxation of a double-well energy, *Continuum mechanics and thermodynamics*, 3 (1991) 193-236.
5. T. Mura, T. Koya, *Variational methods in mechanics*, 1992, Oxford.
6. J De Simone, *ARMA*, 1993, Magnetic.
7. G. Gioia R.D. James, Micromagnetics of very thin films. *Proc. R. Soc. Lond. A* (1997) 453, 213-223.
8. K. Bhattacharya, R.D. James, *JMPS*, 1999, Thin Films.
9. J. De Simone, *JMPS*, 2002, Constraint Theory.
10. K. Bhattacharya, *Microstructure of Martensite* (2003).

Chapter 5

General Continuum Mechanics of Elasto-Electro-Chemical Systems with Moving Boundaries

5.1 Introduction

We model elasto-electro-chemical systems such as conductors, electrodes, and electrolytes near an equilibrium as non-polarizable semiconductors. Effect of heat and temperature changes are skipped in this work. Conductors are modeled as an extreme case of semiconductors in which the charges move extremely fast, such that the charges move so fast to reach the boundaries that no charge can stay inside the material, and thus the electric field inside the material is zero. This easiness of charge passage in a conductor is also accountable to explain why no electric field can exist inside a Faraday's cage either.

In a metal, there are interactions between the electrons and the lattice vibration. Also there are collisions between electrons with impurity atoms or with local distortions or defects of the crystal. Therefore each electron in motion changes its direction of propagation with an average period of 2τ . Assume an applied electric field while keeping all other state parameters constant. The acceleration

of each electron due to an applied electric field E is eE/m_0 . Thus the velocity increment of the electron during a time period of 2τ is $2\tau eE/m_0$, and its time average is $\tau eE/m_0$. Assuming that the velocity change before a collision is not maintained after the collision, then the electron current density due to the electric field is the product of the electric density, ne , and the average velocity $\bar{v} = \tau eE/m_0$,

$$J = ne^2\tau/m_0E = \sigma E \quad (5.1)$$

where n is the density of the electrons. σ is called the electric conductivity. It is seen that in a perfect conductor as the crystal is free of defects and impurities, $\tau \rightarrow \infty$, so that $\sigma \rightarrow \infty$. The situation gets complicated when the material is not a perfect conductor or a perfect isolator. It is even much more complicated when other state parameters, like temperature or chemical concentrations, change in addition to the electric field.

Introducing space charges and ions density as field (state) variables in addition to deformation, a continuum theory of elasto-electro-chemical systems is developed. We consider fixed and moving (first-order phase transformation) boundaries. We assume that no polarization, isothermal conditions, absence of externally applied magnetic field and spontaneous magnetization, or temperature changes.

5.2 Kinematics

Consider a body in an external electric field, which occupies region $\Omega \subset \mathfrak{R}^3$, in the reference configuration (control volume). Assume that an invertible deformation $\mathbf{y} : \Omega \rightarrow \mathfrak{R}^3$ brings the body to the proximity of a conductor $C_v \subset \mathfrak{R}^3$ with fixed potential $\hat{\phi}$ under the action of traction \mathbf{t} .

The deformation gradient is $\mathbf{F} = \nabla_{\mathbf{x}}\mathbf{y}$, and $J = \det\mathbf{F} > 0$ almost everywhere in Ω . We further assume that the conductor C_v is very thin such that it deforms with the body with negligible elastic energy. Here the dot on a quantity, $\dot{\xi}$, denotes the material derivative

$$\dot{\xi}(y(x, t), t) = \frac{d\xi}{dt} = \frac{\partial\xi(y, t)}{\partial t} + \nabla_y\xi(y, t) \cdot \frac{dy(x, t)}{dt} \quad (5.2)$$

where d/dt is defined as $\partial/\partial t|_{y=x}$. We call $\dot{\xi} = \partial\xi(y, t)/\partial t = \partial\xi(y, t)/\partial t|_y$ the spatial time derivative of ξ .

5.3 Deformable solids with mass transport

5.3.1 Conservation of mass

From the Reynolds transport theorem, we get the conservation of mass for an arbitrary volume control Ω :

$$\begin{aligned} \frac{d}{dt} \int_{\Omega} N_{k0} dx &= \int_{\partial\Omega} N_{k0}(\mathbf{v} - \mathbf{v}_k) \cdot \mathbf{m} dS_x + \int_R R_{k0} dx \\ &= \int_{\partial\Omega} N_{k0}(\mathbf{v} - \tilde{\mathbf{v}}) \cdot \mathbf{m} dS_x - \int_{\partial\Omega} \mathbf{J}_{k0} \cdot \mathbf{m} dS_x + \int_R R_{k0} dx \end{aligned} \quad (5.3)$$

where we are working in the reference configuration. N_{k0} , \mathbf{v}_k , m are the mass density, velocity field of species k , and unit outward normal, respectively, and the diffusion flux of species k is defined by $\mathbf{J}_{k0} = N_{k0}(\mathbf{v}_k - \tilde{\mathbf{v}})$. R_{k0} is the rate of generation of material by electrochemical reactions. The convective velocity, $\tilde{\mathbf{v}}$ is defined as

$$\tilde{\mathbf{v}} = \frac{\sum N_{k0} \mathbf{v}_k}{\sum N_{k0}}. \quad (5.4)$$

When there are discontinuities, Γ , we have

$$\begin{aligned} \frac{d}{dt} \int_{\Omega} N_{k0} dx = & \int_{\partial\Omega} N_{k0} \mathbf{v} \cdot \mathbf{m} dS_x - \int_{\Omega} \nabla_x \cdot (N_{k0} \tilde{\mathbf{v}}) dx \\ & - \int_{\Gamma} [[N_{k0} \tilde{\mathbf{v}}]] \cdot \mathbf{m} dS_x - \int_{\Omega} \nabla_x \cdot \mathbf{J}_{k0} dS_x - \int_{\Gamma} [[\mathbf{J}_{k0}]] \cdot \mathbf{m} dS_x + \int_{\Omega} R_{k0} dx. \end{aligned} \quad (5.5)$$

We note that

$$\frac{d}{dt} \int_{\Omega} N_{k0} dx = \int_{\Omega} \frac{d}{dt} N_{k0} - \int_{\Gamma} [[N_{k0}]] U dS_x \quad (5.6)$$

where U is the speed of discontinuity Γ in the direction of its normal.

In the bulk we will have

$$\frac{dN_{i0}}{dt} = -\nabla_x \cdot (N_{i0} \tilde{\mathbf{v}}) - \nabla_x \cdot \mathbf{J}_{N_{i0}} + R_{i0} \quad (5.7)$$

on the discontinuity

$$- [[N_{i0}]] U = - [[N_{i0} \tilde{\mathbf{v}}]] \cdot \mathbf{m} - [[\mathbf{J}_{N_{i0}}]] \cdot \mathbf{m}. \quad (5.8)$$

When there is no net production of mass $\mathcal{R}_0 = \sum R_{i0} = 0$, we have

$$\frac{d\mathcal{N}_0}{dt} + \nabla_x \cdot (\mathcal{N}_0 \tilde{\mathbf{v}}) = 0 \quad (5.9)$$

where $\mathcal{N}_0 = \sum N_{i0}$.

For simplicity we assume that the convective velocity and rate of generation of each species are

zero, $\tilde{\mathbf{v}} = 0$ and $R_k = 0$, we will have

$$\dot{N}_{i0} = \frac{dN_{i0}}{dt} = -\nabla_x \cdot \mathbf{J}_{N_{i0}}, \quad (5.10)$$

and

$$[[N_{i0}]]U = [[\mathbf{J}_{i0}]] \cdot \mathbf{m} \quad (5.11)$$

where u and \mathbf{n} are the counterparts of U and \mathbf{m} in the current configuration.

5.4 Electrostatics

5.4.1 Space charge density

At any point in the system in the current configuration, assume N_i to be the density of ions of i^{th} species (number per unit deformed volume), z_i its valency, and e the coulomb charge per electron.

We denote electronic current by q and the ionic conductivity by $z_i N_i$, then the total charge density is

$$\rho = e \sum z_i N_i + q. \quad (5.12)$$

In the reference configuration, the counterpart of N_i , is defined as N_{i0} (number per unit undeformed volume), then the charge density in the reference configuration is

$$\rho_0 = e \sum z_i N_{i0} + q_0, \quad (5.13)$$

where q_0 stands for charge carried by electrons. We will assume summation over repeated small indices, and will not put the \sum from now on. Similar to what we did for the mass density, we can do for the electrical charges:

$$\frac{\partial \rho}{\partial t} = -\nabla_y \cdot \mathbf{J}_\rho \quad (5.14)$$

and

$$[[\rho]]\mathbf{u} = [[\mathbf{J}_\rho]] \cdot \mathbf{n}. \quad (5.15)$$

In the reference configuration we have

$$\dot{\rho}_0 = -ez_i \nabla_{\mathbf{x}} \mathbf{J}_{N_{i0}} + \dot{q}_0 = -\nabla_{\mathbf{x}} \cdot \mathbf{J}_{\rho 0} \quad (5.16)$$

and

$$[[\rho_0]]\mathbf{U} = [[\mathbf{J}_{\rho 0}]] \cdot \mathbf{m}. \quad (5.17)$$

That is, the total electric charge of an isolated system remains constant regardless of changes within the system itself. The conservation of charge results in the charge-current continuity equation. More generally, the net change in charge density \mathbf{J}_ρ within a volume of integration Ω is equal to the area integral over the current density \mathbf{J}_ρ on the surface of the area $\partial\Omega$, which is in turn equal to the net current I :

$$-\frac{\partial}{\partial t} \int_{\Omega} \rho dV = \int_{\partial} \Omega \mathbf{J}_\rho \cdot \mathbf{n} d\mathbf{S} = I. \quad (5.18)$$

Thus, the conservation of electric charge, as expressed by the continuity equation, gives the result:

$$I = -\frac{dQ}{dt} \quad (5.19)$$

where I is the net outward current through a closed surface and Q is the electric charge contained within the volume defined by the surface. The charge transferred between time t_0 and t is obtained by integrating both sides:

$$Q = -\int_{t_0}^{t_f} I dt. \quad (5.20)$$

5.4.2 Electric field

The space charges in the body as well as the charges on the surfaces of conductors generate an electro-magnetic field in all space. In electrolyte solutions, the presence of diffusion causes certain phenomena which do not occur in solid conductors. At any point in \mathfrak{R}^3 we have

$$\nabla_{\mathbf{y}} \cdot (\epsilon_0 \nabla_{\mathbf{y}} \phi) = -\rho \chi(y(\Omega, t)) \quad \text{in} \quad R^3 \setminus C_v \quad (5.21)$$

$$\nabla_{\mathbf{y}} \phi = 0 \quad \text{on} \quad C_v \quad (5.22)$$

subject to

$$\phi = \hat{\phi} \quad \text{on} \quad C_v \quad (5.23)$$

and

$$\phi \rightarrow 0 \quad \text{as} \quad |\mathbf{y}| \rightarrow \infty \quad (5.24)$$

where $\epsilon_0 = 8.854 \times 10^{-12} \text{ C}^2/\text{Nm}^2$ is the permittivity of the free space, and $\chi(D)$ is the characteristic function of domain D . ϕ is the flux of the electric field through some surface, not necessarily closed.

In the integral form of Maxwell's equation, it can be shown that for each $\psi \in H^1(\mathbb{R}^3)$, $\phi \in H^1(\mathbb{R}^3)$ satisfies the following:

$$\int_{\mathbb{R}^3} (\epsilon_0 \nabla_{\mathbf{y}} \phi) \cdot \nabla_{\mathbf{y}} \psi d\mathbf{y} = \int_{\mathbf{y}(\Omega)} \rho \psi d\mathbf{y} + \int_{\partial C_v} \sigma \psi dS_{\mathbf{y}} \quad (5.25)$$

$$\phi = \hat{\phi} \quad \text{on} \quad C_v \quad (5.26)$$

and from the first and the last equations we have the conservation of charge.

5.4.3 Discontinuities in the electric field

Although ϕ is continuous in \mathbb{R}^3 , other quantities like $\nabla_{\mathbf{y}} \phi$ can be discontinuous across some interfaces, so we need to discuss the jump conditions in a more general setting. In particular, we are interested in time-dependent processes that influence the dissipation rate. We note that the deformation \mathbf{y} could depend on time, and we solve Maxwell's equations at each time to find the electric potential.

Consider any arbitrary curve $\hat{\mathbf{y}}(\alpha)$ on the interface at time t_0 parameterized by α . We have,

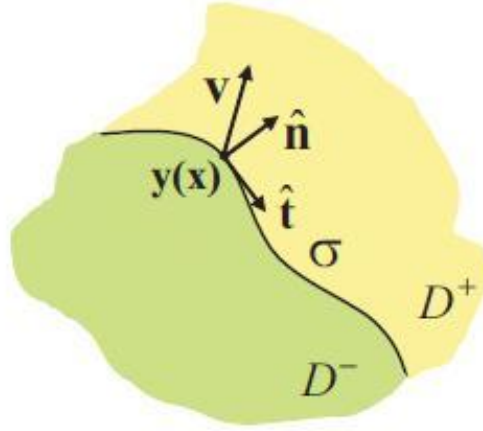


Figure 5.1: A discontinuity separating two regions. Each region can have different elastic or electric behavior. (Xiao and Bhattacharya, 2008)

from the continuity of ϕ ,

$$\phi^-(\hat{\mathbf{y}}(\alpha)) = \phi^+(\hat{\mathbf{y}}(\alpha)). \quad (5.27)$$

Differentiating it with respect to α , we have

$$[[\nabla_{\mathbf{y}}\phi]] \cdot \frac{\partial \hat{\mathbf{y}}}{\partial \alpha} = 0. \quad (5.28)$$

Since this holds for any curve on the interface, we obtain continuity of $\nabla_{\mathbf{y}}\phi$ along the tangent, i.e.,

$$[[\nabla_{\mathbf{y}}\phi]] \cdot \mathbf{t} = 0 \quad \forall \hat{\mathbf{t}} \cdot \hat{\mathbf{n}} = 0. \quad (5.29)$$

So the jump in the electric field can be only in the normal direction to the interface

$$[[\epsilon_0 \nabla_{\mathbf{y}} \phi]] = -\sigma \hat{\mathbf{n}} \quad (5.30)$$

The jump condition across any interface, Γ , separating D^+ and D^- is

$$[[-\epsilon_0 \nabla_{\mathbf{y}} \phi]] \cdot \hat{\mathbf{n}} = \sigma \quad (5.31)$$

where $\sigma : \Gamma \rightarrow \Re$ measurable is the surface charge density on the interface. $\hat{\mathbf{n}}$ is the unit norm of the interface, pointing to D^+ from D^- . The free charge on the boundary, Q_Γ , will be

$$\int_{\Gamma} \sigma dS_y = Q_\Gamma. \quad (5.32)$$

For a fixed boundary, consider a material point \mathbf{x} on the interface. From the continuity of electric potential ϕ we have

$$\phi^-(\mathbf{y}(\mathbf{x}, t), t) = \phi^+(\mathbf{y}(\mathbf{x}, t), t) \quad (5.33)$$

by differentiating with respect to time, we have

$$\dot{\phi}^- = \dot{\phi}^+ \quad or \quad \dot{\phi}^- + \nabla_{\mathbf{y}} \phi^- \cdot \mathbf{v} = \dot{\phi}^+ + \nabla_{\mathbf{y}} \phi^+ \cdot \mathbf{v} \quad (5.34)$$

where, $\dot{\phi}$ denotes the material time derivative of ϕ , and $\acute{\phi}$ denotes the spatial time derivative of ϕ .

Hence,

$$[[\dot{\phi}]] = -[[\nabla_{\mathbf{y}}\phi]] \cdot \mathbf{v} \quad (5.35)$$

where \mathbf{v} is the particle velocity of the material point \mathbf{x}

$$\mathbf{v} = \left. \frac{\partial \mathbf{y}(\mathbf{x}, t)}{\partial t} \right|_{\mathbf{x}}. \quad (5.36)$$

Pulling back the result of the last section, we find

$$[[\epsilon_0 \dot{\phi}_0]] = \sigma(\mathbf{v} \cdot \hat{\mathbf{n}}). \quad (5.37)$$

For a moving boundary, consider a material point \mathbf{x} on the discontinuity. From the continuity of electric potential ϕ we have

$$\phi^-(\mathbf{x}, t) = \phi^+(\mathbf{x}, t). \quad (5.38)$$

where ϕ is the same in both reference and current configurations. By differentiating with respect to time, we have

$$\dot{\phi}^- = \dot{\phi}^+ \quad \text{or} \quad \dot{\phi}^- + \nabla_{\mathbf{x}}\phi^- \cdot \mathbf{V} = \dot{\phi}^+ + \nabla_{\mathbf{x}}\phi^+ \cdot \mathbf{V} \quad (5.39)$$

Hence,

$$[[\dot{\phi}]] = -[[\nabla_{\mathbf{x}}\phi]] \cdot \mathbf{V} \quad (5.40)$$

where \mathbf{V} is the particle velocity of the material point \mathbf{x} , such that $U = \mathbf{V} \cdot \mathbf{m}$. From the last section we find

$$[[-\epsilon_0 \nabla_{\mathbf{x}} \phi]] \cdot \hat{\mathbf{m}} = [[-\epsilon_0 \nabla_{\mathbf{y}} \phi]] \cdot \hat{\mathbf{n}} = \sigma \quad (5.41)$$

so

$$[[-\epsilon_0 \nabla_{\mathbf{x}} \phi]] \cdot \hat{\mathbf{m}} = \sigma \quad (5.42)$$

and from there

$$[[\epsilon_0 \dot{\phi}]] = \sigma(\mathbf{V} \cdot \hat{\mathbf{m}}) = U\sigma. \quad (5.43)$$

5.5 Rate of dissipation of the system

The rate of dissipation of the whole system \mathfrak{D} is defined as the difference between the rate of external working, \mathcal{F} , and the rate of the change of the total energy, $d\mathcal{E}/dt$:

$$\mathfrak{D} = \mathcal{F} - \frac{d\mathcal{E}}{dt}. \quad (5.44)$$

The rate of external working \mathcal{F} includes the mechanical work done by external forces, the electric work done by applying an external field, and chemical and electrical (current) energy fluxes into the system.

The total energy of the system consists of two parts: the energy stored in the material and the

electrostatic field energy generated by external and internal sources, i.e.,

$$\mathcal{E} = \int_{\Omega} W_0 dx + \frac{1}{2} \int_{\mathbb{R}^3} \epsilon_0 |\nabla_y \phi|^2 dy \quad (5.45)$$

where W_0 is the stored energy per unit reference volume in the material and should satisfy frame indifference and material symmetry.

We will divide the dissipation as $\mathfrak{D} = \mathfrak{D}_1 + \mathfrak{D}_2$, where \mathfrak{D}_1 is the elasto-chemical part of the dissipation and \mathfrak{D}_2 is the electrical part of it.

5.6 Elasto-chemical dissipation

$$\mathcal{F}_1 = \int_{y(\partial\Omega)} \mathbf{t} \cdot \mathbf{v} dS_y - \int_{\partial\Omega} \mu_{N_{i0}} \mathbf{J}_{N_{i0}} \cdot \hat{\mathbf{m}} dS_x \quad (5.46)$$

$$\mathcal{E}_1 = \int_{\Omega} W_0 dx \quad (5.47)$$

so we have

$$\mathfrak{D}_1 = \int_{y(\partial\Omega)} \mathbf{t} \cdot \mathbf{v} dS_y - \frac{d}{dt} \int_{\Omega} W_0 dx - \int_{\partial\Omega} \mu_{N_{i0}} \mathbf{J}_{N_{i0}} \cdot \hat{\mathbf{m}} dS_x \quad (5.48)$$

$\mu_{N_{i0}}$ are the chemical potential carried by the flux of the i^{th} ions N_{i0} , $\mathbf{y}(\partial_s\Omega)$ is the part of boundary in the current configuration on which traction, \mathbf{t} , acts. dS_y and dS_x are the differential area in the current and reference configuration, respectively, $\hat{\mathbf{m}}$ the normal to surface in the reference

configuration, and $\hat{\mathbf{n}}$ denotes its counterpart in the current configuration. We will have

$$\mathfrak{D}_1 = \int_{y(\partial\Omega)} \mathbf{t} \cdot \mathbf{v} dS_y - \int_{\Omega} \dot{W}_0 dx + \int_{\Gamma} [[W_0]] U d\Gamma - \int_{\partial\Omega} \mu_{N_{i0}} \mathbf{J}_{N_{i0}} \cdot \hat{\mathbf{m}} dS_x \quad (5.49)$$

using divergence theorem:

$$\begin{aligned} \mathfrak{D}_1 = & \int_{y(\partial\Omega)} \mathbf{t} \cdot \mathbf{v} dS_y - \int_{\Omega} \dot{W}_0 dx + \int_{\Gamma} [[W_0]] U d\Gamma \\ & - \int_{\Omega} \nabla_x \cdot (\mu_{N_{i0}} \mathbf{J}_{N_{i0}}) dS_x - \int_{\Gamma} [[\mu_{N_{i0}} \mathbf{J}_{N_{i0}}]] \cdot \mathbf{m} dS_x \end{aligned} \quad (5.50)$$

from there

$$\begin{aligned} \mathfrak{D}_1 = & \int_{y(\partial\Omega)} \mathbf{t} \cdot \mathbf{v} dS_y - \int_{\Omega} \dot{W}_0 dx + \int_{\Gamma} [[W_0]] U d\Gamma \\ & - \int_{\Omega} \mu_{N_{i0}} \nabla_x \cdot (\mathbf{J}_{N_{i0}}) dS_x - \int_{\Omega} \nabla_x (\mu_{N_{i0}}) \cdot \mathbf{J}_{N_{i0}} dS_x - \int_{\Gamma} [[\mu_{N_{i0}} \mathbf{J}_{N_{i0}}]] \cdot \mathbf{m} dS_x. \end{aligned} \quad (5.51)$$

W_0 is the stored energy per unit reference volume in the material, and should satisfy frame indifference and material symmetry.

We make the constitutive assumption that $W_0 = W_0(\nabla_x \mathbf{y}, N_{i0}, q_0)$, with a possible jump at the phase boundaries, define the deformation gradient, $\mathbf{F} = \nabla_x \mathbf{y}$, we have

$$\int_{\Omega} \dot{W}_0(N_{i0}, \nabla_x \mathbf{y}) dx = \int_{\Omega} \frac{\partial W_0}{\partial N_{i0}} \dot{N}_{i0} dx + \int_{\Omega} \frac{\partial W_0}{\partial q_0} \dot{q}_0 dx + \int_{\Omega} \frac{\partial W_0}{\partial \mathbf{F}} \nabla_x \mathbf{v} dx. \quad (5.52)$$

We will use divergence theorem and push forward to simplify the last term. We also note that

$$\frac{\partial F}{\partial t} = \frac{\partial}{\partial t} \nabla_x \mathbf{y}(\mathbf{x}, t) = \nabla_x \frac{\partial \mathbf{y}}{\partial t} = \nabla_x \mathbf{v}.$$

The elasto-chemical part of dissipation is then

$$\begin{aligned}
\mathfrak{D}_1 = & \int_{y(\partial\Omega)} \mathbf{t} \cdot \mathbf{v} dS_y - \int_{\Omega} \frac{\partial W_0}{\partial N_{i0}} \dot{N}_{i0} dx - \int_{\Omega} \frac{\partial W_0}{\partial q_0} \dot{q}_0 dx + \int_{\Gamma} [[W_0]] U d\Gamma \\
& - \int_{\partial y(\Omega)} \left(\frac{1}{J} \frac{\partial W_0}{\partial \mathbf{F}} \mathbf{F} \mathbf{n} \right) \cdot \mathbf{v} dS_y + \int_{\Gamma} \left[\left[\frac{\partial W_0}{\partial \mathbf{F}} \right] \right] \mathbf{m} \cdot \langle \mathbf{v} \rangle dS_x \\
& - \int_{\Gamma} \left\langle \frac{\partial W_0}{\partial \mathbf{F}} \right\rangle \mathbf{m} \cdot [[\mathbf{F}]] \mathbf{m} U dS_x + \int_{y(\Omega)} \left(\nabla_y \cdot \left(\frac{1}{J} \frac{\partial W_0}{\partial \mathbf{F}} \mathbf{F} \right) \right) \cdot \mathbf{v} dy \\
& - \int_{\Omega} \mu_{N_{i0}} \nabla \cdot (\mathbf{J}_{N_{i0}}) dS_x - \int_{\Omega} \nabla (\mu_{N_{i0}}) \cdot \mathbf{J}_{N_{i0}} dS_x - \int_{\Gamma} [[\mu_{N_{i0}} \mathbf{J}_{N_{i0}}]] \cdot \mathbf{m} dS_x \quad (5.53)
\end{aligned}$$

using the conservation of mass, as stated earlier, we have

$$\begin{aligned}
\mathfrak{D}_1 = & \int_{y(\partial\Omega)} \mathbf{t} \cdot \mathbf{v} dS_y - \int_{\Omega} \frac{\partial W_0}{\partial N_{i0}} \dot{N}_{i0} dx - \int_{\Omega} \frac{\partial W_0}{\partial q_0} \dot{q}_0 dx + \int_{\Gamma} [[W_0]] U d\Gamma \\
& - \int_{\partial y(\Omega)} \left(\frac{1}{J} \frac{\partial W_0}{\partial \mathbf{F}} \mathbf{F} \mathbf{n} \right) \cdot \mathbf{v} dS_y + \int_{\Gamma} \left[\left[\frac{\partial W_0}{\partial \mathbf{F}} \right] \right] \mathbf{m} \cdot \langle \mathbf{v} \rangle dS_x \\
& - \int_{\Gamma} \left\langle \frac{\partial W_0}{\partial \mathbf{F}} \right\rangle \mathbf{m} \cdot [[\mathbf{F}]] \mathbf{m} U dS_x + \int_{y(\Omega)} \left(\nabla_y \cdot \left(\frac{1}{J} \frac{\partial W_0}{\partial \mathbf{F}} \mathbf{F} \right) \right) \cdot \mathbf{v} dy \\
& - \int_{\Omega} \nabla_x \mu_{N_{i0}} \cdot \mathbf{J}_{N_{i0}} dS_x + \int_{\Omega} \mu_{N_{i0}} \dot{N}_{i0} dS_x - \int_{\Gamma} [[\mu_{N_{i0}} \mathbf{J}_{N_{i0}}]] \cdot \mathbf{m} dS_x. \quad (5.54)
\end{aligned}$$

5.7 Electrical dissipation

We idealize C_v as an interface $S_v = \mathbf{y}(S_{v0})$ between the vacuum and the material $\mathbf{y}(\Omega)$ on which the potential is fixed. The interface where $\mathbf{y}(\Omega)$ has direct contact with vacuum is denoted by $S_f = \partial y(\Omega) \setminus S_v$.

$$\mathcal{F}_2 = \hat{\phi} \frac{d}{dt} \int_{y(\partial C_v)} \sigma dS_y - \int_{\partial\Omega} \mu_{\rho_0} \mathbf{J}_{\rho_0} \cdot \hat{\mathbf{m}} dS_x \quad (5.55)$$

$$\mathcal{E}_2 = \frac{1}{2} \int_{\mathbb{R}^3} \epsilon_0 |\nabla_y \phi|^2 dx \quad (5.56)$$

The electrical dissipation is

$$\mathfrak{D}_2 = \hat{\phi} \frac{d}{dt} \int_{y(\partial C_v)} \sigma dS_y - \frac{d}{dt} \frac{1}{2} \int_{\mathfrak{R}^3} \epsilon_0 |\nabla_y \phi|^2 dx - \int_{\partial \Omega} \mu_{\rho_0} \mathbf{J}_{\rho_0} \cdot \hat{\mathbf{m}} dS_x. \quad (5.57)$$

To find the expression for the electric dissipation, we first note that, as the electric energy exists in all space, the calculation of the change of electro-static field energy needs some manipulation. We follow a procedure similar to that used by Xiao and Bhattacharya (2008).

5.7.1 Rate of change of field energy: step 1

From the integral form of Maxwell's equation, by setting $\Psi = \phi$, we have

$$\int_{\mathfrak{R}^3} \epsilon_0 \nabla_y \phi \cdot \nabla_y \phi dy = \int_{y(\Omega)} \phi \rho + \int_{S_v} \hat{\phi} \sigma dS_y \quad (5.58)$$

therefore

$$\begin{aligned} \frac{d}{dt} \int_{\mathfrak{R}^3} \epsilon_0 |\nabla_y \phi|^2 dy &= \frac{d}{dt} \left\{ \int_{y(\Omega)} \phi \rho dy \right\} + \hat{\phi} \frac{d}{dt} \int_{S_v} \sigma dS_y = \\ &= \int_{y(\Omega)} \dot{\phi} \rho dy + \int_{y(\Omega)} \phi \dot{\rho} dy + \hat{\phi} \frac{d}{dt} \int_{S_v} \sigma dS_y - \int_{y(\Gamma)} [[\rho \phi]] \mathbf{v} \cdot \mathbf{n} dS_y \\ &= \int_{y(\Omega)} (\dot{\phi} + \mathbf{v} \cdot \nabla_y \phi) \rho dy + \int_{\Omega} \phi \dot{\rho}_0 dx + \hat{\phi} \frac{d}{dt} \int_{S_v} \sigma dS_y - \int_{\Gamma} [[\rho_0 \phi]] U dS_x \end{aligned} \quad (5.59)$$

where we have used $\rho_o dx = \rho dy$, thus $\rho_o = \rho \det(\mathbf{F})$ in the last equality.

5.7.2 Rate of change of field energy: step 2

By using the Reynold's transport theorem,

$$\begin{aligned}
& \frac{d}{dt} \left(\frac{1}{2} \int_{\mathfrak{R}^3} \epsilon_0 |\nabla_{\mathbf{y}} \phi|^2 dy \right) \\
&= \frac{\epsilon_0}{2} \int_{y(\Omega^+)} \frac{\partial}{\partial t} |\nabla_{\mathbf{y}} \phi|^2 dy + \frac{\epsilon_0}{2} \int_{y(\Omega^-)} \frac{\partial}{\partial t} |\nabla_{\mathbf{y}} \phi|^2 dy - \frac{\epsilon_0}{2} \int_{y(\Gamma)} [|\nabla_{\mathbf{y}} \phi|^2] \mathbf{v} dS_y \\
&+ \frac{\epsilon_0}{2} \int_{\mathfrak{R}^3 \setminus y(\Omega)} \frac{\partial}{\partial t} |\nabla_{\mathbf{y}} \phi|^2 dy - \frac{\epsilon_0}{2} \int_{\partial y(\Omega)} [|\nabla_{\mathbf{y}} \phi|^2] \mathbf{v} \cdot \mathbf{n} dS_y \\
&= \int_{\mathfrak{R}^3} \epsilon_0 \nabla_{\mathbf{y}} \phi \cdot \nabla_{\mathbf{y}} \dot{\phi} dy - \frac{\epsilon_0}{2} \int_{\partial y(\Omega)} [|\nabla_{\mathbf{y}} \phi|^2] \mathbf{v} \cdot \mathbf{n} dS_y - \frac{\epsilon_0}{2} \int_{y(\Gamma)} [|\nabla_{\mathbf{y}} \phi|^2] \mathbf{v} \cdot \mathbf{n} dS_y. \tag{5.60}
\end{aligned}$$

Let $S = \partial y(\Omega)$, then to simplify the first term, we multiply $\dot{\phi}$ on both sides of the differential form of the Maxwell's equation, and integrate over \mathfrak{R}^3 to obtain

$$\int_{y(\Omega)} \rho \dot{\phi} d\mathbf{y} = \int_{\mathfrak{R}^3} \rho \dot{\phi} d\mathbf{y} = - \int_{\mathfrak{R}^3} \nabla_{\mathbf{y}} \cdot (\epsilon_0 \nabla_{\mathbf{y}} \phi) \dot{\phi} d\mathbf{y}. \tag{5.61}$$

The right side can be split to two parts on which divergence theorem can be applied:

$$\begin{aligned}
& \int_{y(\Omega)} \rho \dot{\phi} d\mathbf{y} = \int_{y(\Omega)} \nabla_{\mathbf{y}} \cdot (-\epsilon_0 \nabla_{\mathbf{y}} \phi) \dot{\phi} d\mathbf{y} + \int_{\mathfrak{R}^3 \setminus (y(\Omega))} \nabla_{\mathbf{y}} \cdot (-\epsilon_0 \nabla_{\mathbf{y}} \phi) \dot{\phi} \\
&= \int_{y(\Omega)} \nabla_{\mathbf{y}} \dot{\phi} \cdot (\epsilon_0 \nabla_{\mathbf{y}} \phi) d\mathbf{y} + \int_{\mathfrak{R}^3 \setminus y(\Omega)} \nabla_{\mathbf{y}} \dot{\phi} \cdot (\epsilon_0 \nabla_{\mathbf{y}} \phi) d\mathbf{y} \\
&+ \int_{S^-} \dot{\phi} (-\epsilon_0 \nabla_{\mathbf{y}} \phi) \cdot \hat{\mathbf{n}} dS_y + \int_{S^+} \dot{\phi} (-\epsilon_0 \nabla_{\mathbf{y}} \phi) \cdot (-\hat{\mathbf{n}}) dS_y \\
&+ \int_{y(\Gamma^-)} \dot{\phi} (-\epsilon_0 \nabla_{\mathbf{y}} \phi) \cdot \hat{\mathbf{n}} dS_y + \int_{y(\Gamma^+)} \dot{\phi} (-\epsilon_0 \nabla_{\mathbf{y}} \phi) \cdot (-\hat{\mathbf{n}}) dS_y \\
&= \int_{\mathfrak{R}^3} \epsilon_0 \nabla_{\mathbf{y}} \dot{\phi} \cdot \nabla_{\mathbf{y}} \phi d\mathbf{y} + \int_S [[\dot{\phi}(\epsilon_0 \nabla_{\mathbf{y}} \phi)]] \cdot \hat{\mathbf{n}} dS_y + \int_{y(\Gamma)} [[\dot{\phi}(\epsilon_0 \nabla_{\mathbf{y}} \phi)]] \cdot \hat{\mathbf{n}} dS_y \tag{5.62}
\end{aligned}$$

where S^- , S^+ are the inner and outer surfaces of $y(\Omega)$, respectively. So we will have

$$\int_{\mathbb{R}^3} \epsilon_0 \nabla_{\mathbf{y}} \phi \cdot \nabla_{\mathbf{y}} \dot{\phi} dy = \int_{y(\Omega)} \dot{\phi} \rho dy - \int_S [[\epsilon_0 \dot{\phi} \nabla_{\mathbf{y}} \phi]] \cdot \hat{\mathbf{n}} dS_y - \int_{y(\Gamma)} [[\epsilon_0 \dot{\phi} \nabla_{\mathbf{y}} \phi]] \cdot \hat{\mathbf{n}} dS_y. \quad (5.63)$$

From here we will have

$$\begin{aligned} \frac{d}{dt} \left(\frac{1}{2} \int_{\mathbb{R}^3} \epsilon_0 |\nabla_{\mathbf{y}} \phi|^2 dy \right) &= \int_{y(\Omega)} \dot{\phi} \rho dy - \int_S [[\epsilon_0 \dot{\phi} \nabla_{\mathbf{y}} \phi]] \cdot \hat{\mathbf{n}} dS_y - \int_{y(\Gamma)} [[\epsilon_0 \dot{\phi} \nabla_{\mathbf{y}} \phi]] \cdot \mathbf{n} dy(\Gamma) \\ &- \frac{\epsilon_0}{2} \int_{y(\Gamma)} [|\nabla_{\mathbf{y}} \phi|^2] \mathbf{v} \cdot \hat{\mathbf{n}} dS_y - \frac{\epsilon_0}{2} \int_S [|\nabla_{\mathbf{y}} \phi|^2] \mathbf{v} \cdot \hat{\mathbf{n}} dS_y. \end{aligned} \quad (5.64)$$

Further we note that

$$\begin{aligned} &- \int_S [[\epsilon_0 \dot{\phi} \nabla_{\mathbf{y}} \phi]] \cdot \hat{\mathbf{n}} dS_y - \frac{\epsilon_0}{2} \int_S [|\nabla_{\mathbf{y}} \phi|^2] \mathbf{v} \cdot \hat{\mathbf{n}} dS_y \\ &= \int_S \langle \dot{\phi} \rangle [[-\epsilon_0 \nabla_{\mathbf{y}} \phi]] \cdot \hat{\mathbf{n}} dS_y + \int_S [[\dot{\phi}]] \langle -\epsilon_0 \nabla_{\mathbf{y}} \phi \rangle \cdot \hat{\mathbf{n}} dS_y - \int_S \epsilon_0 \langle \nabla_{\mathbf{y}} \phi \rangle \cdot [[\nabla_{\mathbf{y}} \phi]] \mathbf{v} \cdot \hat{\mathbf{n}} dS_y \\ &= \int_S \langle \dot{\phi} \rangle \sigma dS_y - \int_S \epsilon_0 [[\dot{\phi}]] \langle \nabla_{\mathbf{y}} \phi \rangle \cdot \hat{\mathbf{n}} dS_y - \int_S \epsilon_0 \langle \nabla_{\mathbf{y}} \phi \rangle \cdot [[\nabla_{\mathbf{y}} \phi]] (\mathbf{v} \cdot \hat{\mathbf{n}}) dS_y \\ &= \int_S \langle \dot{\phi} \rangle \sigma dS_y - \int_S \epsilon_0 \left([[\dot{\phi}]] \langle \nabla_{\mathbf{y}} \phi \rangle \cdot \hat{\mathbf{n}} + [[\nabla_{\mathbf{y}} \phi]] \mathbf{v} \cdot \langle \nabla_{\mathbf{y}} \phi \rangle \hat{\mathbf{n}} \right) dS_y \end{aligned} \quad (5.65)$$

where we used $[[ab]] = [[a]] \langle b \rangle + \langle a \rangle [[b]]$ and the jump condition. This can also be written as

$$\begin{aligned}
& - \int_S [[\epsilon_0 \dot{\phi} \nabla_{\mathbf{y}} \phi]] \cdot \hat{\mathbf{n}} dS_y - \frac{\epsilon_0}{2} \int_S [[|\nabla_{\mathbf{y}} \phi|^2]] \mathbf{v} \cdot \hat{\mathbf{n}} dS_y \\
& = \int_S \langle \dot{\phi} \rangle \sigma dS_y - \int_S \epsilon_0 \left([[\dot{\phi}]] + [[\nabla_{\mathbf{y}} \phi]] \cdot \mathbf{v} \right) \cdot \langle \nabla_{\mathbf{y}} \phi \rangle \hat{\mathbf{n}} dS_y \\
& = \int_S \langle \dot{\phi} \rangle \sigma dS_y - \int_S \epsilon_0 [[\dot{\phi} + \nabla_{\mathbf{y}} \phi \cdot \mathbf{v}]] \cdot \langle \nabla_{\mathbf{y}} \phi \rangle \hat{\mathbf{n}} dS_y \\
& = \int_S \langle \dot{\phi} \rangle \sigma dS_y = \int_S (\dot{\phi} - \mathbf{v} \cdot \langle \nabla_{\mathbf{y}} \phi \rangle) \sigma dS_y = \int_S \dot{\phi} \sigma dS_y - \int_S \mathbf{v} \cdot (\nabla_{\mathbf{y}} \phi^- + \frac{1}{2} [[\nabla_{\mathbf{y}} \phi]]) \sigma dS_y \\
& = \int_S \dot{\phi} \sigma dS_y - \int_S \mathbf{v} \cdot \nabla_{\mathbf{y}} \phi^- \sigma dS_y + \frac{1}{2} \int_S \frac{\sigma^2}{\epsilon_0} (\mathbf{v} \cdot \hat{\mathbf{n}}) dS_y. \tag{5.66}
\end{aligned}$$

We introduce the Maxwell's stress tensor as

$$\mathbf{T}_M = \epsilon_0 \mathbf{E} \otimes \mathbf{E} - \frac{\epsilon_0}{2} \mathbf{E} \cdot \mathbf{E} \mathbf{I} \tag{5.67}$$

where $\mathbf{E} = -\nabla_{\mathbf{y}} \phi$ is the electric field. Note that, the discontinuity of \mathbf{E} across an interface leads to the discontinuity of \mathbf{T}_M .

$$\begin{aligned}
[[\mathbf{T}_M \hat{\mathbf{n}}]] & = \epsilon_0 [[\mathbf{E} \otimes \mathbf{E} - \frac{1}{2} \mathbf{E} \cdot \mathbf{E} \mathbf{I}]] = \epsilon_0 (\langle \mathbf{E} \rangle [[\mathbf{E} \cdot \hat{\mathbf{n}}]] + [[\mathbf{E}]] \langle \mathbf{E} \rangle \cdot \hat{\mathbf{n}} - \langle \mathbf{E} \rangle \cdot [[\mathbf{E}]] \hat{\mathbf{n}}) \\
& = \langle \mathbf{E} \rangle \sigma + [[\mathbf{E}]] (\epsilon_0 \langle \mathbf{E} \rangle \cdot \hat{\mathbf{n}}) - \epsilon_0 \langle \mathbf{E} \rangle \cdot [[\mathbf{E}]] \hat{\mathbf{n}} \\
& = (\mathbf{E}^- + \frac{[[\mathbf{E}]]}{2}) \sigma = (\mathbf{E}^- + \frac{[[\mathbf{E}]]}{2}) \sigma = \mathbf{E}^- \sigma + \frac{1}{2\epsilon_0} (\sigma)^2 \hat{\mathbf{n}}, \tag{5.68}
\end{aligned}$$

where $\langle \mathbf{Y} \rangle = \frac{\mathbf{Y}^+ + \mathbf{Y}^-}{2}$.

We have

$$\begin{aligned} & - \int_S [[\epsilon_0 \dot{\phi} \nabla_{\mathbf{y}} \phi]] \cdot \hat{\mathbf{n}} dS_y - \frac{\epsilon_0}{2} \int_S [|\nabla_{\mathbf{y}} \phi|^2] \mathbf{v} \cdot \hat{\mathbf{n}} dS_y \\ & = \int_S \dot{\phi} \sigma dS_y + \int_S [[\mathbf{T}_M \hat{\mathbf{n}}]] \cdot \mathbf{v} dS_y = \int_S [[\mathbf{T}_M \hat{\mathbf{n}}]] \cdot \mathbf{v} dS_y \end{aligned} \quad (5.69)$$

where we used $\dot{\phi} = 0$ on S_v . Finally we will have

$$\frac{d}{dt} \left(\frac{1}{2} \int_{\mathbb{R}^3} \epsilon_0 |\nabla_{\mathbf{y}} \phi|^2 \right) = \int_{y(\Omega)} \dot{\phi} \rho dy + \int_S [[\mathbf{T}_M \hat{\mathbf{n}}]] \cdot \mathbf{v} dS_y + \int_{y(\Gamma)} [[\mathbf{T}_M \hat{\mathbf{n}}]] [[\mathbf{F}]] u dS_y. \quad (5.70)$$

5.7.3 Rate of change of field energy: step 3

Now subtracting the result from step 2 from that of step 1, we obtain

$$\begin{aligned} & \frac{d}{dt} \left(\frac{1}{2} \int_{\mathbb{R}^3} \epsilon_0 |\nabla_{\mathbf{y}} \phi|^2 \right) \\ & = \int_{\Omega} \phi \dot{\rho}_0 d\mathbf{x} + \int_{y(\Omega)} \mathbf{v} \cdot \nabla_{\mathbf{y}} \phi \rho dy + \hat{\phi} \frac{d}{dt} \int_{S_v} \sigma dS_y - \int_{\partial y(\Omega)} [[\mathbf{T}_M \hat{\mathbf{n}}]] \cdot \mathbf{v} dS_y \\ & - \int_{y(\Gamma)} [[\mathbf{T}_M \hat{\mathbf{n}}]] [[\mathbf{F}]] u dS_y + \int_{y(\Gamma)} [[\mathbf{T}_M \hat{\mathbf{n}}]] \mathbf{n} \cdot \langle \mathbf{v} \rangle dS_y - \int_{\Gamma} [[\rho_0 \phi]] U d\Gamma. \end{aligned} \quad (5.71)$$

5.8 Rate of dissipation: the final expression

Putting together the elasto-chemical dissipation and electric dissipation, we now have the final expression for the rate of dissipation of the whole system:

$$\begin{aligned}
\mathfrak{D} &= \int_{y(\partial\Omega)} \mathbf{t} \cdot \mathbf{v} dS_y - \int_{\Omega} \frac{\partial W_0}{\partial N_{i0}} \dot{N}_{i0} dx - \int_{\Omega} \frac{\partial W_0}{\partial q} \dot{q} dx + \int_{\Gamma} [[W_0]] U dS_x \\
&- \int_{\partial y(\Omega)} \left(\frac{1}{J} \frac{\partial W_0}{\partial \mathbf{F}} \mathbf{F} \mathbf{n} \right) \cdot \mathbf{v} dS_y + \int_{\Gamma} \left[\left[\frac{\partial W_0}{\partial \mathbf{F}} \right] \right] \mathbf{m} \cdot \langle \mathbf{v} \rangle dS_x \\
&- \int_{\Gamma} \left\langle \frac{\partial W_0}{\partial \mathbf{F}} \right\rangle \cdot \mathbf{m} \cdot [[\mathbf{F}]] \mathbf{m} U dS_x + \int_{y(\Omega)} \left(\nabla_y \cdot \left(\frac{1}{J} \frac{\partial W_0}{\partial \mathbf{F}} \mathbf{F} \right) \right) \cdot \mathbf{v} dy \\
&- \int_{\Omega} \nabla_x \mu_{N_{i0}} \cdot \mathbf{J}_{N_{i0}} dS_x + \int_{\Omega} \mu_{N_{i0}} \dot{N}_{i0} dS_x - \int_{\Gamma} [[\mu_{N_{i0}} \mathbf{J}_{N_{i0}}]] \cdot \mathbf{m} dS_x \\
&- \int_{\Omega} \phi \dot{\rho}_0 d\mathbf{x} - \int_{\mathbf{y}(\Omega)} \mathbf{v} \cdot \nabla_{\mathbf{y}} \phi \rho dy + \int_{y(\Gamma)} [[\mathbf{T}_M]] \mathbf{n} \cdot \langle \mathbf{v} \rangle dS_y \\
&+ \int_{\partial y(\Omega)} [[\mathbf{T}_M \hat{\mathbf{n}}]] \cdot \mathbf{v} dS_y + \int_{y(\Gamma)} [[\mathbf{T}_M \hat{\mathbf{n}}]] \cdot [[\mathbf{F}]] u dS_y + \int_{\Gamma} [[\rho_0 \phi]] U dS_x \\
&- \int_{\Omega} \nabla_x \mu_{\rho_0} \cdot \mathbf{J}_{\rho_0} dS_x + \int_{\Omega} \mu_{\rho_0} \dot{\rho}_0 dS_x - \int_{\Gamma} [[\mu_{\rho_0} \mathbf{J}_{\rho_0}]] \cdot \mathbf{m} dS_x \tag{5.72}
\end{aligned}$$

or equivalently

$$\begin{aligned}
\mathfrak{D} &= \\
&- \int_{\Omega} \nabla_x \mu_{\rho_0} \cdot \mathbf{J}_{\rho_0} dS_x + \int_{\Omega} \mu_{\rho_0} \dot{\rho}_0 dS_x - \int_{\Omega} \frac{\partial W_0}{\partial N_{i0}} \dot{N}_{i0} dx \\
&- \int_{\Omega} \frac{\partial W_0}{\partial q} \dot{q} dx - \int_{\Omega} \nabla_x \mu_{N_{i0}} \cdot \mathbf{J}_{N_{i0}} dS_x + \int_{\Omega} \mu_{N_{i0}} \dot{N}_{i0} dS_x - \int_{\Omega} \phi \dot{\rho}_0 dx \\
&- \int_{\mathbf{y}(\Omega)} \mathbf{v} \cdot \nabla_{\mathbf{y}} \phi \rho dy + \int_{y(\Omega)} \left(\nabla_y \cdot \left(\frac{1}{J} \frac{\partial W_0}{\partial \mathbf{F}} \mathbf{F} \right) \right) \cdot \mathbf{v} dy \\
&+ \int_{y(\partial\Omega)} \mathbf{t} \cdot \mathbf{v} dS_y - \int_{\partial y(\Omega)} \left(\frac{1}{J} \frac{\partial W_0}{\partial \mathbf{F}} \mathbf{F} \mathbf{n} \right) \cdot \mathbf{v} dS_y + \int_{\partial y(\Omega)} [[\mathbf{T}_M \hat{\mathbf{n}}]] \cdot \mathbf{v} dS_y \\
&+ \int_{y(\Gamma)} [[\mathbf{T}_M \hat{\mathbf{n}}]] [[\mathbf{F}]] u dS_y + \int_{\Gamma} \left[\left[\frac{\partial W_0}{\partial \mathbf{F}} + T_M^0 \right] \right] \mathbf{m} \cdot \langle \mathbf{v} \rangle dS_x - \int_{\Gamma} \left\langle \frac{\partial W_0}{\partial \mathbf{F}} \right\rangle \cdot \mathbf{m} \cdot [[\mathbf{F}]] \mathbf{m} U dS_x \\
&+ \int_{\Gamma} [[W_0]] U dS_x + \int_{\Gamma} [[\rho_0 \phi]] U dS_x - \int_{\Gamma} [[\mu_{\rho_0} \mathbf{J}_{\rho_0}]] \cdot \mathbf{m} dS_x - \int_{\Gamma} [[\mu_{N_{i0}} \mathbf{J}_{N_{i0}}]] \cdot \mathbf{m} dS_x. \tag{5.73}
\end{aligned}$$

We use $\mathbf{n}dS_y = J\mathbf{m}\cdot\mathbf{F}^{-1}dS_x$, and define the pull back of Maxwell's stress tensor as

$$J\mathbf{T}_M\mathbf{F}^{-1} = \mathbf{T}_M^0 \quad \text{or} \quad \mathbf{T}_M = \frac{1}{J}\mathbf{T}_M^0\mathbf{F} \quad (5.74)$$

so we have

$$\begin{aligned} \mathfrak{D} &= \\ &- \int_{\Omega} \nabla_x \mu_{\rho_0} \cdot \mathbf{J}_{\rho_0} dS_x - \int_{\Omega} \nabla_x \mu_{N_{i0}} \cdot \mathbf{J}_{N_{i0}} dS_x \\ &+ \int_{\Omega} \left(\mu_{\rho_0} \dot{\rho}_0 - \frac{\partial W_0}{\partial N_{i0}} \dot{N}_{i0} - \frac{\partial W_0}{\partial q} \dot{q} + \mu_{N_{i0}} \dot{N}_{i0} - \phi \dot{\rho}_0 \right) dx \\ &+ \int_{y(\Omega)} \left(\nabla_y \cdot \left(\frac{1}{J} \frac{\partial W_0}{\partial \mathbf{F}} \mathbf{F} + \mathbf{T}_M \right) \right) \cdot \mathbf{v} dy \\ &+ \int_{y(\partial\Omega)} \left(\mathbf{t} - \left(\frac{1}{J} \frac{\partial W_0}{\partial \mathbf{F}} \mathbf{F} \mathbf{n} \right) + [[\mathbf{T}_M \hat{\mathbf{n}}]] \right) \cdot \mathbf{v} dS_y \\ &+ \int_{\Gamma} \left([[[\mathbf{T}_M^0]]] - \left\langle \frac{\partial W_0}{\partial \mathbf{F}} \right\rangle \mathbf{m} \cdot [[[\mathbf{F}]]] \mathbf{m} + [[[W_0]]] + [[[\rho_0 \phi]]] \right) U dS_x \\ &+ \int_{\Gamma} \left[\left[\frac{\partial W_0}{\partial \mathbf{F}} + \mathbf{T}_M^0 \right] \right] \mathbf{m} \cdot \langle \mathbf{v} \rangle dS_x - \int_{\Gamma} [[[\mu_{\rho_0} \mathbf{J}_{\rho_0}]]] \cdot \mathbf{m} dS_x - \int_{\Gamma} [[[\mu_{N_{i0}} \mathbf{J}_{N_{i0}}]]] \cdot \mathbf{m} dS_x \quad (5.75) \end{aligned}$$

where we also used

$$\begin{aligned} -\rho \nabla_y \phi &= -\rho \phi_{,i} = -\epsilon_0 \phi_{,i} E_{j,j} = -\epsilon_0 (\phi_{,ij} E_j - \phi_{,ij} E_j + \phi_{,i} E_{j,j}) \\ &= -\epsilon_0 (\phi_{,ij} E_j + \phi_{,i} E_{j,j} + \phi_{,ij} \phi_{,j}) = \epsilon_0 (-\phi_{,i} E_j)_{,j} - \epsilon_0 \left(\frac{1}{2} \phi_{,k} \phi_{,k} \delta_{ij} \right)_{,j} \\ &= \epsilon_0 (E_i E_j - \frac{1}{2} |\nabla_y \phi|^2 \delta_{ij})_{,j} = \nabla_y \cdot (\epsilon_0 \mathbf{E} \otimes \mathbf{E} - \frac{\epsilon_0}{2} \mathbf{E} \cdot \mathbf{E} \mathbf{I}) \\ &= \nabla_y \cdot \mathbf{T}_M. \quad (5.76) \end{aligned}$$

We further note that

$$[[\mu_{\rho_0} \mathbf{J}_{\rho_0}]] \cdot \mathbf{m} = \langle \mu_{\rho_0} \rangle [[\mathbf{J}_{\rho_0}]] \cdot \mathbf{m} + [[\mu_{\rho_0}]] \langle \mathbf{J}_{\rho_0} \rangle \cdot \mathbf{m} \quad (5.77)$$

$$[[\mathbf{J}_{\rho_0}]] \cdot \mathbf{m} = [[\rho_0]] U \quad (5.78)$$

$$\langle \mathbf{J}_{\rho_0} \rangle \cdot \mathbf{m} = \langle \rho_0 \rangle U, \quad (5.79)$$

so the last two terms in the dissipation can be written as

$$\begin{aligned} & \langle \mu_{\rho_0} \rangle [[\rho_0]] U + [[\mu_{\rho_0}]] \langle \mathbf{J}_{\rho_0} \rangle \cdot \mathbf{m} + \langle \mu_{N_{i0}} \rangle [[N_{i0}]] U + [[\mu_{N_{i0}}]] \langle \mathbf{J}_{N_{i0}} \rangle \cdot \mathbf{m} \\ &= ([[\mu_{\rho_0}]]) \langle \mathbf{J}_{\rho_0} \rangle + [[\mu_{N_{i0}}]]) \langle \mathbf{J}_{N_{i0}} \rangle \cdot \mathbf{m} + (\langle \mu_{\rho_0} \rangle [[\rho_0]] + \langle \mu_{N_{i0}} \rangle [[N_{i0}]]) U \\ &= ([[\mu_{\rho_0}]]) \langle \rho_0 \rangle + [[\mu_{N_{i0}}]]) \langle N_{i0} \rangle + \langle \mu_{\rho_0} \rangle [[\rho_0]] + \langle \mu_{N_{i0}} \rangle [[N_{i0}]] U. \end{aligned} \quad (5.80)$$

We further note that $\rho = ez_i N_i + q$, $\mu_\rho = \{\mu_{P_{N_{i0}}}, \mu_q\}$, so we have

$$\mu_{\rho_{0i}} \dot{\rho}_{i0} = \mu_{P_{N_{i0}}} ez_i \dot{N}_{i0} + \mu_q \dot{q}_0 \quad (5.81)$$

$$\nabla \mu_{\rho_{0i}} \cdot \mathbf{J}_{\rho_{0i}} = \nabla \mu_{P_{N_{i0}}} \cdot ez_i J_{N_{i0}} + \nabla \mu_q \cdot J_{q_0}. \quad (5.82)$$

As $ez_i\mu_{P_{N_{i0}}}$ and $\mu_{N_{i0}}$ are not independent, we can include one in the other and refer to the total effect as $\tilde{\mu}_{N_{i0}} = ez_i\mu_{P_{N_{i0}}} + \mu_{N_{i0}}$. The rate of total dissipation is

$$\begin{aligned}
\mathfrak{D} &= \\
& - \int_{\Omega} \nabla_x \mu_{q_0} \cdot \mathbf{J}_q dS_x - \int_{\Omega} \nabla_x \tilde{\mu}_{N_{i0}} \cdot \mathbf{J}_{N_{i0}} dS_x \\
& + \int_{\Omega} \left(\mu_{q_0} \dot{q}_0 - \frac{\partial W_0}{\partial N_{i0}} \dot{N}_{i0} - \frac{\partial W_0}{\partial q_0} \dot{q}_0 + \tilde{\mu}_{N_{i0}} \dot{N}_{i0} - \phi(ez_i \dot{N}_{i0} + \dot{q}_0) \right) dx \\
& + \int_{y(\Omega)} \left(\nabla_y \cdot \left(\frac{1}{J} \frac{\partial W_0}{\partial \mathbf{F}} \mathbf{F} + \mathbf{T}_M \right) \right) \cdot \mathbf{v} dy \\
& + \int_{y(\partial\Omega)} \left(\mathbf{t} - \frac{1}{J} \frac{\partial W_0}{\partial \mathbf{F}} \mathbf{F} \mathbf{n} + [[\mathbf{T}_M \hat{\mathbf{n}}]] \right) \cdot \mathbf{v} dS_y \\
& + \int_{\Gamma} \left(([[\mathbf{T}_M^0]] - \langle \frac{\partial W_0}{\partial \mathbf{F}} \rangle) \mathbf{m} \cdot [[\mathbf{F}]] \mathbf{m} + [[W_0]] + [[\rho_0 \phi]] \right) U dS_x \\
& + \int_{\Gamma} \left(-[[\mu_{q_0}]] \langle q_0 \rangle - [[\tilde{\mu}_{N_{i0}}]] \langle N_{i0} \rangle - \langle \mu_{q_0} \rangle [[q_0]] - \langle \tilde{\mu}_{N_{i0}} \rangle [[N_{i0}]] \right) U dS_x \\
& + \int_{\Gamma} \left[\left[\frac{\partial W_0}{\partial \mathbf{F}} + \mathbf{T}_M^0 \right] \mathbf{m} \cdot \langle \mathbf{v} \rangle \right] dS_x. \tag{5.83}
\end{aligned}$$

From the total dissipation inequality we can see that the dissipation of the system has two contributions: dissipation caused by the diffusion of ions and charges, and the contribution from the deformation of the body.

5.9 Governing equations

According to the second law of thermodynamics specialized to isothermal processes which we are currently considering, the rate of dissipation \mathfrak{D} should always be greater or equal to zero. Notice that in the last expression each term is a product of conjugate pairs: generalized velocity (time rate of change of some quality or flux of some quantity) multiplied by a generalized force (a quantity that depends on the state and not the rate of change of the state). Arguing as Coleman and Noll

(1963) to obtain the governing equations, specifically by considering various processes that have the same state at some instant of time but different rates and insisting that $\mathfrak{D} \geq 0$ for all these processes, we conclude that

$$(\nabla \mu_q \cdot \mathbf{J}_q + \nabla_{\mathbf{x}} \tilde{\mu}_{N_{i0}} \cdot \mathbf{J}_{N_{i0}}) \leq 0 \quad \text{in } \Omega. \quad (5.84)$$

We also have

$$\tilde{\mu}_{N_{i0}} - \frac{\partial W_0}{\partial N_{i0}} - e z_i \phi = 0 \quad \text{in } \Omega, \quad (5.85)$$

and also

$$\mu_q - \frac{\partial W_0}{\partial q} - \phi = 0 \quad \text{in } \Omega, \quad (5.86)$$

and

$$[(\boldsymbol{\sigma} + \mathbf{T}_M)] \cdot \mathbf{n} = 0 \quad \text{on } \partial\Omega. \quad (5.87)$$

We recall that the Cauchy stress tensor is defined as

$$\boldsymbol{\sigma} = \frac{1}{J} \left(\frac{\partial W_0}{\partial \mathbf{F}} \right) \mathbf{F}^T, \quad (5.88)$$

so

$$\nabla_{\mathbf{y}} \cdot (\boldsymbol{\sigma} + \mathbf{T}_M) = 0 \quad \text{in } \mathbf{y}(\Omega), \quad (5.89)$$

and

$$\sigma \hat{\mathbf{n}} - [[\mathbf{T}_M \hat{\mathbf{n}}]] - \mathbf{t}_\chi(\mathbf{y}(\partial_s \Omega)) = 0 \quad \text{on } \partial \mathbf{y}(\Omega). \quad (5.90)$$

We note that conservation of angular momentum requires the sum $\sigma + \mathbf{T}_M$ to be symmetric, however there is no requirement for either part to be symmetric by itself.

$$\sigma \hat{\mathbf{n}} + \mathbf{T}_M \mathbf{n} = 0 \quad \text{on } \mathbf{y}(\Gamma) \quad (5.91)$$

We have

$$\tilde{\mu}_{N_{i0}} = \frac{\partial W_0}{\partial N_{i0}} + e z_i \phi, \quad (5.92)$$

$$\mu_q = \frac{\partial W_0}{\partial q} + \phi. \quad (5.93)$$

We see that the chemical potential of ions consists of two parts: a compositional contribution $\partial W_0 / \partial N_{i0}$ which includes chemical and elastic energies, and an electrostatic contribution $e z_i \phi$. Note that the effect of stress field is implicit in this part. In this work we assume that $\frac{\partial W_0}{\partial q} = 0$, so $\mu_q = \phi$.

In order to satisfy the inequalities we make further constitutive assumption that (summation on repeated indices J over all ions, excluding electrons)

$$\mathbf{J}_{N_{I0}} = -K_{IJ} N_{J0} \nabla_{\mathbf{x}} \mu_{N_{J0}} - K_{I,q} \nabla_{\mathbf{x}} \phi, \quad (5.94)$$

and

$$\mathbf{i} = \mathbf{J}_q = -K_q \nabla_{\mathbf{x}} \phi - K_{q,J} \nabla_{\mathbf{x}} \mu_{N_{J0}}, \quad (5.95)$$

where the non-negative coefficients K can have very different values for different charged species, (diffusion of free charges (electrons) is usually much faster than that of the ions. The condition on K_{IJ}, K_{JI} is that,

$$\mathbf{J}_{N_{i0}} \cdot \nabla_{\mathbf{x}} \mu_{N_{i0}} \leq 0 \quad \text{in } \Omega, \quad (5.96)$$

which shows that we should have (Onsager's reciprocal relation)

$$K_{IJ} = -K_{JI} \quad \text{for any } I, J. \quad (5.97)$$

The same way we should have

$$K_{I,q} = -K_{q,I} \quad \text{for any } I. \quad (5.98)$$

In the special case that the species chemical potentials are continuous across the discontinuity curve, Γ , we have

$$U = K_P \left[W - \frac{\partial W}{\partial N_{i0}} N_{i0} - \frac{\partial W}{\partial q} q - (\mathbf{T}_M^0 + \frac{\partial W}{\partial \mathbf{F}}) \mathbf{F} + \rho_0 \phi \right] \quad \text{on } \Gamma \quad (5.99)$$

for a positive coefficient K_P .

So the driving force, or configurational force or the J-integral, for any discontinuity, say a crack

or a phase boundary in an elasto-electro-chemistry system, including semiconductors is

$$\mathcal{F} = \left[[W - \frac{\partial W}{\partial N_{i0}} N_{i0} - \frac{\partial W}{\partial q} q - (\mathbf{T}_M^0 + \frac{\partial W}{\partial \mathbf{F}}) \mathbf{F} + \rho_0 \phi] \right]. \quad (5.100)$$

Note that we could consider $W_0(N_{i0}, \mathbf{F}, \mathbf{E})$. This would add a term $\frac{\partial W}{\partial E} \dot{E}$ to the dissipation. Dissipation being always non-negative would require $\frac{\partial W}{\partial E} = 0$ which shows that no electric energy is stored in a neutral material.

5.10 References

1. B. D. Coleman, W. Noll, "The thermodynamics of elastic materials with heat conduction and viscosity.", Arch. Ration. Mech., 13:167-78. 1963.
2. F.C. Larche, J.W. Cahn, JRNBS, 1984.
3. M. Silhavy, The mechanics and thermodynamics of continuous media, 2002.
4. M. Jabbour, K.Bhattacharya, A continuum model of multi species film growth by chemical vapor deposition. J. Elasticity 73: 13-74, 2003.
5. K. Bhattacharya, Microstructure of martensite. Oxford: Oxford University Press; 2003.
6. G. Chen, X. Song and TJ Richardson, Electrochem. Solid-State Lett. 9 (2006).
7. N. Meethong, H.-Y. S. Huang, S.A. Speakman, W. C. Carter, Y.-M. Chiang, Adv. Funct. Mater., 17, 1115-1123 (2007).
8. H.-Y. S. Huang, W. C. Carter, Y.-M. Chiang, Electrochem. Solid State Lett., 10[5] 134-138, (2007).

9. Y. Xiao, K. Bhattacharya. A continuum theory of deformable, semiconducting ferroelectrics. *Arch. Rat. Mech. Anal.*, 189: 59-95, 2008.
10. C. Delmas¹, M. Maccario, L. Croguennec, F. Le Cras F. Weill , "Lithium deintercalation in LiFePO₄ nanoparticles via a domino-cascade model", *Nature Materials* 7, 665 - 671 (2008).
11. G. M. Singh, G. Ceder, M. Z. Bazant, *Electrochemica Acta*, 2008.
12. Z. Zhang, R.D. James, S. Muller, "Energy barriers and hysteresis in martensitic phase transformations.", *Acta Materialia* 57(15), 4332-4352 (2009).
13. W. Dreyer, J. Jamnik, C. Gohlke, R. Huth, J. Moskon, M. Gaberscek, " The thermodynamic origin of hysteresis in insertion batteries", *NATURE MATERIALS VOL 9 MAY 2010*.